MATHEMATICAL MODELING OF OPTICAL AND THERMAL BEHAVIOUR OF A NEW CASCADE NANOFLUID-BASED PV/T SYSTEM

SAMIR HASSANI

THESIS SUBMITTED IN FULFILMENT OF THE REQUIREMENT FOR THE DEGREE OF DOCTOR OF PHILOSOPHY

FACULTY OF ENGINEERING
UNIVERSITY OF MALAYA
KUALA LUMPUR

2017

UNIVERSITI MALAYA

ORIGINAL LITERARY WORK DECLARATION

Name of Candidate: **Samir Hassani**   (I.C/Passport No.: ▮▮▮▮▮▮▮)

Registration/Matric No: **KHA130044**

Name of Degree: **Doctor of Philosophy (PhD)**

Title of Project Paper/Research Report/Dissertation/Thesis ("this Work"):

Mathematical modeling of optical and thermal behaviour of a new cascade nanofluid-based PV/T system

Field of Study: **Energy**

I do solemnly and sincerely declare that:

(1) I am the sole author/writer of this Work;
(2) This Work is original;
(3) Any use of any work in which copyright exists was done by way of fair dealing and for permitted purposes and any excerpt or extract from, or reference to or reproduction of any copyright work has been disclosed expressly and sufficiently and the title of the Work and its authorship have been acknowledged in this Work;
(4) I do not have any actual knowledge nor do I ought reasonably to know that the making of this work constitutes an infringement of any copyright work;
(5) I hereby assign all and every rights in the copyright to this Work to the University of Malaya (UM), who henceforth shall be owner of the copyright in this Work and that any reproduction or use in any form or by any means whatsoever is prohibited without the written consent of UM having been first had and obtained;
(6) I am fully aware that if in the course of making this Work I have infringed any copyright whether intentionally or otherwise, I may be subject to legal action or any other action as may be determined by UM.

Candidate's Signature ▮▮▮▮▮▮▮   Date: 03/03/2017

Subscribed and solemnly declared before,

Witness's Signature ▮▮▮▮▮▮▮   Date: 3/3/2017

Name: PROF DR MAHMOUD MOGHAVVEMI
Professor
Designation: Department of Electrical Engineering
University of Malaya
50603 Kuala Lumpur

ii

ABSTRACT

In the last few decades, scientists and engineers have increasingly focused on maximizing the efficiency of solar-harvesting technologies. Photovoltaic/thermal (PV/T) solar systems, which produce both electrical and thermal energy simultaneously, represent a method to achieve very high conversion rates of sunlight into useful energy. In recent years, nanofluids have been proposed as efficient coolant fluids and as a means to filter sunlight for PV/T systems.

In the present study, a new architecture of nanofluid-based PV/T hybrid system with separate channels is proposed, where one channel controls the optical properties while the other enhances heat removal from the PV cells. That is, the first nanofluid, optical nanofluid, acts as a liquid optical bandpass filter above the PV cells while the second, thermal nanofluid, removes heat from the back of the PV cells.

The proposed PV/T system was simulated for both GaAs and Si-based PV cells at various solar concentration ratios, and its electrical and thermal performance were determined numerically using advanced modeling and simulation approaches.

Nanofluids' thermal conductivities were optimized using a new correlation for predicting the thermal conductivity of nanofluids developed herein. The correlation has been developed using Vaschy-Buckingham theorem and derived from 196 values of nanofluids thermal conductivity, 86% of them are correlated within a mean deviation of ±5%, while 98% of them belong to an interval of ±10%.

An improved algorithm for Mie theory was developed to measure nanofluid optical properties. In addition, a modified electrical model was established to predict electrical efficiency of Si and GaAs cells.

To verify the design performance of the proposed nanofluid-based PV/T system with separate channels (D-1), a comparative analysis, in terms of electrical and thermal output, is

conducted between the latter and a nanofluid-based PV/T with double-pass channel (D-2). In concentrated solar systems, it was found that the separate channel system (D-1) outperformed the double-pass design (D-2) by ~8.6%, in terms of the electrical efficiency of GaAs and Si. The overall efficiency of the D-1 system with GaAs and Si have been improved by ~5.8% and ~4.6%, respectively, by increasing the volume fraction of the thermal nanofluid. Generally, it was found that the proposed PV/T configuration with separate channels has potential for further development in high-concentration (C >100) solar systems.

In order to assess the environmental and exergy life cycle of the proposed PV/T system D-1, another comparative analysis has been conducted between the system D-1, standard PV panel and conventional PV/T system.

The life cycle exergy analysis revealed that system D-1 showed the best performance compared to a standard PV and PV/T systems. In instance, the system D-1 produces $\sim$1.3 MWh/m^2 of high-grade exergy annually with the lowest exergy payback time of 2 years, whereas these are $\sim$0.36,$\sim$0.79$MWh/m^2$and 3.48, 2.55 years for standard PV and PV/T systems, respectively. In addition, the nanofluids-based PV/T system type D-1 can prevent the emissions ~448 $kg\ CO_2eq\ m^{-2}.yr^{-1}$.

Overall, this study presents a rigorous research analysis of an improved nanofluid-based PV/T design – a design which opens up a new approach for hybrid solar collectors.

ABSTRAK

Dalam beberapa dekad yang lalu, ahli-ahli sains dan jurutera telah semakin memberi tumpuan kepada memaksimumkan kecekapan teknologi solar-penuaian. Photovoltaic/haba (PV/T) sistem solar, yang menghasilkan kedua-dua tenaga elektrik dan haba pada masa yang sama, mewakili satu kaedah untuk mencapai kadar penukaran yang tinggi cahaya matahari kepada tenaga yang berguna. Dalam tahun-tahun kebelakangan ini, nanofluids telah dicadangkan sebagai cecair penyejuk cekap dan sebagai satu cara untuk menapis cahaya matahari untuk sistem PV/T.

Dalam kajian terkini, konfigurasi melata PV/T berdasarkan nanofluid-dengan saluran berasingan dicadangkan, di mana satu saluran mengawal ciri-ciri optik manakala saluran yang lain meningkatkan kapasiti penyingkiran haba dari sel-sel PV. Lapisan nanofluid pertama, nanofluid optik, bertindak sebagai penapis laluan jalur optik cecair di atas sel-sel PV manakala yang kedua, nanofluid haba, mengurangkan suhu dari belakang sel-sel PV.

Sistem PV/T yang dicadangkan itu simulasi untuk sel-sel PV berasaskan Si dan GaAs pada pelbagai nisbah kepekatan solar, dan prestasi elektrik dan haba yang ditentukan secara berangka menggunakan pemodelan dan simulasi pendekatan maju.

Nanofluids keberaliran haba mereka telah dioptimumkan dengan menggunakan korelasi baru untuk meramalkan keberaliran haba nanofluids. Korelasi ini telah dijalankan menggunakan teori Vaschy-Buckingham dan pangkalan data eksperimen telah diambil dari kajian literasi. Korelasi tersebut berasal daripada 196 nilai nanofluids kekonduksian terma, 86% daripada mereka ini sentiasa bergandingan dalam sisihan min $\pm 5\%$, manakala 98% daripada mereka tergolong dalam selang $\pm 10\%$.

Algoritma yang telah ditambah baik untuk teori Mie telah dibangunkan untuk mengukur sifat nanofluid optik. Di samping itu, model elektrik diubahsuai telah ditubuhkan untuk meramalkan kecekapan elektrik sel Si dan GaAs.

Untuk mengesahkan kelebihan reka bentuk PV/T berdasarkan nanofluid-cadangan dengan saluran berasingan (D-1), analisis perbandingan, dari segi output elektrik dan haba, yang dijalankan antara kedua dan PV/T sistem dengan dua saluran-pass (D-2).

Dalam system solar pekat, didapati bahawa sistem saluran yang berasingan (D-1) mengatasi reka bentuk dua-pass (D-2). Peningkatan sebanyak~ 8.6%, dari segi kecekapan elektrik GaAs (pada C=45) dan Si (pada C= 30) telah direkodkan. Kecekapan keseluruhan sistem D-1 dengan GaAs (pada C=160) dan Si (pada C=100) telah dipertingkan sebanyak~ 5.8% dan ~ 4.6%, masing-masing, dengan meningkatkan pecahan isipadu nanofluid haba dari 0,001 kepada 1.5%. Secara keseluruhan, didapati bahawa cadangan PV/T konfigurasi dengan saluran berasingan mempunyai potensi untuk terus dimajukan pada kepekatan sistem solar yang tinggi (C>100).

Dalam usaha untuk menilai kitaran hidup alam sekitar dan exergy D-1 sistem yang dicadangkan, satu lagi analisis perbandingan telah dijalankan antara sistem D-1, panel PV standard dan PV/T konvensional sistem (iaitu tanpa unit penapisan optik). Analisis exergy kitaran hidup mendedahkan bahawa sistem D-1 menunjukkan prestasi yang terbaik berbanding dengan PV standard dan sistem PV/T. Dalam contoh, sistem D-1 menghasilkan ~1.3 MWh/m^2 bermutu tinggi exergy setiap tahun dengan masa exergy bayaran balik yang paling rendah 2 tahun, sedangkan ini adalah ~0.36,~0.79MWh/m^2 dan 3.48, 2.55 tahun untuk PV standard dan sistem PV/T, masing-masing. Di samping itu, berdasarkan nanofluids-jenis PV/T sistem D-1 boleh menghalang pelepasan kira-kira 448 $kg\ CO_2 eq\ m^{-2}.yr^{-1}$.

Secara keseluruhan, kajian ini membentangkan analisis penyelidikan yang ketat yang lebih baik reka bentuk PV/T berdasarkan nanofluid- reka bentuk yang membuka pendekatan baru untuk hibrid pengumpul suria.

ACKNOWLEDGMENT

First and Foremost, Alhamdulillah, all praise is to ALLAH, the Almighty, the greatest of all, on whom ultimately we depend for sustenance and guidance. I would like to thank Almighty Allah for giving me opportunity, determination and strength to do my research. His continuous grace and mercy was with me throughout my life and ever more during the tenure of my research. I do believe sincerely that without the help and blessing of Allah the achievement of this thesis will be not possible.

The Prophet Muhammad, peace and blessings be upon him, said, "He has not thanked Allah who has not thanked people." Now, I would like to thank and express my deep and sincere gratitude to my supervisor Prof. Dr. Saad Mekhilef for his continuous support, guidance and encouragement. In addition to being an excellent supervisor, he is a man of principles and has immense knowledge of research in general and his subject in particular. I appreciate all his contributions of time, support and ideas.

My sincere appreciation goes to my former supervisor Prof. Dr. Saidur Rahman for his invaluable advice and supervision at the initial stages of this study. His timely and efficient contribution helped me shape this into its final form and I express my sincerest appreciation for his assistance in any way that I may have asked.

I also would like to thank Dr. Robert A. Taylor for his valuable comments and suggestions. Indeed, his feedback and constructive comments were really inspiring and helpful.

I owe everything to my family who encouraged and helped me at every stage of my personal and academic life and longed to see this achievement come true. I dedicate this work to my pious grandfather Arezki Yahia, my sincere and generous father Hassani Mohand Tahar, and my loving mother Arezki Tadj, this is my precious gift to you for all your sacrifice to give me this life. To my lovely wife Mekki Faouzia for her patience, assistance, continuous

support and understanding in everything I done. To my brothers; Abd Elhak, and Abd Eslam, to my sisters; Haoua, Malika, and Saliha.

Last but not least, I would like to dedicate this work to all Hassani and Arezki family to my friends, namely Djamel Benaziz, Said Arezki and Sabeur Nassereddine for their support and encouragement.

Samir Hassani.

.

TABLE OF CONTENT

LIST OF FIGURES

LIST OF TABLES

LIST OF SYMBOLS AND ABBREVIATIONS

A area, $1m^2$

C solar concentration

$CExC$ cumulative exergy consumption, kWh/m^2

cp specific heat, $J\ kg^{-1}\ K^{-1}$

D_h hydraulic diameter, m

d diameter, m

e electron charge, $1.6021 \times 10^{-19} C$

E annual exergy production, kWh

E_g band gap energy, J

e_n nanofluid thickness, m

EQE external quantum efficiency

$ExPBT$ exergy payback time, years

F photon flux, $s^{-1}m^{-2}\mu m^{-1}$

d_{ref} reference diameter

d_p diameter of the nanoparticle, m

T_b boiling point temperature of the base fluid, K

T_{fr} freezing point of the base fluid, K

FF fill factor

G solar radiation, Wm^{-2}

h heat transfer coefficient, $Wm^{-2}K^{-1}$

hr radiation transfer coefficient, $Wm^{-2}K^{-1}$

I radiation intensity, $Wm^{-2}\mu m^{-1}$

J current density, $A\ m^{-2}$

K	conversion factor
k	thermal conductivity, $Wm^{-1}K^{-1}$
k_b	Boltzmann constant, $1.38 \times 10^{-23} \, JK^{-1}$
l	collector length, m
L_c	characteristic length, m
$\dot{m}$	mass flow rate, $kg \, s^{-1}$
Nu	Nusselt number
PE	pollutant emitted, kg
PS	pollutant saved, kg
Pr	Prandtl number
q	heat flux, $W \, m^{-2}$
Q_e	extinction efficiency
R	thermal resistance, $K \, W^{-1}$
Ra	Rayleigh number
Re	Reynolds number
T	temperature, K
v	velocity, $m \, s^{-1}$
V	voltage, V

Greek symbols

α	absorption coefficient, Thermal diffusivity, m^2 s^{-1}
$\bar{\alpha}$	geometrical absorption coefficient
β'	temperature coefficient, K^{-1}
β	linear extinction coefficient, m^{-1}
Δx	spatial step, m

ε	emissivity
η	efficiency
κ	linear absorption coefficient, m^{-1}
λ	wavelength, μm
υ	kinematic viscosity, $m^2\ s^{-1}$
υ_{Br}	Brownian velocity, m s^{-1}
σ	linear scattering coefficient, m^{-1}
τ	transmittance
ϕ	volume fraction

Subscripts

a	air gap
eq	equivalent
np	nanoparticles
bc	back cover
f	base fluid
TH	Therminol
el	electrical
th	thermal
ex	exergy
w	water
c 1,2,3	cover glass 1, 2 and 3
n, 1,2	nanofluid 1 and 2
i	the node number in the flow direction, or insulation
am	ambient

p	plate
con.	convection
rad.	radiation
cond.	conduction
wf	working fluid
0	electrical efficiency at 298K
s	exergy factor of solar radiation

Abbreviations

TH66	Therminol 66
RC	Radiator Coolant
D-1	PV/T hybrid system using separate channel
D-2	Double-pass PV/T hybrid system
PV/T	photovoltaic/thermal
CPV/T	Concentrating photovoltaic/thermal
AM	Air mass
LCA	Life cycle assessment
LCEA	Life cycle exergy assessment
PExI	Profitability exergetic index
GHG	Greenhouse gas
Mod.	Modeling
Exp.	Experimental

LIST OF APPENDICES

CHAPTER 1: INTRODUCTION

1.1 Background

Energy is one of the sign of the universe's existence, and based on the human scale of knowledge, cosmos consists of matter and energy. This physical quantity characterizes the state of a system, and it is generally conserved during transformations. In thermodynamic, energy is defined as the ability of a system to do work, produce heat or electricity. Besides to this thermodynamic definition, the term "energy" also is used in different areas such as technology, economy and ecology, to evoke energy resources, their consumption, their development, their exhaustion, and their ecological impact. Since 19th century fossil fuels are the main energy resources used by the humanity to face the growing up worldwide energy demand. According to the International Energy Agency the world total primary energy produced in 2012 was 13.371 Btoe, in which 40.7% of this energy has been supplied by oil, 15.2% by naturel gas and 10.1% coal (*International Energy Agency, 2014 Key world energy statistics*, Accessed 09.10.2015). Unfortunately the energy produced from the combustion of fossil fuels is not safe in ecological terms. For instance, emissions of $PM_{2.5}$ from coal-fired power plants alone were estimated to cause over 13,000 deaths, 9700 hospitalizations, and 20,000 heart attacks in 2010 with a total monetized value of more than $100 billion (Bridges, Felder, McKelvey, & Niyogi, 2015). Moreover, due to the non-renewable character at human time scale of fossil fuels the conventional energy resources will not be able to ensure a sustainable energy security. For example, Malaysia proven oil reserve represent 0.2% of world's reserve (Petroleum, June 2015), this is expected to be consumed totally within the next 15.8 years if the daily production remains at same level than that on 2014 with 666000 barrels per day.

The negative impact of the combustion of fossil fuels on the ecosystem and their sustainable limitations make the humanity to think again on how to solve the energy problem which is

the most important challenge humankind has to face in the 21st century (Armaroli & Balzani, 2007).

Is there any solution? Definitively yes. On the year 1980 the German Öko-Institut has published an article titled "Energy transition" in which the principal idea of the publication appeals for the complete abandonment of nuclear and petroleum energy (Krause, Bossel, & Müller-Reißmann, 1980).

The concept of Energy transition means the passage from the current energy system using non-renewable resources (i.e. finite resource) to an energy system based mainly on renewable energy resources.

1.2 Use of renewable energy

Prior to the European industrial revolution in the mid-19th century, the humanity was nearly dependent on renewable energy resources to meet her energy needs. Renewable energy is generally defined as a source of energy which is naturally and continually replenished on a human timescale such as sunlight, wind, rain, biomass, waves, and geothermal heat (Ellabban, Abu-Rub, & Blaabjerg, 2014).

Based on REN21's 2015 report (*Renewables 2015: Global status report*, 2015) renewables energy represented approximately 59% of net additions to global power capacity in 2014. By year's end, renewables covered an estimated of 27.7% of the world's power generating capacity, enough to supply an estimated 22.8% of global electricity.

The Sun is the main source of different forms of renewable energy: its radiation is the transport vehicle of the useful energy named solar energy. Solar energy is an effective alternative solution to fossil fuel. For example, according to Malaysia Energy Statistics Handbook 2015, the total energy consumption during the year of 2013 was 51,583 ktoe or ~600,000 GWh, only 1h50min of solar radiation on Malaysia's area is sufficient to cover this amount of energy, or incident solar energy on a surface area of 410 km^2 of PV panels with

20% of conversion efficiency is enough to meet Malaysia's electricity demand for an entire year.

1.3 Solar energy harvesting techniques

Two main techniques are known to be used to harvest solar energy which are either passive or active solar energy systems. In passive solar techniques, building parts such as windows, walls, roofs, and floors are utilized to collect and store solar radiation in the form of thermal energy, which is a useful heating source during winter season. In other hand, active solar technique consist of the use of photovoltaic panels, concentrated or thermal solar collectors. Thermal solar collector converts solar radiation to the heat via an absorber plate (conventional method) or via a volumetric absorber, in which the sunlight energy is absorbed and converted simultaneously by the participating medium (i.e. working fluid) (Todd P. Otanicar, Phelan, Taylor, & Tyagi, 2011; Robert A. Taylor, Patrick E. Phelan, Todd P. Otanicar, Chad A. Walker, et al., 2011). Then, the thermal energy harvested is carried out from the system via a working fluid, and stored or can be used for domestic water heating, industrial processes and electricity generation.

Photovoltaic panels or PV cells are able to convert sunlight into direct current electricity using semiconducting materials. The direct conversion of sunlight to electricity occurs without any environmental emissions during the process. After hydro and Wind, solar PV is the third most important renewable energy source in terms of worldwide installed capacity (*Renewables 2015: Global status report*, 2015).

The main negative side of the usage of PV technology solely is that only a fraction of the total incident radiation is convertible to the electricity and the remaining radiation is either lost or converted to the heat, as shown in the Figure 1.1.
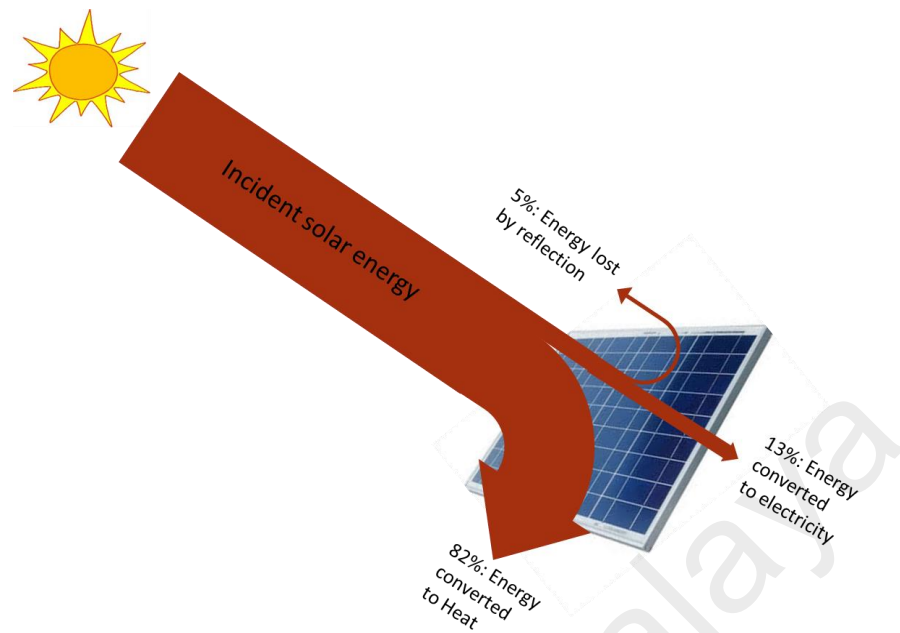
Figure 1.1: Energy conversion in a PV panel

1.4 Photovoltaic/thermal solar collector (PV/T)

The converted solar radiation to the heat, if is not removed, increases the temperature of the PV cells which affect negatively their efficiency of conversion (Dubey & Tiwari, 2008). Based on the aforementioned limitations of using PV technologies alone, scientists have proposed a new kind of solar collector which is PV/T hybrid systems. The first authors who worked on PV/T were Kern & Russell (1978). PV/T collector is a combination of photovoltaic (PV) and solar thermal component systems which leads into an integrated product which can produce both electricity and heat simultaneously (Al-Shamani et al., 2014). In a conventional PV/T system water or air are used as coolant to cool down the PV cells and collect the useful heat. The overall efficiency of PV/T systems is greater than PV systems (Kasaeian, Eshghi, & Sameti, 2015), theoretically a hybrid PV/T collector can be designed to run at roughly 80% of combined efficiency (T. T. Chow, 2010). Therefore, the effective costs for PV/T systems are lower.
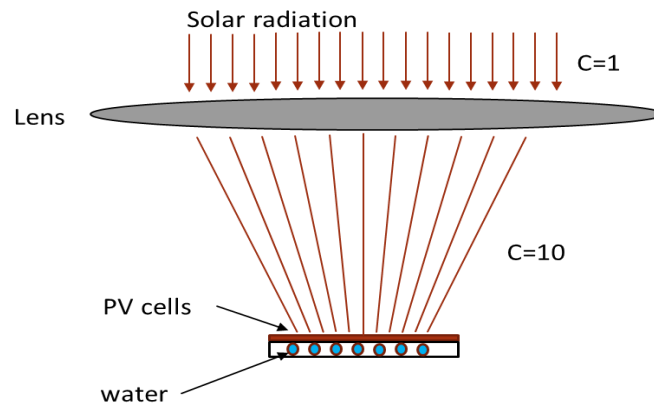
Figure 1.2: Concentrated PV/T systems

However, at height solar concentration PV/T (CPV/T), i.e. Figure 1.2, the electrical efficiency of conventional PV/T system drops down due to the poor thermal properties of the working fluids used to carry the heat generated by the PV cells. Therefore, in order to save the efficiency of the CPV/T system at elevated solar concentrations, a technical solution is needed.

1.5 Optical filtering technique

As mentioned previously, the efficiency of the PV cells decrease when the temperature of the cells increase due to absorption of photons at energy levels below the cells bandgap (T. P. Otanicar, Taylor, & Telang, 2013).

The common characteristic of the PV cells is that their external quantum efficiency is lower within the whole spectrum of incident solar irradiance. For example, the most suitable spectral band for silicon cells, as the most common type of PV cells, is roughly between $700nm$ and $1100nm$ (Mojiri, Stanley, Taylor, Kalantar-zadeh, & Rosengarten, 2015). That is, the UV and IR spectrum are unwanted radiation and once absorbed by the cells it turns to the heat which leads, if not or poorly collected, to a drop in electrical efficiency.

Optical filters methods were proposed firstly by Osborn et al. (1986) in order to absorb unwanted incident radiation on the PV cells. Among the optical filters used in PV/T system

5

there is liquid based optical filter which involve the use of water or organic fluid to intercept the UV and the IR spectrum. In this case the liquid acts as selective absorber by absorbing the unwanted radiation and transmitting the useful spectrum to the PV cells. It is possible as well to use a pure fluid as selective filter and coolant simultaneously (Michael, S, & Goic, 2015).

Water is an excellent absorber of sunlight radiation in the infrared region (Palmer & Williams, 1974). Moreover, water is a highly conductive pure fluid which makes it a good heat carrier fluid to remove the extra heat generated by PV modules. However, water absorbs poorly the UV spectrum, and the energy laying in UV region also considered as unwanted radiation for the PV cells. Therefore, pure water cannot be considered as an ideal liquid based optical filter.

1.6 Nanofluid as coolant and liquid based optical filter

Pure fluids are generally limited heat transfer fluids in terms of optical and thermophysical properties. Recently, researchers have discovered a new kind of heat transfer fluid named nanofluid (Chol, 1995) which is a fluid containing small particles at size of "nano", called nanoparticles. Nanofluid is more flexible in term of optical property control (Q. He, Wang, Zeng, & Zheng, 2013; Todd P. Otanicar, Phelan, Prasher, Rosengarten, & Taylor, 2010; Sajid Hossain, Saidur, Mohd Sabri, Said, & Hassani, 2015; R. Taylor et al., 2013) and more attractive in term of thermal conductivity compared to pure fluids (Saidur, Leong, & Mohammad, 2011; Younes, Christensen, Li, Hong, & Ghaferi, 2015).

Several researchers have investigated the use of nanofluids as coolants and optical filters in PV/T hybrid systems via a double pass geometry design as shown in the Figure 1.3:
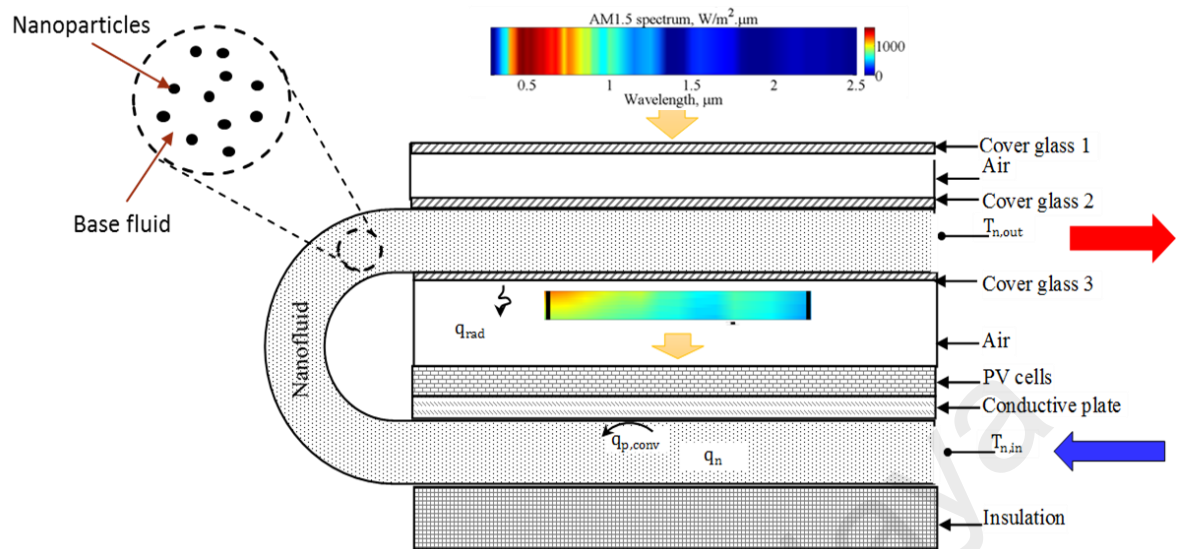
Figure 1.3: Double pass PV/T system operated by unique nanofluid

Firstly, the nanofluid flows through the first channel under the PV cells to cool them down, then it pass to the second channel above the PV cells to absorb the unwanted radiation. All this process involves only the use of one nanofluid. The efficiency of the nanofluid depends on several parameters such as; volume fraction and the material of the nanoparticles, and the physical nature of the base fluid. *So, is it a good solution to use a unique fluid for both cooling and optical filtering?*

1.7 Problem statement

After reviewing references (Brekke, Otanicar, DeJarnette, & Hari, 2016; DeJarnette, Otanicar, Brekke, Hari, & Roberts, 2015; DeJarnette et al., 2014; Jing, Hu, Liu, Wei, & Guo, 2015; Todd P. Otanicar, Chowdhury, Prasher, & Phelan, 2011; Saroha et al., 2015; Zhao et al., 2011), it has been found that a gap exists in the literature where no studies have investigated the use of separate nanofluids for the optical filtering and for the cooling process. In fact, using the same nanofluid for optical filtering and cooling in PV/T systems is disadvantageous since it imposes conflicting requirements in the particle volume fractions and materials, as it is shown in Figure 1.4:
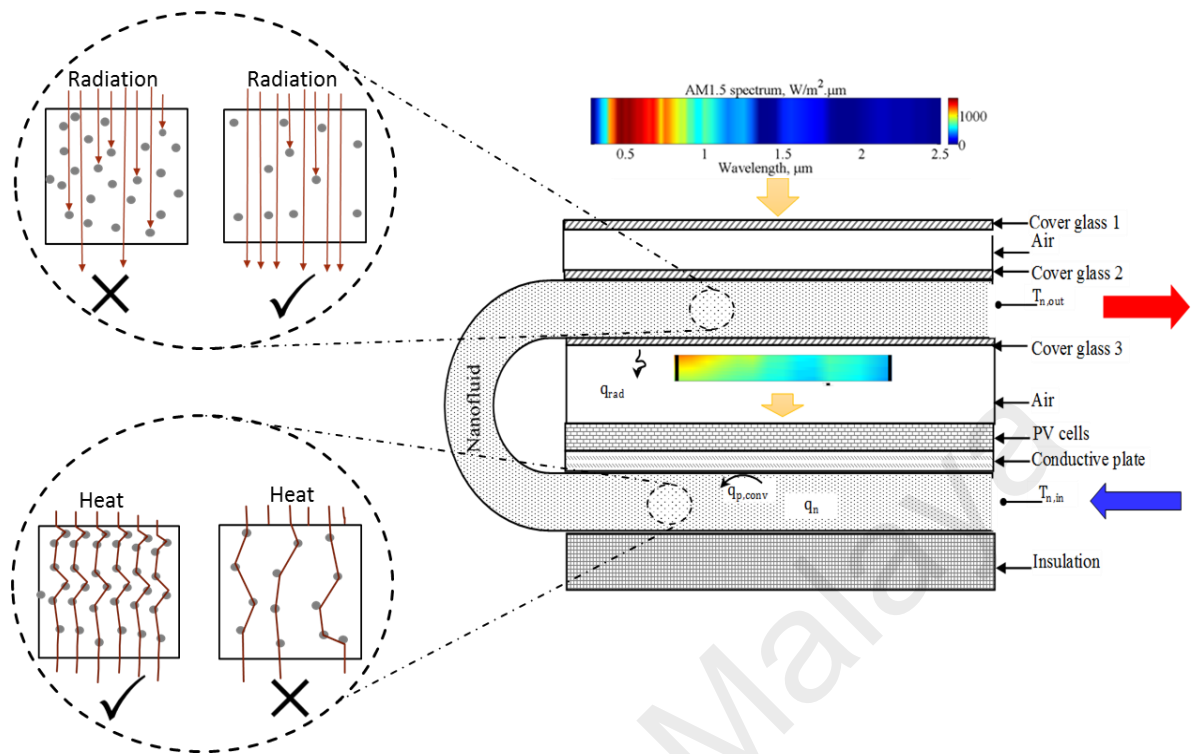
Figure 1.4: Disadvantageous of the double pass PV/T hybrid system

Increasing the volume fraction of the nanoparticles will enhance the thermal conductivity of the nanofluid and promote heat transfer between the nanofluid and PV cells, but will considerably degrade the optical properties of the nanofluid filter. Similarly, a good nanofluid-based optical filter is obtained at a low volume fraction and no measureable change is possible in the thermal properties.

Therefore, a new nanofluid-based PV/T design with separate channels is proposed herein which uses two different nanofluids. The first nanofluid – the 'optical nanofluid' – is optimized to obtain the best liquid optical filter (high transmittance at the visible spectrum and high absorbance at the UV–IR spectrum). The second nanofluid – the 'thermal nanofluid' – is designed to enhance heat removal from the PV cells. This approach is missing in the open literature.

To verify the benefit of the proposed PV/T system configuration, a comparative analysis is conducted between a separate and a double-pass channel configuration.

The evaluation of the thermal and electrical performance of the proposed PV/T will be conducted numerically. Therefore, a robust numerical model has to be developed to investigate the different output performance, and to optimize the thermal conductivity and optical properties of the nanofluids.

Several numerical correlations exist to predict the thermal conductivity of nanofluids. However, most of these correlations were inconsistent with the experimental data. Moreover, it was not clear which is the best model in predicting the thermal conductivity of nanofluids. Therefore, in order to design an appropriate thermal nanofluid for the proposed PV/T system, a new correlation has to be developed as well.

Overall, this research presents a rigorous study of an improved PV/T design – a design which opens up a new approach for hybrid solar collectors.

1.8 Objective of this study

The aim of this study is to propose a novel architecture of nanofluids-based hybrid PV/T system, and determine how nanofluids enhance heat transfers, absorb light selectively, improve the output performances and sustainability of the proposed PV/T hybrid system. The following are the specific objectives of this research:

1. To propose a new architecture of nanofluids-based PV/T system, with a better output performance.

2. To develop new mathematical models to evaluate; the thermal conductivity, optical properties of nanofluids, electrical and thermal performance of the proposed PV/T hybrid systems.

3. To investigate the effect of nanofluid on the electrical and thermal performance of the PV/T.

4. To assess the sustainability of the proposed nanofluids-based PV/T system against the existing PV and PV/T technologies.

1.9 Outline of the thesis

This thesis is consisted of five chapters. Chapter 1 is an introductory chapter that emphasizes the importance of the renewable energy and draws the attention to the advantage of the use of PV/T system to harvest the solar energy. It also highlights about how the use of nanofluids can improve the electrical and thermal efficiency of the PV/T hybrid system. The gap in the literature, problem statement and the objectives of this study are included, as well.

Required information related to the study has been extensively reviewed in chapter 2. To show the 'state-of-the-art' in the area of nanofluid heat transfer, firstly backgrounds regarding nanofluid, its thermophysical-optical properties, and techniques for preparing nanofluids, are presented. Secondly, a brief statement of numerical models used for nanofluid thermal conductivity prediction, available in the literature, and their drawbacks are reported and discussed. Finally, a summary of previous studies on the use of nanofluid, and the applicability of Life Cycle Analysis in PV/T systems are reported.

In spite of all the research works reported in the chapter 2, nanofluids are still far to be well understood. As a result, innovative methods are needed to be developed. Therefore, chapter 3 presents the advanced modeling procedures employed in this research to attempt to predict nanofluid thermophysical-optical properties, thermal, electrical, exergy and environmental performance for a nanofluid-based PV/T hybrid system.

The results and discussion of study are presented in chapter 4. Firstly, the numerical models proposed in chapter 3 have been validated by comparing the theoretical results against experiments data taken from the open literature. Secondly, the simulation results of output performance resulted from the comparative study between the proposed and existing nanofluid-based PV/T architecture has been presented and discussed. Finally, life cycle exergy analysis of five PV/T configurations operated with nanofluid and conventional fluid has been presented and discussed. The results obtained from the life cycle exergy analysis

helps the reader to understand well how the nanofluid-based PV/T hybrid system could be a good energy device solution in real-world applications.

Finally, chapter 5 summarizes the outcomes of this research, and presents some recommendation for possible future work that can be formed from these efforts.

CHAPTER 2: LITERATURE REVIEW

2.1 Introduction

Firstly, general information on nanofluid, its preparation and stability enhancement are provided in this chapter. Secondly, a critical review on existing models for nanofluid thermal conductivity determination has been presented. Finally, a research gap in the literature on the application of nanofluids and life cycle energy analysis in PV/T systems has been reported.

2.2 Definition and generalities

A nanofluid is an engineered colloidal suspension of nanometer-sized particles, named nanoparticles, in the base fluid. The nanoparticles used in nanofluids are typically made of metals, oxides, carbides, or carbon nanotubes. The common base fluids include water, ethylene glycol and oil.

Nanofluids have remarkable thermophysical properties that make them potentially useful in many heat transfer applications (Minkowycz, Sparrow, & Abraham, 2012), including electronic cooling systems, fuel cells, engine cooling/vehicle thermal management, solar thermal collectors, domestic refrigerators, chillers, and heat exchangers. Over the last few years, nanofluids have attracted the interest of a growing number of scientists, and a significant research effort was devoted to this subject. The main findings have been summarized in the recent review papers written by Wen, Lin, Vafaei, and Zhang (2009), (Mahian, Kianifar, Kalogirou, Pop, & Wongwises, 2013), (Saidur et al., 2011), (Aybar, Sharifpur, Azizian, Mehrabi, & Meyer, 2015), (Haddad, Abid, Oztop, & Mataoui, 2014), and (Younes et al., 2015).

In this chapter, the preparation and stability of nanofluid are reviewed briefly. A major attention was devoted to the thermophysical-optical properties of nanofluid, and the energy benefits when nanofluid is used in PV/T hybrid systems as working fluid.

2.3 Preparation methods for stable nanofluids

In general, the dispersion of nanoparticles in a base fluid can be carried out using two methods:

2.3.1 One-step Method

The single-step method is a process combining simultaneously the production and dispersion of the nanoparticles within the base fluid. Several techniques are used in one-step method. Physical Vapor Deposition (Richter, Birkner, & Mudring, 2010), Physical Vapor Condensation (Eastman, Choi, Li, Yu, & Thompson, 2001), and Submerged Arc Nanoparticle Synthesis System (Lo, Tsung, Chen, Su, & Lin, 2005) are among these techniques.

The advantage of one-step method is that drying, storage, transportation, and dispersion of nanoparticles are avoided, so the agglomeration of nanoparticles is minimized and the stability of the nanofluids is increased (Y. Li, Zhou, Tung, Schneider, & Xi, 2009). However, one-step method has its disadvantages which limits its applicability. The disadvantages of this method is that it is impossible to scale it up for great industrial purposes, and applicable only for low vapor pressure base fluids (Ghadimi, Saidur, & Metselaar, 2011). In addition, the residual reactants are left in the nanofluids due to incomplete reaction or stabilization (Wei Yu & Xie, 2012).

2.3.2 Two-step Method

Tow-step method is the most widely method utilized for producing nanofluids. In this method, nanoparticles are firstly produced as dry nanometric scaled powder by chemical or physical techniques, then in a second process dispersed into a base fluid. Due to high surface energy in the nanoparticles, aggregation and clustering will be appeared easily. Afterward, agglomeration and sedimentation of nanoparticles will take place in the mixture. In order to minimize the aggregation and improve dispersion behavior, some techniques are used such

as dispersants, ultrasound, and addition of surfactants (Sidik, Mohammed, Alawi, & Samion, 2014).

Unlike one-step method, two-step method is scald up for great industrial functions, and there are potential economic advantages in using two-step synthesis methods (Ghadimi et al., 2011; Y. Li et al., 2009). This method is effective for oxide nanoparticles, primarily because oxide particles are facile to produce and chemically stable in solution (Das, Choi, & Patel, 2006). However, also two-step method has its drawbacks, such as the quickness agglomeration, poor dispersion, and nanoparticles sedimentation which leads to decrease thermophysical properties of nanofluid.

2.4 Stability enhancement of nanofluids

Stability of nanofluids is one of the fundamental condition that has to be satisfied in order to ensure a better use of the nanofluid in heat transfer applications.

The dispersion of nanoparticles in a base fluid usually involves physical and / or chemical processes to homogenizing the distribution of nanoparticles in the base fluid and improve the stability of the suspension (Sarkar, Ghosh, & Adil, 2015).

In a physical process, a strong mechanical action using a rotary agitator or ultrasound, is applied to break the agglomerated nanoparticles and ensure a better dispersion of the nanoparticles in the base fluid. However, the duration and intensity of mechanical action can have negative effects on the thermophysical properties of nanofluids (Babita, Sharma, & Mital, 2016).   Sadri et al. (2014) investigated the effect of ultrasonication on MWCNTs/Distilled water nanofluid, and they noted that the heat generated through the ultrasonication treatment increased the temperature of the nanofluid which, consequently, affected various parameters like thermophysical and radiative properties.

High shear homogenizer is another physical process used instead of ultrasonication to break agglomerated nanoparticles and helps to get stable nanofluids (Wen & Ding, 2005).

E.P. Bandarra Filho et al (2014) prepared a Silver/Deionized water nanofluid using high shear homogenizer method (up to 400 bar). The nanofluid was found to be stable for more than 3 months.

In chemical treatment researchers add surfactants, change the pH of the solution, or modify the surface of nanoparticles by functionalization. The chemical treatment helps to reduce Van Der Walls attractive forces which forms nanoparticles clustering.

The stabled suspension results from a balance between van der Waals attractive and electrical double layer repulsive forces that exist between particles as they approach each other due to the Brownian agitation (Wei Yu & Xie, 2012).

Surfactants are used when nanoparticles are hydrophobic and dispersed into polar base fluids, or are hydrophilic and dispersed into non-polar base fluids. That is, surfactant acts as a connector between nanoparticles and base fluids (Babita et al., 2016; Mukherjee & Paria, 2013).

The pH treatment is also one of the solution to improve nanofluid's stability. For instance, in a case where acidity of nanofluid is properly controlled, the hydrophobic-to-hydrophilic conversion of the surface nature will occur, and this is due to hydrophobic hydroxyl groups generated by water and leads to increase the nanofluid's Zeta potential (Ghadimi et al., 2011; Hachey, Nguyen, Galanis, & Popa, 2014). Therefore, the repulsive forces between nanoparticles suspended in base fluid increase and the coagulation phenomenon is avoided, consequently, the stability of nanofluid will be improved.

For further improvement of nanofluids' stability, researchers propose to modify the surfaces of nanoparticles by functionalization. Adding functionalized nanoparticles into the base fluid, ensure to the nanofluid a long term stability.

Hordy et al. (2014) have produced a stable multi-walled carbon nanotubes nanofluid using plasma functionalized. The authors claims that the produced nanofluid was stayed stable during 8 months.

Some of the details on how researchers prepare their nanofluids, and different method used for the enhancement of the nanofluids stability are summarized on Table 2.1.

Table 2.1: Summary on preparation and stability enhancement method of nanofluids

Authors	Nanofluids	Preparation method	Stability enhancement method	Stability analysis
(Eastman et al., 2001)	Cu/EG	One-step	Thioglycolic acid	Stored up to two months.
(S. W. Lee, Park, & Bang, 2012)	CuO/H$_2$O	One-step/ Two-step	NA/ sonicate the mixture for 6 h	Nanofluid produced by one-step method is much stable than that produced by two-step method
(De Robertis et al., 2012)	Cu/EG	One-step	Polyvinyl pyrrolidone	The particles settlement is about 28.5% in 50 days
(Botha, Ndungu, & Bladergroen, 2011)	Ag-silica/ Transformer oil	One-step	No dispersant was employed	Particles started settling within 1 h
(Munkhbayar, Tanshen, Jeoun, Chung, & Jeong, 2013)	Ag-CNT/H$_2$O	One-step	Ultrasonication	The nanofluids remain stable for several days (without indicting the number of days)
(Nagvenkar, Deokar, Perelshtein, & Gedanken, 2016)	Zn(acetate)/ 2H$_2$O	One-step	Polyvinyl alcohol	Minimum stability of the nanofluid was found 30 for a ratio of Zn(acetate)·2H2O:PVA equal to 1:15.
(Xuan & Li, 2000)	Cu/H$_2$O	Two-step	Laurate salt+ ultrasonic vibrator	More than 30 h in the stationary state
(Raykar & Singh, 2010)	ZnO/H$_2$O	Two-step	Acetylacetone	Over 9 months to 1 year
(Witharana, Palabiyik, Musina, & Ding, 2013)	ZnO, Al$_2$O$_3$ and TiO$_2$ in PG, EG and 50 wt.% mixtures of PG and EG in H$_2$O	Two-step	Several surfactant were used, pH control, and sonication process.	Samples were visually stable for 2 months
(Mo, Chen, Jia, & Luo, 2012)	TiO$_2$/ DI-H$_2$O	Two-step	SDS as surfactant, pH control, 10min of magnetic stirring, and 40 min of sonication.	Nanofluids kept stable for about 12 days
(Y. Y. Song, Bhadeshia, & Suh, 2015)	Stainless steel 316L /H$_2$O	Two-step	SDS, SDBS and CTAB as surfactants, NaOH for pH control, and 1h sonication.	The overall long term stability was 10 days for pH 11.
(X. Li, Zou, Lei, & Li, 2015)	SiC/EG	Two-step	PVP as dispersant, NaOH for pH control, and 12h of ultrasonication.	No visually observable sedimentation or stratification was found even after 30 days.
(Abdolbaqi, Azmi, Mamat, Sharma, & Najafi, 2016)	BioGlycol:H$_2$O (60:40%)/ Al$_2$O	Two-step	2h of the sonication process.	After 30 days the sedimentation rate was found less than 5%.
(Menbari, Alemrajabi, & Ghayeb, 2016)	γ-Al$_2$O$_3$/H$_2$O, CuO/H$_2$O, γ-Al2O$_3$–CuO/H$_2$O	Two-step	pH control, Sodium Hexa Meta Phosphate as surfactant.	30 days after preparation nanofluids still remain stable
(Oliveira, Cardenas Contreras, & Bandarra Filho, 2016)	MWCNT/H$_2$O	Two-step	High-pressure homogenization process	Not indicated
(Iyahraja & Rajadurai, 2016)	Ag/H$_2$O	Two-step	Poly vinyl pyrrolidone and sodium dodecyl sulfate as surfactants, and magnetic stirrer followed by 3 h ultrasonication	The stability increases with SDS as surfactant as against PVP. However, 11 days was the maximum attained period of stability.

To date, despite the number of research works published on the stability of nanofluid, there is still a big challenge regarding the stability issue, which delays the commercialization at large scale of the nanofluids. Therefore, more basic theoretical and experimental work is required for improving the long term stability of nanofluids.

Although nanofluid preparation and stability are not the scope of the present thesis, it has been found necessary to report some of these notions for better understanding this new generation of heat transfer fluid.

2.5 Thermophysical properties of nanofluids

Thermophysical properties, such as thermal conductivity, viscosity, density, and specific heat, of a heat carrier fluid are drastically modified by the addition of nanoparticles to the base fluid. The qualitative order of the resulting thermophysical properties are mainly depending on a number of factors such as preparation method (include stability treatment), base fluid, material, shape, volume fraction, and size of nanoparticles.

One of the objective of the present research work is to determine theoretically, with enough accuracy, the nanofluids thermophysical properties in order to evaluate the output performance of the PV/T systems involving nanofluid as heat carrier fluid. Therefore, it seems necessary to report the main findings and approaches already developed in the literature for the evaluation of the different thermophysical properties.

2.5.1 Dynamic viscosity

Viscosity (viscum in Latin) can be defined as the resistance to uniform flow occurring in a given mass of fluid. In a laminar flow, the dynamic viscosity of a fluid is the ratio of the shear stress to the velocity gradient perpendicular to the plane of shear (Book, 2014).

The numerical value of viscosity is fundamental, and must to be determined in the case of all applications involving fluids in motion. The viscosity is one of the parameter that allows to

engineers to predict the pumping power needed to keep the fluid in motion. A viscous fluid require more pumping power than watery fluid.

The addition of nanoparticles to base fluid enhances its thermal conductivity, but may leads to an undesirable increase in its viscosity, which means more pumping power (Solangi et al., 2015).

Various theoretical and experimental studies have been conducted to predict or measure the dynamic viscosity of nanofluids and investigate the effect of some physical parameters, such temperature or nanoparticles materials, on the variation of nanofluid viscosity. The interested reader can peruse the main findings summarized in the following recent review papers (W. H. Azmi, Sharma, Mamat, Najafi, & Mohamad, 2016; Bashirnezhad et al., 2016; A. K. Sharma, Tiwari, & Dixit, 2016). Moreover, a large number of theoretical models which are often used by researchers to predict nanofluid viscosity are listed in the following paper (Meyer, Adio, Sharifpur, & Nwosu, 2016).

The viscosity of nanofluid is not necessary to be always larger than that of its base fluid. At low volume concentration researchers R. A. Taylor et al. (2011) reported that there is no significant change in pumping power between nanofluid and base fluid, and this is due to the insignificant change in dynamic viscosity. This fact can be demonstrated using the following relation:

$$\mu_{eff} = \mu_f.(1 + 2.5\phi_v + 6.5\phi_v^2) \tag{2.1}$$

If we plug in $\phi_v < 1 \times 10^{-3}$, we can see that there is a negligible change in viscosity (i.e. $\mu_{eff} \sim \mu_f$). If viscosity is unchanged, this leads to negligible pumping power from frictional losses. It seems that, to be innovative in terms of nanofluid design, a low volume concentration nanofluid with higher performance will be the target in this study.

2.5.2 Specific heat and density

Specific heat is also an important property to be calculated with a proper precision, since the latter is incorporated in energy equation. To determine specific heat of nanofluids, mainly researchers use equations (2.2) and (2.3), which are the most frequently referenced in nanofluids literature:

$$cp_n = \phi_v cp_{np} + (1 - \phi_v)cp_{bf} \tag{2.2}$$

$$cp_n = \frac{\phi_v(\rho.cp)_{np} + (1 - \phi_v)(\rho.cp)_{bf}}{\rho_n} \tag{2.3}$$

Equation (2.2) is proposed by (Pak & Cho, 1998), which is based on mixing theory for ideal gas mixtures, while equation (2.3) is proposed by (Xuan & Roetzel, 2000), and is based on the assumption of thermal equilibrium between the particles and the surrounding fluid (O'Hanley, Buongiorno, McKrell, & Hu, 2012).

The denominator in equation (2.3) is the nanofluid density and is determining using the famous equation (2.4) reported by (Pak & Cho, 1998)

$$\rho_n = \phi_v \rho_{np} + (1 - \phi_v)\rho_{bf} \tag{2.4}$$

O. Mahian et al. (2016) experimentally measured density of SiO_2/H_2O nanofluid and compared their data to theoretical results predicted using equation (2.4), they have found that 1.5% was the maximum deviation between experimental and predicted results.

Although several researchers prefer to use equation (2.2) for nanofluid specific heat due to its simplified form (Polidori, Fohanno, & Nguyen, 2007), however equation (2.3) has been found more fit than equation (2.2) (Shahrul, Mahbubul, Khaleduzzaman, Saidur, & Sabri, 2014).

Several researchers (S. M. Sohel Murshed, 2011a; O'Hanley et al., 2012; Zhou, Wang, Peng, Du, & Yang, 2010) have compared their experimental data on nanofluids specific heat against

predicted data obtained by equations (2.2) and (2.3), they confirmed that their findings match better with those predicted by equation (2.3) than (2.2).

Based on the finding reported in literature review, equation (2.3) for specific heat and equation (2.4) for nanofluid density will be selected for the rest of our calculation.

2.5.3 Thermal conductivity

Nanofluids exhibit the enhanced thermal conductivity and the convective heat transfer coefficient compared to the base fluid. The development of models for predicting the thermophysical properties of nanofluids, such as the thermal conductivity, attracted the interest of several researchers. There are several analytical models that allows engineers and scientists to estimate the thermal conductivity values of nanofluids. Former models, such as Maxwell (1873), Hamilton-Crosser (1962), and Bruggemen (1935), which are based on the classical theory of composites and mixtures containing particles of the order of millimeter or micrometer, fail dramatically in predicting the abnormal thermal conductivity of nanoparticle suspensions. This is essentially due to the nature of the models, which take into consideration only the effect of the nanoparticle concentration. For example, S. M. S. Murshed et al. (2005) found that the results obtained from the Hamilton- Crosser, and Bruggemen models differed from their experimental data by 17% for a 5% particle volumetric concentration.

Thereby, new insights and mathematical models on the thermal conductivity have been proposed. They mainly considered the nanolayering of the liquid at the liquid/nanoparticle interface (L. Li, Zhang, Ma, & Yang, 2008; Lin, Hsiao, & Chieng, 2011; W. Yu & Choi, 2004), and/or Brownian motion of the nanoparticles (Jang & Choi, 2004; Keblinski, Phillpot, Choi, & Eastman, 2002; Xuan, Li, & Hu, 2003; Wenhua Yu, Hull, & Choi, 2003), and/or the effects of nanoparticle clustering (Prasher, Phelan, & Bhattacharya, 2006; Wang, Zhou, & Peng, 2003; Yongjin, Boming, Peng, & Mingqing, 2007). In addition, other models which were in the form of empirical correlations, based on the experimental data, considered the

variation of the temperature, the volume concentration and the diameter of nanoparticles (W H Azmi, Sharma, Mamat, Alias, & Misnon, 2012; Chon, Kihm, Lee, & Choi, 2005; Corcione, 2011; H. Patel, Sundararajan, & Das, 2010; K. V. Sharma, Sarma, Azmi, Mamat, & Kadirgama, 2012).

Although numerous models have been suggested, some of them were inconsistent with the experimental data. Moreover, it is not clear which is the best model to use for thermal conductivity of nanofluids (Aybar et al., 2015). Some of the models proposed contain empirical constants that are either heavily dependent on the experimental observation, or poorly defined (Aybar et al., 2015; Corcione, 2011).

2.5.4.1 Existing correlations for nanofluids thermal conductivity

Based on the existing literature on thermal conductivity of nanofluids, few correlations found to be available on this subject. The validity of most existing correlations is limited to a certain extent. For example, most of them are valid only for oxide or metallic nanoparticles suspended in water or ethylene glycol. It has been noticed that none of these correlations could be used as a general reference to predict the thermal conductivity for a large variety of nanofluids. This limitation is essentially due to the shortage of the experimental databases used to drive these correlations. A summary of selective correlations on the thermal conductivity of nanofluids and their validity range are listed in Table 2.2.

Table 2.2: A summary of selected correlations on thermal conductivity of nanofluids

References	Correlations	Remarks
J. Koo et al. (2005)	$$k_n = \left[\frac{k_p + 2k_f - 2\phi(k_f - k_p)}{k_p + 2k_f + \phi(k_f - k_p)}\right]k_f + \left[5 \times 10^4 \beta\phi\rho_f cp_f\sqrt{\frac{k_bT}{\rho_p d_p}}f(T,\phi)\right]$$ $$f(T,\phi) = (-6.04\phi + 0.4705)T + (1722.3\phi - 134.63)$$ $\beta = 0.0011(100\phi)^{-0.7272}$ for CuO $\phi > 1\%$ $\beta = 0.0017(100\phi)^{-0.0841}$ for Al$_2$O$_3$ $\phi > 1\%$	The term $f(T,\phi)$ is obtained based only on the experimental data of SK Das et al. (2003) for CuO ($d_p = 28.6\ nm$)-water nanofluid. The range of validity of $f(T,\phi)$ is; $1\% < \phi < 4\%$ and $300 < T < 325K$.
R. Prasher et al. (2005a)	$$k_n = (1 + ARe^m Pr^{0.333}\phi)\left[\frac{[k_p(1+2\alpha)+2k_m]+2\phi[k_p(1-\alpha)-k_m]}{[k_p(1+2\alpha)+2k_m]-\phi[k_p(1-\alpha)-k_m]}\right]k_f$$ $$\alpha = \frac{2R_b k_m}{d_p}\ ;\ k_m = k_f\left[1 + \left(\frac{1}{4}\right)Re.Pr\right];\ Re = \frac{1}{v_f}\sqrt{\frac{18k_bT}{\pi\rho_p d_p}}$$	According to R. Prasher et al. (2005b) L. Xue et al. (2003) the thermal interface resistance R_b was not clearly defined. The authors have assumed $R_b \approx 0.77 \times 10^{-8}\ \text{Km}^2\text{W}^{-1}$ for water, $R_b \approx 1.2 \times 10^{-8}\ \text{Km}^2\text{W}^{-1}$ for EG, and $R_b \approx 1.9 \times 10^{-8}\ \text{Km}^2\text{W}^{-1}$ for oil. For the empirical constants A and m, the authors assumed $A = 40000$ for all types of nanofluids. However, the second constant m has been found to depend on the type of base fluid and diameter of the nanoparticles. Because of the need for curve-fitting parameters, A and m, Prasher's model lacks generality(Kleinstreuer & Feng, 2011).

Table 2.2: continued.

R.S. Vajjha et al. (2009)	$$k_n = \left[\frac{k_p + 2k_f - 2\phi(k_f - k_p)}{k_p + 2k_f + \phi(k_f - k_p)}\right]k_f + \left[5 \times 10^4 \beta \phi \rho_f cp_f \sqrt{\frac{k_b T}{\rho_p d_p}} f(T,\phi)\right]$$ $$f(T,\phi) = (2.8217 \times 10^{-2}\phi + 3.917 \times 10^{-3})\frac{T}{T_0}$$ $$+ (-3.0669 \times 10^{-2}\phi - 3.91123 \times 10^{-3})$$ $\beta = 9.881(100\phi)^{-0.9446}$ for CuO $\beta = 8.4407(100\phi)^{-1.07304}$ for Al_2O_3 $\beta = 8.4407(100\phi)^{-1.07304}$ for ZnO	This model is the improved version of Koo & Kleinstreuer model (2005). The new empirical correlations for β and $f(T,\phi)$ are limited only for 60:40 EG/water, and water based fluid. The range of validity of the empirical correlations is; $298 < T < 363K$, and concentration range is $1 < \phi < 6\%$ for CuO, $1 < \phi < 10\%$ for Al_2O_3, and $1 < \phi < 7\%$ for ZnO.
Chon et al. (2005)	$$k_n = \left(1 + 64.7.\phi^{0.746}\left(\frac{d_f}{d_p}\right)^{0.369}\left(\frac{k_p}{k_f}\right)^{0.746} Pr^{0.9955} Re^{1.2321}\right)k_f$$ $$Pr = \frac{\mu_f}{\rho_f \alpha_f}; \quad Re = \frac{\rho_f k_b T}{3\pi \mu_f^2 l_f}$$	The correlation was obtained using Buckingham-Pi theorem and valid only for Al2O3-water nanofluids. The mean-free path l_f was taken as 0.17 nm for water. The authors did not provide the precise value of molecular diameter of a base fluid. In the literature, one can found several values for molecular diameter of water; $d_f = 0.384\ nm$ (Pil Jang & Choi, 2006), $d_f = 0.272\ nm$ (Mathai et al., 1996).The correlation is valid for nanoparticle sizes ranging between 11 and 150 nm. For temperature, the related validity range is 294–344k. Only two points of volume fractions have been investigated; 1% and 4%.

W.H. Azmi et al. (2012)	$$k_n = k_f 0.8938 \left(1 + \frac{\phi}{100}\right)^{1.37} \left(1 + \frac{T}{70}\right)^{0.2777} \left(1 + \frac{d_p}{150}\right)^{-0.0336} \left(\frac{\alpha_p}{\alpha_f}\right)^{0.01737}$$ ϕ in %, T in °C and d_p in nm.	The correlation is only for oxide nanoparticles incorporated in water based fluid. The correlation is valid for a volume concentration less than 4.0%, diameters in the range of $20 - 150nm$, and temperature of $293 - 343K$. (K. V. Sharma et al., 2012)
Corcione (2011)	$$k_n = k_f \left(1 + 4.4 Re^{0.4} Pr^{0.66} \left(\frac{T}{T_{fr}}\right)^{10} \left(\frac{k_p}{k_f}\right)^{0.03} \phi^{0.66}\right)$$ $$Re = \frac{2\rho_f k_b T}{\pi \mu_f^2 d_p}$$	The correlation is for oxide and metal nanoparticles suspended in water or ethylene glycol based nanofluids. The correlation is based on experimental data with 1.86% standard deviation of error. The ranges of the nanoparticle diameter, volume fraction and temperature are $10 - 150 \, nm$, $0.002 - 0.09$ and $294 - 324 \, K$, respectively.
H. Patel et al. (2010)	$$k_n = k_f \left(1 + 0.135 \left(\frac{k_p}{k_f}\right)^{0.273} \left(\frac{T}{20}\right)^{0.547} \left(\frac{100}{d_p}\right)^{0.234} \phi^{0.467}\right)$$	The correlation is based on an experimental database for water, ethylene glycol and transformer oil based nanofluids only. The correlation is valid for nanofluids with spherical nanoparticles shapes of $10 - 150$ nm diameter, thermal conductivity of $20 - 400$ W/mK, base fluid having thermal conductivity of $0.1 - 0.7$ W/mK, volume fraction of $0.1 < \phi < 3\%$ and temperature range from $293 \, to \, 323K$.
H. E. Patel et al. (2008)	$$k_n = k_f \left(1 + \frac{k_p \phi d_f}{k_f (1 - \phi) d_p}\right)$$	The model supposed to be a general tool to predict the thermal conductivity of CNT-Nanofluids. However, the model is not able to predict well at higher temperature of nanofluids (Kumaresan & Velraj, 2012).

Most of the research works which have been published throughout the past two decades concerning the theoretical evaluation of nanofluids thermal conductivity are far from satisfactory. Therefore, an accurate and adaptable model or correlation is needed to be developed, and it is also essential to determine a model, which must take into account the experimental observations available in the literatures. This leads to the possibility of achieving one of the aforementioned objectives (i.e. objective 2).

Having a right correlation is a critical requirement in order to predict, with faultless, the thermal conductivity of nanofluids that will be used in the present proposed PV/T hybrid systems.

2.6 Optical properties of nanofluids

Besides to the area of research activity on thermal properties of nanofluids, several researchers are recently interested to study the optical properties of nanofluids in order to profit from their advantage in direct solar energy absorption applications.

Nanoparticles have been found excellent electromagnetic wave absorber within UV-Visible range where ~85% of solar energy is available. On the other hand, conventional base fluids absorb only the sunlight energy laid within the IR spectrum having ~15% of solar energy (Sajid Hossain et al., 2015). Recently researchers demonstrate that addition of nanoparticles in a conventional base fluid causes significant changes on base fluid optical properties (Said, Sajid, Saidur, Kamalisarvestani, & Rahim, 2013). Absorption, scattering and extinction coefficients are mainly the most investigated optical properties since they allow us to evaluate the performance of nanofluids used as volumetric or selective (i.e. optical filtering) absorbers. Scattering and absorption are linked to each other by the extinction phenomenon. Extinction is the attenuation of light by scattering and absorption as it passes through a medium.

In homogeneous media, such as base fluid, absorption coefficient defines the quantity of incident light absorbed by the working fluid. In mixture media, such as nanofluids, both

nanoparticles and base fluid absorb the incident light. In the other hand, scattering is also a loss of intensity of incident light caused by the obstacle molecules in the medium which force the incident light to be deviated from its straight trajectory (Sajid Hossain et al., 2015).

At low volume concertation and small size of nanoparticles (i.e. <0.6%, <10nm), scattering effect is usually neglected (Robert A Taylor, Phelan, Adrian, Prasher, & Otanicar, 2011), and extinction coefficient only will depends on absorption coefficient.

Like thermal conductivity, optical properties depend on several parameters, such as base fluid, and shape, volume fraction, material, and size of nanoparticles. A good solar nanofluid, that absorbs efficiently sunlight energy and converted it to heat, is optimized taking into account all the aforementioned parameters.

In order to assess nanofluids optical properties theoretically, several approaches are used by researchers. Amongst the most used models we have: Maxwell–Garnett effective medium, Lambert–Beer law, Rayleigh scattering approach and Mie theory. A Summary on research works on optical properties of nanofluids using different approach and comparing their accuracy to the experimental data are presented in Table 2.3.

Table 2.3: Summary on experimental and theoretical works on optical properties of nanofluids

References	Particle types	Base fluid(s)	Model(s)	Remarks
TP. Otanicar et al. (2013)	Ag	Ethylene glycol.	Mie theory	The location of the Plasmon resonance peak for the absorption has been confirmed by the model. The model does not well predict the measured transmittance.
R.A. Taylor et al. (2011)	Ag, Al, Au, Cu, TiO$_2$ graph	Water/VP-1 oil	Rayleigh scattering, and Maxwell Garnett effective medium approach.	Maxwell model fails for all nanofluids studied. Rayleigh scattering approach predicts well extinction coefficient values for graphite/water whereas for other nanoparticle types the model fails.
S. Mahendia et al. (2011)	Au	Poly(vinyl alcohol)	Mie theory	The absorption spectrum of the Au nanofluid shows the SPR peak at 530 nm in agreement with that predicted from calculations based on Mie theory.
Menbari & Alemrajabi (2016)	γ-Al$_2$O$_3$, CuO, and γ-Al$_2$O$_3$+CuO	Water and EG	Mie theory	The extinction coefficients were measured experimentally and comparted to those predicted by Mie theory. Authors have concluded that Mie theory provides a suitable method for predicting the extinction coefficient of the collection of similar particles
Zhu et al. (2013)	AlN	Water	Mie theory, Lambert Beer's law	The transmittance values obtained by models are inaccurate with those measured. An equivalent diameter has been proposed by the author which is 130nm, the results obtained have been found to be in faultless with the experimental.
He et al. (2013)	Cu	Water	Lambert–Beer law.	Extinction coefficient has been calculated. At short wavelength a large discrepancy between obtained, theoretical and experimental, data, whereas at large wavelength the model is in good agreement with experimental data.

Gan & Qiao `(2012)	CNTs MWCNTs Al	Ethanol	Rayleigh scattering approach	The extinction coefficient was determined. In the case of CNTs and MWCNTs, at visible range the predicted data were in a qualitative agreement with those measured, while a significant discrepancy has been noted at UV region. In the case of Al nanofluid a significant dissimilarity between predicted and measured coefficients at both regions UV-Visible.
S.H. Lee & Jang (2013)	MWCNTs	water	Maxwell-Garnett and Rayleigh scattering approach	Maxwell-Garnett model's values were completely incompatible with experimental data. By using hydrodynamic diameter measured by DLS technique Rayleigh scattering was able to predict extinction coefficient of nanofluid. For more accuracy in extinction coefficient the author suggests to adjust the hydrodynamic size of nanoparticles.
D. Song et al. (2016)	Al_2O_3	Deionized water and pure ethyl alcohol	Rayleigh theory, and Mie theory	Using both Rayleigh theory and Mie theory to predict the optical properties of the Al_2O_3/water based nanofluid after aggregation. The results indicate that values obtained by Rayleigh theory are several orders higher than experimental values but Mie theory match reasonably the experimental results.
Moreira et al. (2013)	Ag and Au	water	Mie theory	The absorption and the scattering cross section have been determined using Mie theory. The resulting data for the spectral extinction coefficient were found close to the experimental data.

Based on the reported literature review above, it has been noticed that, in general, Mie theory is more acceptable than other approaches. In the present study, an improved algorithm for Mie theory is proposed in order to optimize and predict optical properties of all the nanofluids designed for optical filtering involved in the proposed PV/T system.

2.7 Application of nanofluid in PV/T hybrid systems

A number of studies have examined the ability for nanoparticles and nanofluids to achieve tunable optical properties (Murray-Méthot, Ratel, & Masson, 2010; T. Otanicar et al., 2013; Said, Sajid, Saidur, Mahdiraji, & Rahim, 2015; Wu, Zhou, Du, & Yang, 2015).

R. A. Taylor et al. (2011) studied the optical property performance of copper, aluminum, silver, graphite, and gold nanoparticles dispersed in water and Therminol VP1. The objective of their study is to determine the potential use of the resulted nanofluids in direct absorption solar collectors. They found that each of the nanofluids can absorbs over 95% of incoming direct normal radiation for a 10cm fluid depth, and this can be achievable even at very low nanoparticle volume fractions (less than $1 \times 10{-5}$, or 10 ppm).

Chen et al. (2015) investigated the photo-thermal conversion efficiency of Ag based nanofluid, and comparing the results to water, ZnO and TiO_2 nanofluids. They revealed that the conversion efficiency of Ag nanofluid (mass concentration of 80.94 ppm) was found equal to 84.61% after 5 min under simulated radiation, which was almost double that of water, and much efficient than that of ZnO and TiO2 nanofluids.

In other research works, researchers revealed that nanofluid if applied as a direct absorption medium (volumetric absorption) of sunlight energy can enhance the output performance of solar thermal devices.

T. P. Otanicar et al. (2010) studied experimentally and theoretically the application of nanofluids for direct solar absorption on a solar collector. The nanofluids were prepared from a variety of nanoparticles (graphite, carbon nanotubes, and silver) mixed with water as the base fluid. They reported that the efficiency of the solar collector was improved up

to 5% by using silver nanofluids as the absorption medium in comparison to a dark flat-plate absorber.

Luo et al. (2014) performed a numerical study to investigate the performance of a direct absorption collector (DAC) by utilizing nanofluids and pure base fluid as absorption mechanism. The photo-thermal efficiency was determined by combining the radiative heat transfer in participating medium with conduction and convection heat transfer mode. The nanofluids were made by; CNT, C, Cu, Ag, TiO_2, SiO_2, Al_2O_3 dispersed in oil as the base fluid. The predicted results show that nanofluids perform better than oil base fluid, and could increase the outlet temperature and the efficiency by 30–100 K and by 2–25%, respectively. In addition, they reported that the photo-thermal efficiency of C based nanofluid is 122.7% superior to that of a coating absorbing surface.

Recently, researchers propose a new idea on the potential use of nanofluids as selective absorbing fluids (Todd P. Otanicar, Chowdhury, et al., 2011; Robert A. Taylor, Otanicar, & Rosengarten, 2012; Zhao et al., 2011). The working principal of a selective absorbing fluid is the ability of nanofluid to absorb the electromagnetic waves laying within a certain range of solar spectrum and to transmit the remaining waves. This principle is similar to a conventional optical solid filter used in PV systems which transmit only the electromagnetic waves laid within the spectral response of the PV cells, and reflect the remaining waves. The energy carried by the reflected waves is considered as unwanted energy because once absorbed by the PV it turns to heat, which induces temperature elevation in the PV cells, hence it causes a decrease in electrical efficiency of the PV panel. The working principal of a nanofluid based optical filter is shown in Figure 2.1.

The advantage to use nanofluid based optical filter instead conventional optical solid filter is that nanofluid has the ability to transmit the waves of interest and absorbs volumetrically the energy carried by the waves laying out of spectral response range. In

addition, the absorbed sunlight energy will be converted to heat and then can be stored and/or used in heating purpose.

(a) Nanofluid based optical filter   (b) Convectional solid filter
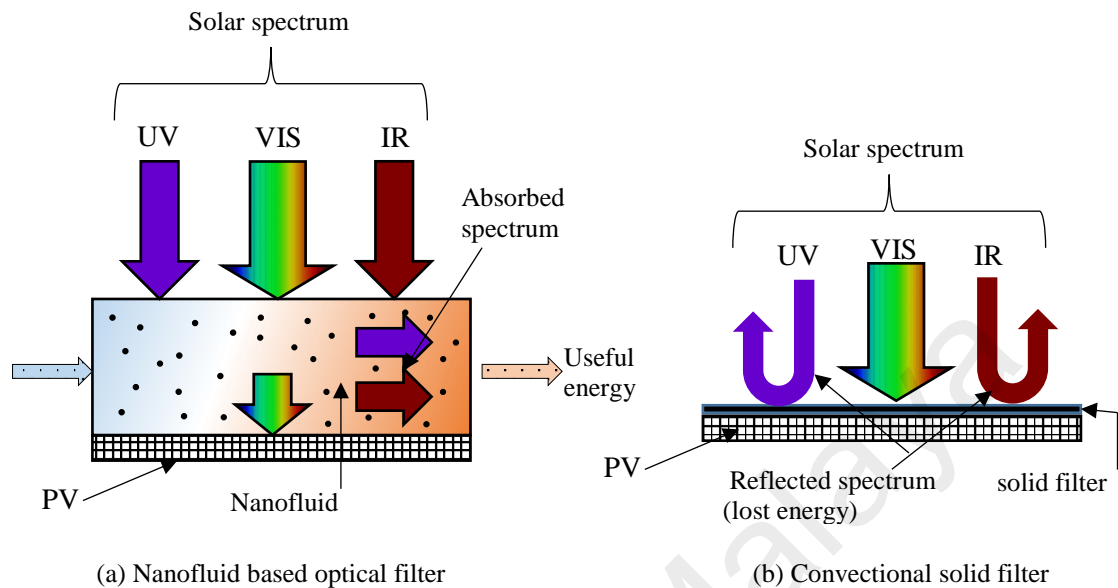
Figure 2.1: Working principal of a nanofluid optical filter and Convectional solid filter

Someone may ask the following question; *how we can use nanofluid based optical filter in a PV system?* PV/T hybrid system is the ideal answer to this question. In a conventional PV/T system, the PV/T consists of two principal units; one is the PV panel, and the second is the thermal solar collector usually placed under the PV cells for cooling purpose. The addition of a second thermal solar collector, as direct absorption collector (DAC), in upper side of the PV cells allows to incorporate the nanofluid based optical filter, as shown in Figure 2.1.

The application of nanofluid as optical liquid filter in PV/T systems is a new field of research, and only a few research works are available in the literature. Some of these works are reported in the present study.

Zhao et al. (2011) presented the ideal nanofluid for a hybrid double-pass PV/T solar collector.
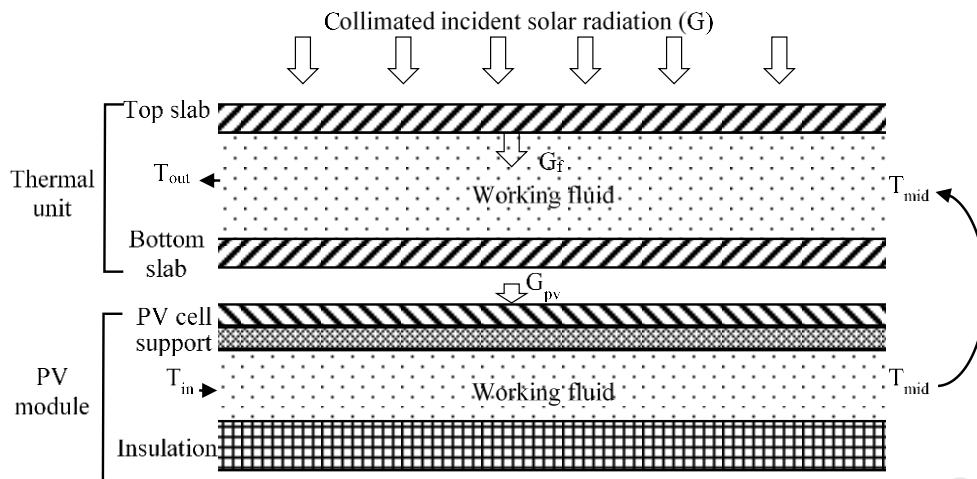
Figure 2.2: Schematic of the double-pass PV/T system proposed by Zhao et al. (2011). T_{mid} is the outlet temperature of the coolant channel and the inlet temperature of filtering channel (thermal unit)

In Zhao's work the same nanofluid was used as both an optical filter and a coolant fluid as shown in Figure 2.2. The thermophysical properties optimization of nanofluids has not been considered in their study. The theoretical results show that increasing the mass flow rate improves the thermal efficiency of the thermal unit, and the electrical efficiency of the PV cells is not influenced by variations in the mass flow rate. At high solar concentration, this does not hold true because decreasing the mass flow rate slows down the cooling process, and increases the working fluid temperature. Consequently, increases the solar cell temperature, which subsequently decreases the electrical efficiency.

T. P. Otanicar (2011) proposed a hybrid PV/T configuration using nanofluid as optical liquid filter to absorb selectively the energy below the band-gap of the PV cells. The PV/T system was studied using numerical one dimensional heat transfer and radiation model. The drawback in their PV/T collector is that it was not provided by a cooling system to remove the extra heat from the PV cells as shown in the Figure 2.3. Consequently, to keep the PV cells temperature below the allowed working temperature range of the PV cells, the PV/T configuration proposed by T. P. Otanicar (2011) should run only at low solar concentration.
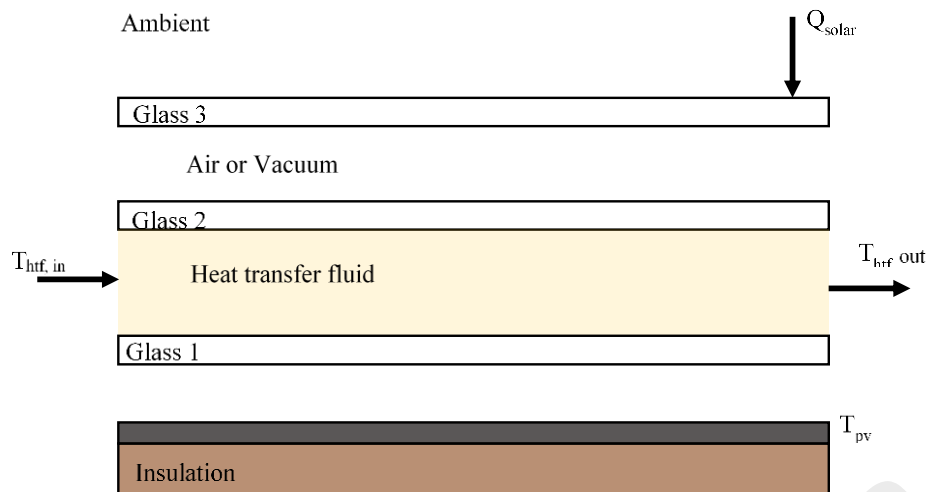
Figure 2.3: PV/T system utilizing a selective nanofluid filter proposed by T. P. Otanicar (2011)

R. A. Taylor et al. (2012; 2013) conducted a theoretical study on the optimization of nanofluid-based optical filters in PV/T systems and investigated the various combinations of base fluids, nanoparticle materials, nanoparticle shapes, and volume fraction to discover a set of potential nanoparticle-based fluid filters. The optical properties were numerically modeled for optimal performance in five PV cell materials, namely Si, Ge, InGaP, InGaAs, and CdTe. The results show that nanofluid-based optical filters can achieve the same level of control as conventional optical solids filters, although some of the materials may be difficult to fabricate with the necessary geometric tolerances. To obtain the desired optical properties, authors claims that a very low volume fractions (on the order of 0.001%) were found to be needed for an optimum PV/T filter, which makes nanofluids potentially inexpensive spectrally selective optical filters.

T. P. Otanicar et al. (2013) applied the resulting nanofluid-based optical filters developed by R. A. Taylor et al. (2012) to concentrated PV/T systems and compared the output performance with different conventional thin-film-based optical fluid filters. The results demonstrate that nanofluid-based filters have a slightly lower overall efficiency than conventional thin-film filters. T. P. Otanicar et al. (2013) did not consider the heat removed from the PV cells, q_{back} in Figure 2.4, in calculating the overall efficiency of

the PV/T system – an unexploited source of thermal energy. In other words, the amount of q_{back} shown in Figure 2.4 has been considered by the authors as a lost energy.
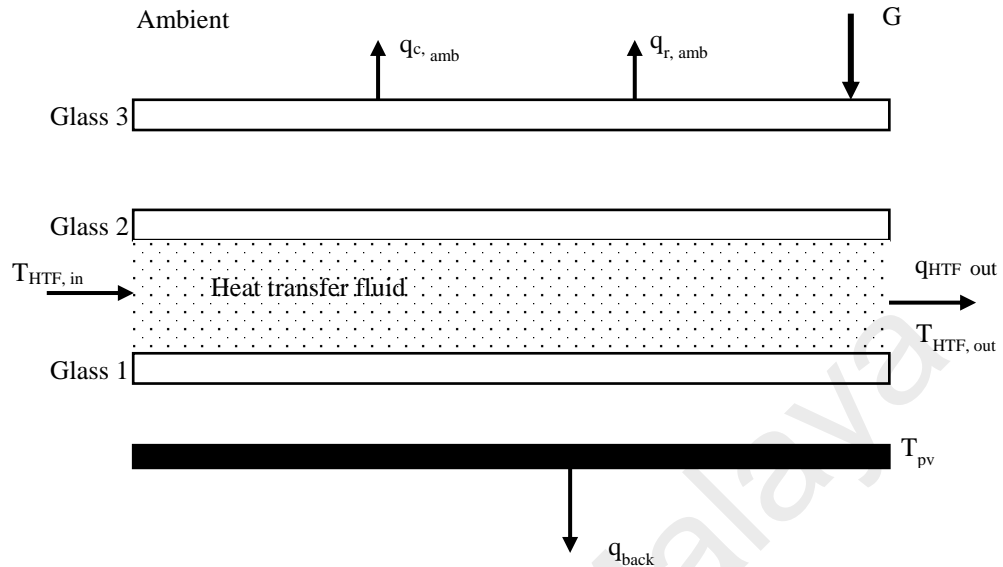
Figure 2.4: Energy balance and modeling schematic proposed by T. P. Otanicar et al. (2013) for their PV/T system

Yun and Qunzhi (2012) experimentally explored the effect of nanofluids in a PV/T system. In their study, MgO-water nanofluids were used as a coolant and applied to the top of a silicon photovoltaic panel to cool down solar cells and collect heat. The results show that the increase of both particle volume fraction and nanofluid film thickness decreases the transmittance of visible light, which leads to a reduction in the output power of solar cells in the PV/T system.

Saroha et al. (2015) proposed a new design of a nanofluid based PV/T hybrid collector with double pass channels. Silver and gold nanoparticles have been used to design the nanofluids filters. The thermophysical properties optimization of nanofluids has not been considered in their study. The PV/T system has been numerically modeled with a zero dimensional model. Indeed, application of such a model for analyzing the performance of a PV/T system is under question. How accurate the results of such a model will be for a real PV/T system in practice? Moreover, assumptions considered in their study render the theoretical model exceedingly simplified and need proper justifications which are ignored in their manuscript. Similar approaches were adopted in Zhao et al. (2011) work.

DeJarnette et al. (2015) studied numerically a spectral selective nanofluid based solar filter for use in double-pass nanofluid based PV/T concentrating system. The optimization of the nanofluid filter has been based on temperature dependent bandgap of GaAs solar cell. They reported that the optimized nanofluid can absorb 86% of below bandgap sunlight energy, while transmitting to the PV cells 82% above bandgap solar radiation. In addition, they have noted that the placement of a nanofluid filter above the PV cell is shown to absorb an additional 2% of the total solar energy reflected off the PV panel.

Jing et al. (2015) produced SiO_2/H_2O spectral selective nanofluid using one step sol–gel process. Thus, the resulted nanofluid has been applied as coolant fluid and optical liquid filter in a double pass PV/T system with Si cells. The transmittance and thermal conductivity of the prepared nanofluids were measured. They have found that the transmittance of SiO_2/H_2O nanofluid, with a diameter size of 5 nm and volume concentration of 2%, was higher than 97%, which is very close to pure water. They reported that the nanofluid absorbs only the IR spectrum. It seems that with 97% of transmitted light the nanofluid optical filter was poorly optimized. For instance the UV spectrum (which is an unwanted spectral energy for Si cells) was not absorbed by the nanofluid and this is due to optical property of SiO_2 (i.e. linear absorption coefficient of the refractive index) which is of the order of zero along the whole solar spectrum. In addition, water is a fullfor transmitter of UV spectrum, and only absorbs IR spectrum. Consequently, one can say that the nanofluid based PV/T system proposed by Jing et al. (2015) in terms of geometry design and optical properties optimization is far from perfection.

Due to the few research works on nanofluid based PV/T systems, the previous optimization of these kind of devices are far from satisfactory. A little effort to date has gone into optimizing (i) the geometry of nanofluid based PV/T system, (ii) thermal and optical properties of the nanofluid inside the PV/T system. Therefore, a considerable

effort will be devoted in the present study in order to achieve a high efficient nanofluid based PV/T system with optimized geometry, and thermo-optical properties. Using advanced mathematical approach, and realistic assumptions will make the present study fairly comparable to a real scenario of a nanofluid based PV/T hybrid system.

2.8 Life cycle analysis of PV/T hybrid systems

The conventional hybrid PV/T collector is a sustainable technology (Tripanagnostopoulos, Souliotis, Battisti, & Corrado, 2005). Several publications (S. Agrawal & Tiwari, 2013; Battisti & Corrado, 2005; T.-T. Chow & Ji, 2012; Good, 2016; Tiwari, Raman, & Tiwari, 2007; Tripanagnostopoulos et al., 2005) reported the economic and environmental competitiveness of conventional PV/T hybrid systems.

Battisti and Corrado (2005) carried out LCA (i.e. life cycle analysis) on a conventional multi-crystalline silicon PV and PV/T systems with a heat recovery system for the domestic hot water supply. The LCA was conducted based on energy replaced, either by electricity or natural gas. Based on their results, the EPBT (Energy Payback Time) and GPBT (Greenhouse Gas Payback Time) of PV system were found to be 3.3 and 4.1 years, whereas those of PV/T systems designed for electricity replacement were 1.7 and 1.6 years.

In another study, Tripanagnostopoulos et al. (2005) applied the methodology of LCA to perform an energy and environmental assessment of a standard PV, and water-cooled glazed/unglazed PV/T system. The output power of the both systems was 3kWp. Both of these devices were analyzed for both free-stand and integrated building installations. The EPBT of the PV and BiPV system were found to be 2.9 and 3.2 years, whereas the GPBT were 2.7 and 3.1 years, respectively. For glazed PV/T system at 45℃ operating temperature, the EPBT for PV/T and BiPV/T were found to be 2.6 and 2.7 years, and GPBT were 3 and 3.1 years, respectively.

Chow and Ji (2012) reported an evaluation of the EPBT and GPBT of a tilted free-stand PV/T and vertical-mounted BiPV/T systems in Hong Kong. Their results showed that the EPBT of PV/T and BiPV/T were 2.8 and 3.8 years, thus the GPBT were 3.2 and 4 years, respectively. The performance of a vertical-mounted BiPV/T was found to be better than that of roof-top BiPV/T system.

Further research works available in literature on LCA of conventional PV/T systems have been summarized by Bahaidarah et al. (2016) and Good (2016).

After searching the literature on LCA of PV/T systems, it has been noted that the LCA method was applied only on a standard PV/T system that uses conventional fluids such as water or air, flowing behind the PV cells, as a working fluid to recover the heat for thermal applications. To the best of the author's knowledge, no research works to date have been done on life cycle analysis of a nanofluid –based PV/T systems.

In this study, exergetic life cycle analysis and environmental impact of various nanofluid-based PV/T configurations will be investigated. In addition, a comparative analysis to a standard PV-only and conventional PV/T system operated by a pure fluid will be reported. Life cycle exergy method will be considered as a verification tool for the sustainability of the PV/T configurations. One of the central objective of the present work (i.e objective number 4) is to answer the following question; *how the use of optimized nanofluid as a coolant and optical filter can improve the energetics and ecological performance of a PV/T hybrid system?*

2.9 Summary

Based on the previous literature, it has been noticed that most of the existing models on nanofluids thermal conductivity determination are lacking precision, and a general model to predict this thermal properties for a large variety of nanofluids with enough accuracy is still needed.

The application of nanofluids in PV/T system is a new field of research, and the proposed design for such systems by the previous researchers need improvement in terms of physical architecture and thermo-optical properties optimization. In addition, existing numerical models for predicting the different performances of PV/T system are practically overmuch simplified and the assumptions taken into consideration are not realistic, which leads to a fault prediction of the output performance of the system. Therefore, in this study an advanced mathematical model will be developed to solve the different physical phenomenon involved in the system, and based on more realistic assumptions. To the best of the author's knowledge, this study offers the first investigation on the life cycle exergy analysis of a PV/T collector operated by nanofluids based optical filter and coolant.

.

CHAPTER 3: METHODOLOGY

3.1 Introduction

In this chapter, a description of methods and procedures to achieve the objectives listed in the first chapter are provided. This chapter has been divided into few subsections. Firstly, the working principal of the proposed new architecture of nanofluids-based PV/T system with separate channels will be presented.

Secondly, the mathematical descriptions of thermal and electrical performance calculations, procedure to develop a new correlation for nanofluid thermal conductivity, and modeling procedure used to investigate nanofluid optical properties will be provided. Finally, a detailed description of an exergy and environmental life cycle analysis, including mathematical modeling of electrical and thermal assessment, of the proposed nanofluids-based PV/T design, and of four conventional configurations have been presented.

3.2 A cascade nanofluid-based PV/T system

In this section the proposed design of the nanofluids-based PV/T system, using two nanofluids for cooling and optical filtering purposes, will be described in minutiae way. This will include the structural design and mathematical models utilized to assess the output performance of the system.

3.2.1 Physical model and working principal of the nanofluids-based PV/T system

The optical and thermal flows of proposed PV/T design as compared to the existing double-pass design available in literature are presented in Figure 3.1a and 3.1b, respectivly. In Figure 3.1a, solar radiation reaches the PV cells after crossing the cover glasses and the optical nanofluid filtration channel. After the optical nanofluid channel only the radiation within the spectral response of the PV cells remains. The choice of the nanoparticle material type, base fluid, size, and volume concentration for the optical nanofluid depends on the bandgap of the PV cells and the thickness of the channel. The

function of air gaps 1 and 2 is to reduce heat loss by conduction and convection, and to enable the optical nanofluid thermal receiver to operate at significantly higher temperature than the PV cells.

The metal plate on the rear side of the PV module acts like a heat sink. The heat generated by the PV cells is removed by the thermal nanofluid in the second channel. The thermal nanofluid contains metal nanoparticles at a concentration on the order of 0.001% to 1%, and is designed to have high thermal conductivity to enhance the extraction of heat from the PV cells.
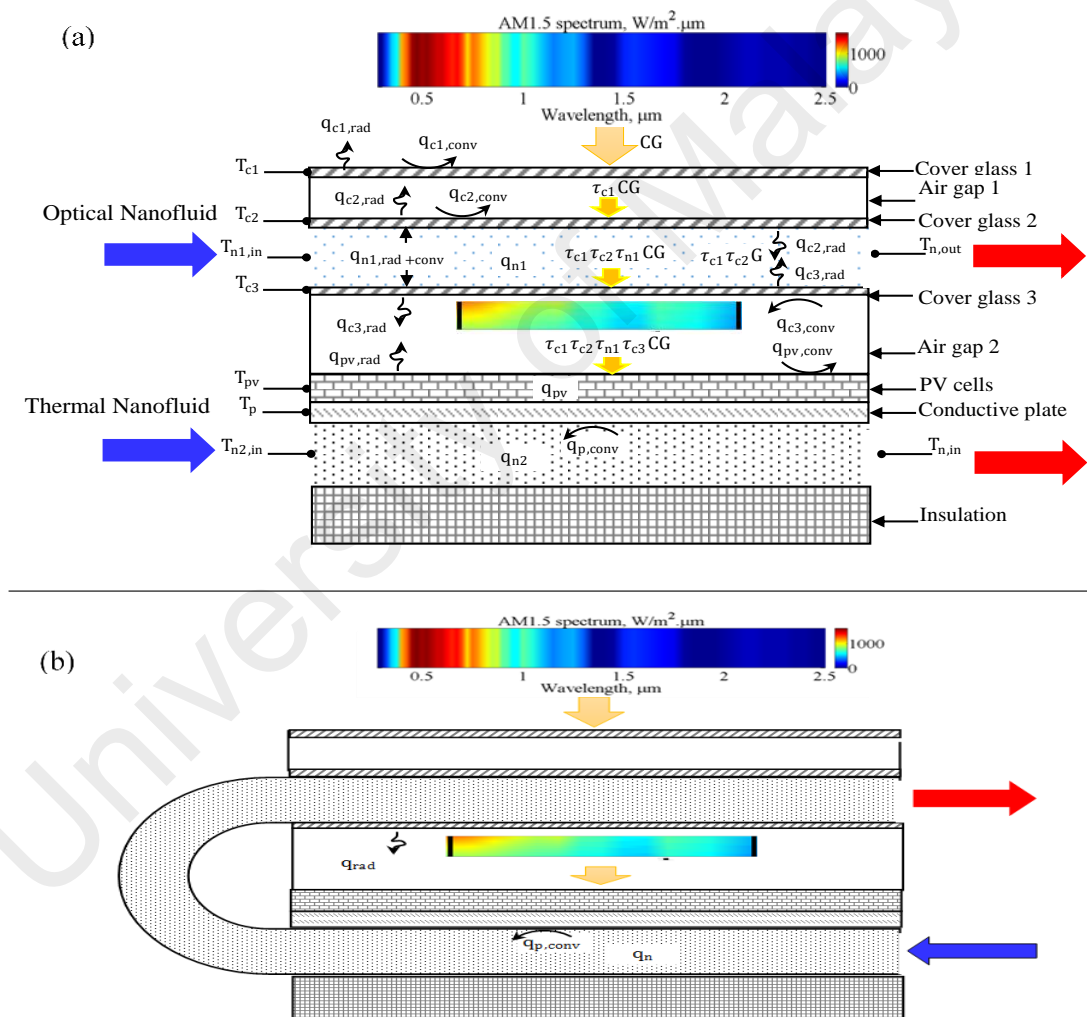
Figure 3.1: Sketch of PV/T hybrid system; (a) separate channels and (b) double-pass channel

To show the advantages of the PV/T system with separate channels, a comparative study will be conducted between the systems presented in Figure 3.1a and Figure 3.1b – e.g. separated channels and a commonly employed double-pass channel. In this study, the

notations D-1 and D-2 refer to the systems presented in Figure 3.1a and Figure 3.1b, respectively.

3.3 Mathematical modeling of the nanofluids-based PV/T system

The general numerical model presented below was used to predict system temperatures, electrical performance, and efficiencies, if the optical and thermal properties are known. In the following sub-sections, a brief description of this model is given, based on how it relates to the pertinent literature.

3.3.1 Thermal model

The mathematical model used in the present study was derived by applying the first law of thermodynamics (i.e. the energy balance equation) for each element of the PV/T collector. For one-dimensional heat transfer, the general energy balance equation is given by:

$$\frac{\partial U}{\partial t} = \dot{Q}_{in} - \dot{Q}_{out} + \dot{Q}_g \tag{3.1}$$

where $\frac{\partial U}{\partial t}$ is the change in the internal energy, $\dot{Q}_{in}$ is the heat transfer rate into the system, $\dot{Q}_{out}$ is the heat transfer rate out of the system, and $\dot{Q}_g$ is the heat generation rate into the system. A set of reasonable assumptions are made and presented in Table 3.1:

Table 3.1: Assumptions considered in the present study

No.	Assumptions
1	Steady state
2	Normal incident irradiation
3	Uses a thin, uniform temperature cover glass (Duffie & Beckman, 2013)
4	Variation of the temperature along the flow direction is considered
5	The thermophysical properties of the base fluid and nanofluids are temperature dependent, and are determined from the most relevant equations in the literature (Duangthongsuk & Wongwises, 2010; Maïga, Palm, Nguyen, Roy, & Galanis, 2005; NIST, accessed December, 2015; O'Hanley et al., 2012)
6	The thermal nanofluid under the PV module is pressurized
7	Thermal energy is transferred in the flow direction by mass transfer
8	Cover glass, plate, and air gaps properties are independent of temperature
9	Electrical pumping power is considered negligible due to low mass flow rates, a justification for this statement is provided in chapter 4.

Steady state assumption may not _always_ hold, however it is a reasonable assumption (to focus on rated conditions) when doing this type of comparative analysis. This is in-line with several other studies. H.A. Zondag et al. (2002) have evaluated the thermal and electrical yield of a PV-thermal collector using four numerical models: a 3D dynamical model and three steady state models that are 3D, 2D and 1D. Their results were compared to experimental data and it was found that for the daily yield, a simple 1D steady state model performs almost as good as the much more time-consuming 3D dynamical model. Similar findings are reported in the following Ref. (Candanedo, Athienitis, Candanedo, O'Brien, & YuXiang, 2010; Hj. Othman, Yatim, Sopian, & Abu Bakar, 2005; Zondag et al., 2002).

With a tracking system steady state near-normal incidence are achievable. The constant temperature cover and property assumptions are also reasonable. In fact, it is worth to be mentioned that the assumptions considered in the present work are more realistic and rigorous that several previous studies in this field such as; (DeJarnette et al., 2015; Elmir, Mehdaoui, & Mojtabi, 2012; Jing et al., 2015; Zhao et al., 2011).

Before any energy balance equation is provided for the parts of the collector, the method in which heat is transferred from one element to another should be understood. Starting from top (cover glass 1) to bottom (insulation), the different heat transfer modes involved in the system are resumed in Table 3.2:

Table 3.2: Heat transfer mechanism occurring in the PV/T

Exchange Element	Heat transfer mode
Cover glass 1 and outside air	Radiation and forced convection
Cover glass 1 and 2	Radiation and free convection
Cover glass 2 and 3	Internal forced convection and radiation in participating medium
Optical nanofluid	The nanofluid is considered as an absorbing and emitting medium, justified by the fact that in concentrating PV/T, the nanofluid temperature is high with non-negligible thermal radiation
PV and Cover glass 3	Natural convection in air gap 2 is neglected, since the PV module has a lower temperature than cover glass 3. Thus, only radiation heat transfer mode is considered between the cover glass 3 and the PV module
PV and rear plate	Pure heat conduction
Rear plate and thermal nanofluid	Internal forced convection
Insulation	A well-insulated bottom with a liquid barrier – e.g. adiabatic/impermeable boundary

The temperature variation along the flow direction is considered. Therefore, a backward scheme for the spatial coordinate (x) is adopted to discretize the derived thermal energy balance equations for each element of the PV/T collector. The resulting discretized equations are summarized in Table 3.3:

Table 3.3: Energy balance equations for the PV/T system model described in Figure 3.1a

$$h_{c1-a}(T_{a,i} - T_{c1,i}) + hr_{c1-c2}(T_{c2,i} - T_{c1,i}) + \alpha_{c1}CG - h_{eq(c1-am)}(T_{c1,i} - T_{am}) = 0 \tag{3.2}$$

$$h_{c2-a}(T_{c2,i} - T_{a,i}) - h_{c1-a}(T_{a,i} - T_{c1,i}) = 0 \tag{3.3}$$

$$h_{c2-n1}(T_{n1,i} - T_{c2,i}) + hr_{c2-c3}(T_{c3,i} - T_{c2,i}) + hr_{c2-n1}(T_{n1,i} - T_{c2,i}) + \alpha_{c2}\tau_{c1}CG - hr_{c2-c1}(T_{c2,i} - T_{c1,i}) - h_{c2-a}(T_{c2,i} - T_{a,i}) = 0 \tag{3.4}$$

$$\tau_{c1}\tau_{c2}C\int_{0.28\mu m}^{2.5\mu m}\alpha_{\lambda,n1}G_\lambda - h_{c2-n1}(T_{n1,i} - T_{c2,i}) - h_{c3-n1}(T_{n1,i} - T_{c3,i}) - hr_{c2-n1}(T_{n1,i} - T_{c2,i}) - hr_{c3-n1}(T_{n1,i} - T_{c3,i}) \\ - \dot{m}_{n1}cp_{n1}\frac{T_{n1,i} - T_{n1,i-1}}{l\,\Delta x} = 0 \tag{3.5}$$

$$h_{c3-n1}(T_{n1,i} - T_{c1,i}) + hr_{c3-n1}(T_{n1,i} - T_{c3,i}) + \alpha_{c3}\tau_{c1}\tau_{c2}C\int_{0.28\mu m}^{2.5\mu m}\tau_{\lambda,n1}G_\lambda - hr_{c2-c3}(T_{c3,i} - T_{c2,i}) - hr_{c3-pv}(T_{c3,i} - T_{pv,i}) = 0 \tag{3.6}$$

$$\tau_{c1}\tau_{c2}\tau_{c3}\alpha_{pv}C\int_{0.28\mu m}^{2.5\mu m}\tau_{\lambda,n1}G_\lambda(1 - \eta_{el}^*) = \frac{(T_{pv,i} - T_{p,i})}{R_p} - hr_{c3-pv}(T_{c3,i} - T_{pv,i}) \tag{3.7}$$

$$\frac{(T_{pv,i} - T_{p,i})}{R_p} - h_{p-n2}(T_{p,i} - T_{n2,i}) = 0 \tag{3.8}$$

$$h_{p-n2}(T_{p,i} - T_{n2,i}) - q_{back} - \dot{m}_{n2}cp_{n2}\frac{T_{n2,i} - T_{n2,i-1}}{l\,\Delta x} = 0 \tag{3.9}$$

Note: The thermal conductivity determination for nanofluids is described in section **3.3.4.1**. The heat transfer correlations appearing in the above equations are given in the Appendix A. All other parameters and coefficients involved in solving equations (3.2) to (3.9) are presented in Table 4.4.

3.3.2 Electrical model

In the aim of the comparative study between separate and double-pass nanofluid based PV/T (D-1 and D-2), two types of photovoltaic materials, Si and GaAs, are investigated. The electrical model to evaluate adjusted electrical efficiency η_{el}^* in equation (3.7) at different temperatures is based on references (Fan, 1986; Freeman, 2010; T. Otanicar, Chowdhury, Phelan, & Prasher, 2010; T. P. Otanicar et al., 2013; Silverman et al., 2013). The dark saturation current J_{00} in the cell is calculated as follow (Fan, 1986):

$$J_{00} = K' T_{pv}^{3/n} exp\left(\frac{-E_g}{m k_b T_{pv}}\right) \tag{3.10}$$

where K', n, and m are empirical constants. E_g is the energy gap that corresponds to the PV cells.

The short circuit current J_{sc} can be computed from (T. P. Otanicar et al., 2013):

$$J_{sc} = \int_{0.28\mu m}^{\lambda_g} e EQE_\lambda \tau_{sys,\lambda} F_\lambda d\lambda \tag{3.11}$$

where λ_g is the wavelength of solar radiation, which corresponds to the band-gap of the PV material, e is the electron charge, and F_λ is the photon flux. EQE_λ is the PV cell's quantum efficiency, which is wavelength-dependent and were adapted from (Green, Emery, Hishikawa, Warta, & Dunlop, 2012, 2014). Considering the AM1.5 spectral range, $\tau_{sys,\lambda}$ is the spectral transmittance of the upper channels ($\tau_{sys,\lambda} = \tau_{c1}\tau_{c2}\tau_{c3}\tau_{n1,\lambda}$) in the transmission window between $0.28 \ \mu m - \lambda_g$, τ_c is the transmittance of the cover glass, and $\tau_{n1,\lambda}$ is the optical filtering efficiency of the nanofluid based optical filter

determined using equation (3.29). Methods on how $\tau_{\lambda,n1}$ is determined is described in section **3.3.4.2**.

The open-circuit voltage V_{oc} is then calculated as follows (T. P. Otanicar et al., 2013):

$$V_{oc} = \frac{A' k_b T_{pv}}{e} ln \left(\frac{C J_{sc}}{J_{00}} + 1\right) \tag{3.12a}$$

where A' is the diode factor and C is the solar concentration ratio.

At standard temperature of $T_{pv} = 25°C$, equation (3.12b) effectively predicts the efficiency of the PV cells. However, it has been found that equation (3.12b) is less accurate at temperatures higher than $25°C$. Therefore, in the present study, a new formula for V_{oc} is introduced as follows:

$$V_{oc} = V_{oc,0} \left(1 - \beta'(T_{pv} - T_0)\right) \tag{3.12b}$$

where T_0 is the reference temperature equal to 25 °C, $V_{oc,0}$ is the open-circuit voltage at T_0, and β' is the coefficient temperature taken from (Silverman et al., 2013).

The fill factor FF is given by (Fan, 1986; T. Otanicar et al., 2010):

$$FF = \frac{V_{mp}}{V_{oc}} \left[1 - \frac{exp\left(\frac{e V_{mp}}{k_b T_{pv}}\right) - 1}{exp\left(\frac{e V_{oc}}{k_b T_{pv}}\right) - 1}\right] \tag{3.13}$$

where V_{mp} is the voltage at the maximum power point of the *I-V* curve and is calculated using the following relationship:

$$V_{mp} = k \times V_{oc}. \tag{3.14}$$

The k value is typically between 0.70 and 0.80 (Freeman, 2010).

The final step is the expression of the electrical efficiency of the PV cells, which can be calculated by (Fan, 1986; T. P. Otanicar et al., 2013):

$$\eta_{el} = \frac{V_{oc} J_{sc} FF}{G} \tag{3.15}$$

To account for the spectral filtering assured by the nanofluid, an expression for adjusted electrical efficiency is proposed by (T. P. Otanicar et al., 2013) as follows:

$$\eta_{el}^* = \frac{V_{oc}J_{sc}FF}{\tau_{c1}\tau_{c2}\tau_{c3} \int_{0.28\mu m}^{2.5\mu m} \tau_{\lambda,n1}G_{\lambda}} \tag{3.16}$$

Regarding the equations reported above most of them are from other references, but it is necessary to report them in the main text since they lead to my contributions of equations (3.12b) and (3.14). In addition, the numerical value of the empirical constants K', n, m and A' appearing in equations (3.10) and (3.12b) have been adjusted using an optimization algorithm, and presented in Table 4.4.

At a cursory level it may seem standard model, but the electrical model presented herein is actually a modified model from (Fan, 1986; T. Otanicar et al., 2010).

It should be noted that this model is only applicable for advanced solar cells technologies.

3.3.3 Overall efficiency of PV/T

The interdependence of the different temperatures and the efficiency of the PV cells requires a coupled iterative method between the electrical and thermal models. In other words, equations (3.2) to (3.16) should be solved simultaneously. In the present study, the overall thermal efficiency of the PV/T system is the sum of the thermal efficiency of the first and second channels. In (T. P. Otanicar et al., 2013), the thermal energy in the second channel is considered as lost energy. In the strategy described in (T. P. Otanicar et al., 2013), the thermal efficiency analysis does not enable one to directly calculate the thermal energy extracted from the second channel, certainly this could be considered as useful energy source.

When all the unknown temperatures have been computed, the thermal efficiency of the PV/T can be calculated by adding the useful energy obtained from both channels, defined as:

$$\eta_{th} = \dot{m}_{n1} \frac{cp_{n1}\left(T_{n1,out} - T_{n1,in}\right)}{CGA} + \dot{m}_{n2} \frac{cp_{n2}\left(T_{n2,out} - T_{n2,in}\right)}{CGA} \tag{3.17}$$

The overall or exergy efficiency of the PV/T system can be calculated using equation (3.18) as follows:

$$\eta_{ov} = \eta_{el} + K \sum_{i=1}^{2} \left(1 - \frac{T_0}{T_{n,i}}\right)\eta_{th,i} \tag{3.18}$$

where i is the channel's number, $i = 1$ is the first channel and $i = 2$ is the second channel, T_n is the nanofluid outlet temperature.

K is the fraction of thermal exergy converted to electrical output and assumed to be 0.5 for high solar concentration (T. Otanicar et al., 2010; T. P. Otanicar et al., 2013; Vorobiev, González-Hernández, & Kribus, 2005). More insights about equation (3.18) are available in section **3.4.2.6**.

N.B: equation (3.18) has been derived by the author of this thesis.

3.3.4 Thermal conductivity and optical properties modeling

Using trustable models for predicting nanofluid's thermal conductivity and optical properties is a priority need in modeling study of solar thermal devices such as the above proposed design of nanofluid based PV/T system. Therefore it has been found that it is necessary to develop confident models for these two key properties with less possible prediction error. In this study, development procedure of a new correlation for nanofluid thermal conductivity predicting, as well as an optimized algorithm for optical properties determination are presented.

3.3.4.1 Proposed correlation for nanofluid thermal conductivity

Since nanofluid's thermal conductivity is one of the main factor prompting the quality of the heat transfer in the PV/T system, its determination need a robust numerical model in order to avoid imprecision when the thermal performance of the PV/T are determined. In the following, a detailed description on how the proposed correlation was developed.

a) Correlation database

The present correlation is derived from a wide variety of experimental data of the thermal conductivity of nanofluids. Several alternative base fluids, such as water, ethylene glycol, methanol, engine oil (EO), Therminol 66, ethylene glycol based coolant used in car radiator (RC), R141a, containing different types of nanoparticles, like TiO_2, Al, Al_2O_3, Fe, Cu, Ag, SiO_2, CuO, CNTs and MWCNTs were considered in developing this correlation. The experimental database used to develop the present correlation is obtained from the following open literature: (Choi, Zhang, Yu, Lockwood, & Grulke, 2001; Chon et al., 2005; Das et al., 2003; Elias et al., 2014; Garg et al., 2008; Godson, Raja, Lal, & Wongwises, 2010; Hong, Hong, & Yang, 2006; Hwang et al., 2006; Jiang et al., 2014; S. H. Kim, Choi, & Kim, 2006; S. Lee, Choi, Li, & Eastman, 1999; Liu, Ching-Cheng Lin, Huang, & Wang, 2005; Mahbubul, Fadhilah, Saidur, Leong, & Amalina, 2013; Masuda, Ebata, Teramae, & Hishinuma, 1993; Mintsa, Roy, Nguyen, & Doucet, 2009; S. Murshed, Leong, & Yang, 2008; S. M. Sohel Murshed, 2011b; Pang, Jung, Lee, & Kang, 2012); Singh et al. (2014); (Wen & Ding, 2004), and shown in Table 3.4.

Table 3.4: Database for the proposed correlations

References	Nanoparticles	d_p(nm)	Base fluid	Volume fraction (%)	Temperature (K)	Number of data
S. M. Sohel Murshed (2011b)	TiO$_2$	15	Ethylene glycol	$1 < \phi < 5$	296	49
S. M. Sohel Murshed (2011b)	TiO$_2$	10		$1 < \phi < 5$	296	
S. Murshed et al. (2008)	Al	80		$1 < \phi < 5$	296	
S. Murshed et al. (2008)	Al$_2$O$_3$	80		0.5	294<T<333	
Garg et al. (2008)	Cu	200		$0.4 < \phi < 2$	298	
(2006)	Fe	10		$0.1 < \phi < 0.55$	306	
Liu et al. (2005)	CNTs	20		$0.2 < \phi < 2$	296	
Hwang et al. (2006)	MWCNTs	25		$0.25 < \phi < 1$	296	
S. H. Kim et al. (2006)	TiO$_2$	34	Water	$1 < \phi < 3$	298	86
Chon et al. (2005)	Al$_2$O$_3$	47		1	293<T<343	
Chon et al. (2005)	Al$_2$O$_3$	47		4	293<T<343	
Chon et al. (2005)	Al$_2$O$_3$	150		1	293<T<343	
Masuda et al. (1993)	Al$_2$O$_3$	13		$1.3 < \phi < 4.3$	320	
Chon et al. (2005)	Al$_2$O$_3$	11		1	293<T<343	
Das et al. (2003)	CuO	33		$1 < \phi < 4$	298	
Mintsa et al. (2009)	CuO	29		$1 < \phi < 14$	293	
S. Lee et al. (1999)	CuO	18		$1 < \phi < 14$	298	
Godson et al. (2010)	Ag	60		0.3	323<T<363	
Godson et al. (2010)	Ag	60		0.6	323<T<363	
Godson et al. (2010)	Ag	60		0.9	323<T<363	
Wen and Ding (2004)	MWCNTs	40		$0.05 < \phi < 0.84$	296	
Hwang et al. (2006)	MWCNTs	20		$0.25 < \phi < 1$	296	
Elias et al. (2014)	Al$_2$O$_3$	13	RC	$0.2 < \phi < 1$	283<T<323	25
Mahbubul et al. (2013)	Al$_2$O$_3$	13	R141b	$0.5 < \phi < 2$	293	4
S. Murshed et al. (2008)	Al	80	Engine oil	1	294<T<333	15
S. Murshed et al. (2008)	Al	80		3	294<T<333	
Choi et al. (2001)	CNTs	25		$0.04 < \phi < 0.2$	296	
Liu et al. (2005)	CNTs	25		$1 < \phi < 2$	296	
Jiang et al. (2014)	Cu	20	TH 62, 66	$0.5 < \phi < 2$	333	7
Singh et al. (2014)	Cu	160		$0.5 < \phi < 2$	393	
Pang et al. (2012)	Al$_2$O$_3$	45	Methanol	$0.005 < \phi < 0.5$	293	10
Pang et al. (2012)	SiO$_2$	15		$0.005 < \phi < 0.5$	293	

There are a total of 196 data points for six base fluids; water, ethylene glycol, methanol, radiator coolant, R141b, engine oil and Therminol 66 and 62.

b) Correlation development for effective thermal conductivity

The thermal conductivity of nanofluid depends on several parameters related either, to the medium (i.e. base fluid) such as, the temperature, the thermal conductivity, the specific heat, the viscosity, the density, or to the physical properties of nanoparticles, such as the Brownian velocity, the volume fraction, nanoparticle's thermal conductivity, the density and the size. The Brownian velocity is introduced due to the Brownian motion of nanoparticles within the base fluid. Therefore, the resulting relationship between the thermal conductivity and the selected variables is represented in a functional form, as given by equation (3.19):

$$k_n = f\left(\phi, k_f, k_p, v_{Br}, cp_f, d_{ref}, d_p, T, v_f, T_b\right) \tag{3.19}$$

The main question is how to build up a correlation, which is able to combine all the aforementioned physical variables in only one expression? The answer to this question is the Vaschy-Buckingham theorem (Buckingham π −theorem) (Buckingham, 1914; Vaschy, 1892), which is one of the basic theorems for the dimensional analysis. The theorem states that if there is a physical equation with n number of physical variables which depend on k of fundamental units, then there is an equivalent equation involving $n − k$ dimensionless parameters $\pi_1, \pi_2, \ldots \pi_{n-k}$ constructed from the original variables. By applying the Vaschy-Buckingham theorem to the physical parameters aforementioned, seven dimensionless π −groups are generated with four repetitive variables, k_f, d_p, v_{Br}, and T.

The resulting π −groups are given in Table 3.5.

A generalized empirical correlation for the dimensionless thermal conductivity of the nanofluids, k_n, normalized by the base fluid thermal conductivity, k_f, is developed based on the generated π −groups, as given in equation (3.20). The coefficients and exponents

of the correlations, $\alpha_{1...n}$ and $\beta_{1...n'}$, will be obtained by applying a non-linear regression analysis for the experimental data mentioned in Table 3.4.

$$\pi_1 = \alpha_1 + \pi_2^{\beta_1} \pi_3^{\beta_2} \pi_4^{\beta_3} \left[\frac{\alpha_2}{\pi_4^{\beta_3}} - \frac{\alpha_3}{\pi_3^{\beta_2}} + \left(\alpha_4 \, \pi_5^{\beta_4} \, \pi_6^{\beta_5} \, \pi_7^{\beta_6} \, \pi_8^{\beta_7} \right) \right] \quad (3.20)$$

Table 3.5: Dimensionless π-groups of the present correlations

π −group	Parameter
π_1	$\dfrac{k_n}{k_f}$
π_2	ϕ
π_3	$\dfrac{k_p}{k_f}$
π_4	Pr
π_5	$\dfrac{d_{ref}}{d_p}$
π_6	$\dfrac{v_f}{d_p \, v_{Br}}$
π_7	$\dfrac{cp}{T^{-1} v_{Br}^2}$
π_8	$\dfrac{T_b}{T}$

v_{Br} is the Brownian velocity, given by equation (3.21) (Junemoo Koo & Kleinstreuer, 2004);

$$v_{Br} = \sqrt{\frac{18 \, k_b \, T}{\pi \, \rho_p \, d_p^3}} \quad (3.21)$$

where k_b is the Boltzmann constant, $1.3807 \times 10^{-23} \, J/K$ and ρ_p is the density of nanoparticles.

The d_{ref} is the molecular diameter of hydrogen, and equal to 2.9Å, (Kumar, Salih, Lu, Müller, & Rodríguez-Reinoso, 2011; X. Xu, Yang, Song, Liu, & Lin, 2003).

The thermophysical properties of the nanoparticles integrated in the calculation have been presented in Table 3.6.

Table 3.6: Thermophysical properties of nanoparticles

Nanoparticles	Density (g/cm³)	TC[*] (W/m.K)	References
Al₂O₃	3.97	40	Oztop and Abu-Nada (2008)
TiO₂	4.1	8.9538	Oztop and Abu-Nada (2008)
Ag	10.5	419	P.D. Shima et al. (2014)
Fe	7.87	80	B.N. Reinecke et al. (2008)
Cu	8.94	400	M.S. Liu et al. (2006)
CuO	6.4	20	A. Azari (2015)
SiO₂	2.2	1.2	E.V Timofeeva et al. (2011)
Al	2.7	237	Syam and Singh (2013)
CNTs	2.1	1282	J. Jianwei et al. (2000)

[*] Thermal conductivity

It has to be noted that temperature of base fluids was considered for this analysis, and all thermophysical properties of the base fluids have been calculated using data taken from the following Refs. (Cengel & Ghajar, 2011; NIST, accessed December, 2015).

The statistical relations employed to verify the accuracy of the present correlation, equation (3.20), are as follows:

Mean deviation:

$$\frac{1}{n}\sum_{1}^{n} \text{ABS}[100 \times (\pi_{1,prd} - \pi_{1,exp})/\pi_{1,exp}] \tag{3.22}$$

Average deviation:

$$\frac{1}{n}\sum_{1}^{n}[100 \times (\pi_{1,prd} - \pi_{1,exp})/\pi_{1,exp}] \tag{3.23}$$

Standard deviation:

$$\sqrt{\left(\frac{1}{n}\sum_{1}^{n}[100 \times (\pi_{1,prd} - \pi_{1,exp})/\pi_{1,exp}]^2 - \text{Average dev.}^2\right)} \tag{3.24}$$

3.3.4.2 Optical properties modeling

Optical properties are critical parameters to design a nanofluid based optical filter. The aim, of course, is to design the nanofluid-based optical filter to be transparent across

spectral response curve of the PV cells. Moreover, the nanofluid should highly absorb the undesired sunlight to obtain a high quality thermal output.

Silver (Ag) nanoparticles suspended in Therminol VP-1 were chosen to design two nanofluids-based optical filters for the comparison study between the proposed nanofluid-based PV/T design with separate channels and the commonly employed double-pass channels. Therminol VP-1 is a High Temperature Fluid (HTF) suitable at high working temperature application, which gives an advantage to compare both PV/T systems at advanced solar concentration applications. Silver nanoparticles were used to absorb shorter wavelength.

The radiative transfer equation (3.7) is used to determine the intensity variation of the incoming solar radiation in the first channel as shown in Figure 3.1.

$$\frac{\partial I_\lambda}{\partial y} = -(\kappa_{n1,\lambda} + \sigma_{n1,\lambda})I_\lambda = -\beta_{n1,\lambda}I_\lambda \tag{3.25}$$

where I_λ is the spectral solar irradiance. AM1.5 Global ASTM G-173 (International standard ISO 9845-1 (Accessed in July 2015)) is used as solar spectra in the present study, and its range is from 0.28μm to 2.5μm, which has an integrated power of $992W/m^2$. $\kappa_{n1,\lambda}$, $\sigma_{n1,\lambda}$, and $\beta_{n1,\lambda}$ are the linear absorption, scattering, and extinction coefficients of the nanofluid, respectively.

Pure base fluid (such as water or VP-1) does not scatter sunlight– e.g. independent from the nanoparticles; thus, only the linear absorption coefficient for base fluid $\kappa_{bf,\lambda}$ is considered as follows (Tyagi, Phelan, & Prasher, 2009):

$$\kappa_{bf,\lambda} = \frac{4\pi k_{bf,\lambda}}{\lambda} \tag{3.26}$$

where $k_{bf,\lambda}$ is the imaginary part of the refractive index of base fluid.

Since they are independent, the extinction coefficient of the nanofluid is the sum of the absorption coefficient of the base fluid and extinction coefficient of nanoparticles (Robert A. Taylor et al., 2012):

$$\beta_{n1,\lambda} = \kappa_{bf,\lambda} + \beta_{np,\lambda} \tag{3.27}$$

where $\beta_{p,\lambda}$ is the sum of the linear absorption and scattering coefficient of nanoparticles and is defined as follow (R. A. Taylor et al., 2013):

$$\beta_{np,\lambda} = \frac{3}{2}\frac{\phi Q_{e,\lambda}}{d_{np}} \tag{3.28}$$

where $Q_{e,\lambda}$ is the extinction efficiency of the nanoparticles and is calculated using the Mie theory described in (Bohren & Huffman, 2008), see Appendix C.

Then, after extinction coefficient of the nanofluid is determined, the spectral transmittance of the nanofluid is calculated using the Beer–Lambert–Bouguer law as follows (Siegel & Howell, 1992):

$$\tau_{n1,\lambda} = \frac{I_\lambda}{I_{0,\lambda}} e^{-e_{n1}\beta_{n1,\lambda}} \tag{3.29}$$

where I_λ is the transmitted irradiation, $I_{0,\lambda}$ is the incident irradiation (AM1.5 Global [ASTM G-173]), and e_{n1} is the fluid thickness for the optical nanofluid (depth of the first channel in Figure 3.1). The extinction coefficient in equation (3.29) formally includes scattering, but, the loss of solar energy by scattering is ignored because the nanoparticles are extremely small (~10 nm).

The total transmittance of the nanofluid-based optical filter in the first channel is then calculated using equation (3.30a).

$$\tau_{n1} = \frac{\int_{0.28\mu m}^{2.5\mu m} \tau_{n1,\lambda} I_{0,\lambda} d\lambda}{\int_{0.28\mu m}^{2.5\mu m} I_{0,\lambda} d\lambda} \tag{3.30a}$$

The nanofluids based optical filters' performance is adjusted by monitoring two parameters namely; the semi-ideal filter transmittance τ_{semi} and total absorption coefficient of nanofluid α_{n1}. The semi-ideal filter transmittance is define as the amount of useful solar radiation reaching the solar cells within the boundaries of the ideal filter $\lambda_1 - \lambda_2$, and is given as follow:

$$\tau_{semi} = \frac{\int_{\lambda_1 \mu m}^{\lambda_2 \mu m} \tau_{n1,\lambda} I_{0,\lambda} d\lambda}{\int_{\lambda_1 \mu m}^{\lambda_2 \mu m} I_{0,\lambda} d\lambda} \qquad (3.30b)$$

The total absorption of nanofluid α_{n1} is determined by subtracting τ_{n1} from unity.

The proposed algorithm for τ_{n1}, τ_{semi} and α_{n1} optimization is presented in the Figure 3.2. The target of the algorithm is to maximize as much as possible both semi-ideal filter transmittance τ_{semi} and total absorption of nanofluid α_{n1}. The Matlab code for nanofluid optical properties computation is presented in Appendix D.

Input parameters; refractive index of base fluid and silver nap., solar spectrum, volume fraction and channel thickness interval, nap. radius, ideal filter interval.

$i = 1$

$i = i + 1$

$m = 1$

$m = m + 1$

$j = 1$

$j = j + 1$

$r = 1$

$r = r + 1$

Spherical Bessel and Henkel functions calculation

$\beta_{n1,\lambda}$ (Equation (3.28)), spectral absorption, $\tau_{n1,\lambda}$ (Equation (3.30)), spectral geometric absorption Equation (A.20)

Use Equation (C.7) and (C.9) for spherical Bessel function of the first and second kind

if $j == 1$ Yes

No

Mie coefficient (a_n and b_n)

Numerical integration to determine total value of the coefficient
$\alpha_{n1}, \bar{\alpha}_{n1}$
τ_{semi}, τ_{n1}

a_n (j+1)=0
b_n(j+1)=0   Yes

if $j == n_{max}$ (Equation (C.13))

No

Compute Extinction and Scattering factors

No

Yes

if $r \geq r_{max}$

No

if $j \geq n_{max}$

Yes

No

Is required condition for τ_{semi} and α_{n1} satisfied?

Compute extinction efficiency: $Q_{e,\lambda}$

Yes

end

if $i \geq i_{max}$ (length of solar spectrum array)   No

Display results

Yes

Figure 3.2: Flowchart of proposed algorithm optimization for nanofluid optical properties

3.4 Environmental impact and exergy benefit of the proposed PV/T system

One of the objective of this research work (i.e. objective No. 4) is to theoretically analyze the life cycle exergy of the proposed nanofluids-based PV/T hybrid systems with separate channels (D-1), and comparing its performance to a standard PV and three others conventional PV/T systems. The electrical and thermal performance of the analyzed solar collectors were investigated numerically.

In the framework of the present analysis, the different PV/T configurations were designed for the domestic use only -i.e. low solar concentration, under semi-realistic operating conditions.

3.4.1 Physical model of the analyzed PVT systems

The physical description of the different PV/T configurations (i.e. M-1 to M-5) are provided in this section. The solar module M-1 consists of only one PV module. The PV/T configurations M-2 and M-3 consist of one PV module and one thermal unit for the cooling purpose placed under the PV module. Water and CNTs/water nanofluid have been used as working fluids in M-2 and M-3 configurations, respectively. The PV/T hybrid configurations M-4 and M-5 consist of one PV module and two thermal units. One of the thermal unit is placed under the PV module for the cooling purpose using CNTs/water as working fluids. The second unit is placed above the PV module to act as an optical filter. The PV/T type D-1, previously described, will be analyzed for two different cases of working fluids based optical filters. Hence, water base fluid, and Ag/water nanofluids based optical filters were used as working fluids in the second thermal unit in M-4 and M-5 configurations, respectively. Figure 3.3, presents a schematic description of the four PV/T configurations M-2, M-3, M-4 and M-5. The components, their materials and geometries in the PV/T hybrid systems were taken from Ref. (T.-T. Chow & Ji, 2012). It is to be noted that the working principles of M-4 and M-5 for the present study is different from Ref. (T.-T. Chow & Ji, 2012).

Components and the specifications of all 5 collectors' configurations are presented in Table 3.7.
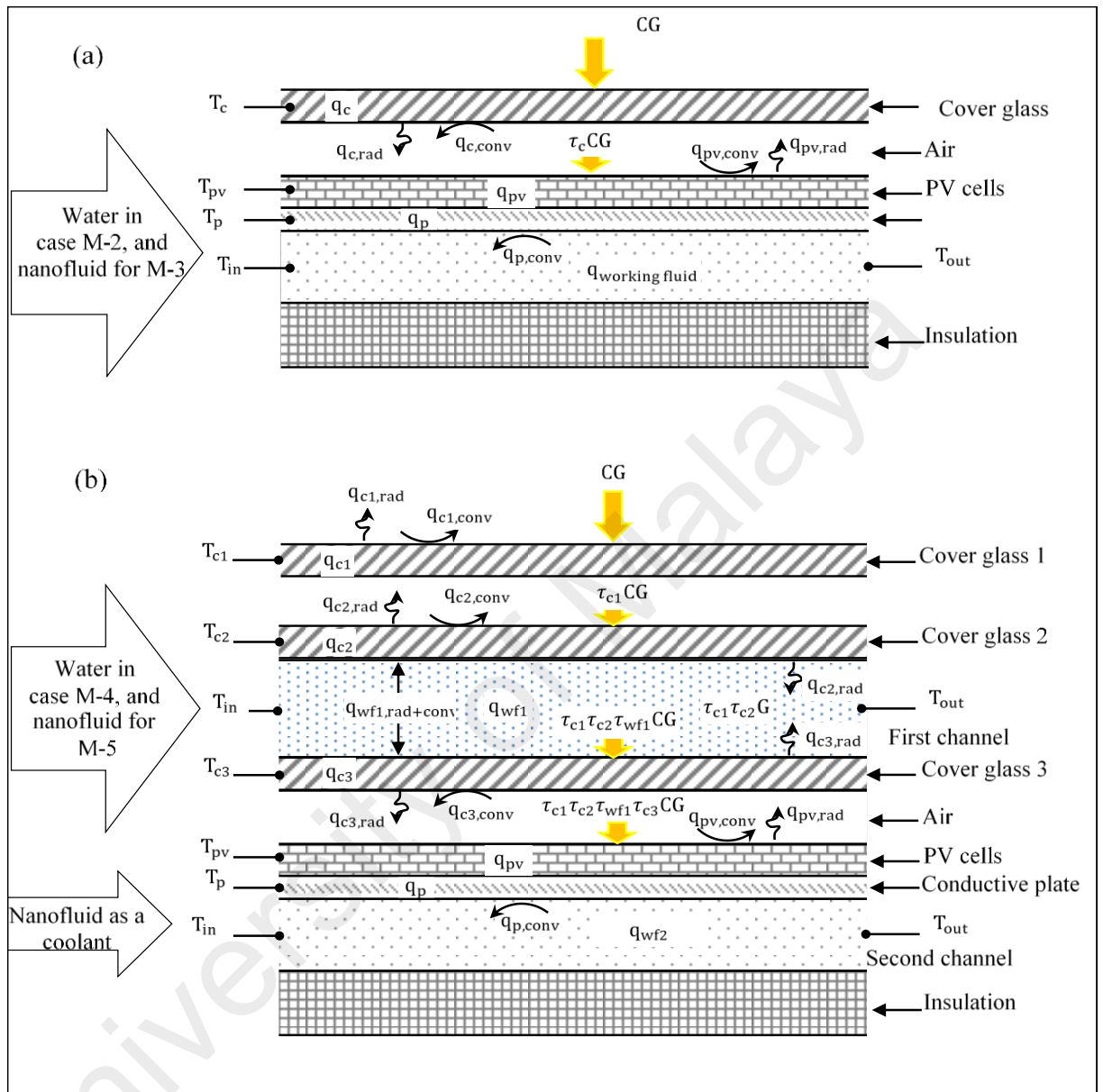
Figure 3.3: Sketch of the PV/T hybrid system for the four studied configurations; (a) M-2 and M-3 (b) M-4 and M-5

Table 3.7: Technical design data of the different solar collectors investigated in the present analysis

Elements	specifications	M-1	M-2	M-3	M-4	M-5
Glass cover	Thickness: 3mm Transmittance: 0.925 1 unit for M-2 and M-3, and 3 units for M-4 and M-5		✓	✓	✓	✓
PV cells	Si single-crystalline Efficiency: 13% Temperature coefficient β': 0.005/K	✓	✓	✓	✓	✓
Absorber	Two aluminum plates Thickness: 2 mm		✓	✓	✓	✓
Insulation	Glass wool Thickness: 30mm		✓	✓	✓	✓
Back cover	Galvanized iron Thickness: 1mm		✓	✓	✓	✓
Working fluid	Nanofluid based optical filter: Ag/water.					✓
	Nanofluid based coolant: CNTs/water			✓	✓	✓
	Water based optical filter				✓	
	Water based coolant		✓			
Storage	Storage capacity for working fluid based coolant: 150kg		✓	✓	✓	✓
	Storage capacity for working fluid based optical filter: 150kg				✓	✓
Additional elements	Solar concentrator, tracking system, structural support and electrical accessories	✓	✓	✓	✓	✓

The area of collectors (including the solar concentrator) is $= 1m^2$.

3.4.2 Mathematical modeling of the analyzed PV/T configurations

A detailed numerical model of the various PV/T configurations was developed herein which included the physical optical, thermal and electrical coupling of the system. A systematic study of the salient operational parameters and the physical geometry were investigated to determine the performance of the analyzed PV/T configurations relative to a more conventional design. Overall, the mathematical tools used to evaluate the

performance can be considered a push forward from previous physical PV/T models in the literature.

3.4.2.1 Thermal model

The thermal model used in the present analysis was derived by applying the first law of thermodynamics (i.e. the energy balance equation) for each element of the four PV/T configurations (see equation (3.12b)). The set of assumptions considered for this analysis is same than that described in Table 3.1.

A backward scheme for the spatial coordinate (x) is adopted to discretize the derived thermal energy balance equations for each element of the PV/T configurations. The resulting discretized equations corresponding to each configuration are summarized in Table 3.8.

Table 3.8: Energy balance equations of the all PV/T configurations presented in Figure 3.3

Con.	Thermal model	No.
M-1	$C \displaystyle\int_{0.28\mu m}^{2.5\mu m} G_\lambda \left(\alpha_{pv} - \eta_{el}(1 - \beta'(T_{pv} - 298))\right)d\lambda - 2 \times h_{eq(c1-am)}(T_{pv} - T_{am}) = 0$	(3.31)
M-2 and M-3	$h_{c-a}(T_{a,i} - T_{c,i}) + hr_{c-pv}(T_{pv,i} - T_{c,i}) + \alpha_c CG - h_{eq(c-am)}(T_{c,i} - T_{am}) = 0$	(3.32)
	$h_{pv-a}(T_{pv,i} - T_{a,i}) - h_{c-a}(T_{a,i} - T_{c,i}) = 0$	(3.33)
	$\tau_c C \displaystyle\int_{0.28\mu m}^{2.5\mu m} G_\lambda \left(\alpha_{pv} - \eta_{el}(1 - \beta'(T_{pv} - 298))\right)d\lambda = \dfrac{(T_{pv,i} - T_{p,i})}{R_p} + hr_{c-pv}(T_{pv,i} - T_{c,i})$	(3.34)
	$\dfrac{(T_{pv,i} - T_{p,i})}{R_p} - h_{p-n}(T_{p,i} - T_{n,i}) = 0$	(3.35)
	$h_{p-n}(T_{p,i} - T_{n,i}) - \dot{m}_n cp_n \dfrac{T_{n,i} - T_{n,i-1}}{l\,\Delta x} - h_{p-n}(T_{n,i} - T_{p2,i}) = 0$	(3.36)
	$h_{p-n}(T_{n,i} - T_{p2,i}) - \dfrac{(T_{p2,i} - T_{i,i})}{R_i} = 0$	(3.37)
	$\dfrac{(T_{p2,i} - T_{i,i})}{R_i} - \dfrac{(T_{i,i} - T_{bc,i})}{R_{bc}} = 0$	(3.38)
	$\dfrac{(T_{i,i} - T_{bc,i})}{R_{bc}} - h_{eq(bc-am)}(T_{bc} - T_{am}) = 0$	(3.39)

	$h_{c1-a}\big(T_{a,i} - T_{c1,i}\big) + hr_{c1-c2}\big(T_{c2,i} - T_{c1,i}\big) + \alpha_{c1}CG - h_{eq(c1-am)}\big(T_{c1,i} - T_{am}\big) = 0$ (3.40)

$h_{c1-a}\big(T_{a,i} - T_{c1,i}\big) + hr_{c1-c2}\big(T_{c2,i} - T_{c1,i}\big) + \alpha_{c1}CG - h_{eq(c1-am)}\big(T_{c1,i} - T_{am}\big) = 0 \qquad (3.40)$

$h_{c2-a}\big(T_{c2,i} - T_{a,i}\big) - h_{c1-a}\big(T_{a,i} - T_{c1,i}\big) = 0 \qquad (3.41)$

$h_{c2-n1}\big(T_{n1,i} - T_{c2,i}\big) + \alpha_{c2}\tau_{c1}CG - hr_{c2-c1}\big(T_{c2,i} - T_{c1,i}\big) - h_{c2-a}\big(T_{c2,i} - T_{a,i}\big) = 0 \qquad (3.42)$

$\tau_{c1}\tau_{c2}C \int_{0.28\mu m}^{2.5\mu m} \alpha_{\lambda,n1}G_\lambda \, d\lambda - h_{c2-n1}\big(T_{n1,i} - T_{c2,i}\big) - h_{c3-n1}\big(T_{n1,i} - T_{c3,i}\big) - \dot{m}_{n1}cp_{n1}\dfrac{T_{n1,i} - T_{n1,i-1}}{l\,\Delta x} = 0 \qquad (3.43)$

$h_{c3-n1}\big(T_{n1,i} - T_{c1,i}\big) + \alpha_{c3}\tau_{c1}\tau_{c2}C \int_{0.28\mu m}^{2.5\mu m} \tau_{\lambda,n1}G_\lambda d\lambda - hr_{c3-pv}\big(T_{c3,i} - T_{pv,i}\big) = 0 \qquad (3.44)$

$\tau_{c1}\tau_{c2}\tau_{c3}C\left(\alpha_{pv}\int_{0.28\mu m}^{2.5\mu m}\tau_{\lambda,n1}G_\lambda d\lambda - (1-\beta'(T_{pv}-298))\int_{0.28\mu m}^{2.5\mu m}\tau_{\lambda,n1}\eta_{el,\lambda}G_\lambda d\lambda\right) = \dfrac{(T_{pv,i}-T_{p,i})}{R_p} - hr_{c3-pv}\big(T_{c3,i}-T_{pv,i}\big) \qquad (3.45)$

M-4
and
M-5

$\dfrac{(T_{pv,i}-T_{p,i})}{R_p} - h_{p-n2}\big(T_{p,i}-T_{n2,i}\big) = 0 \qquad (3.46)$

$h_{p-n2}\big(T_{p,i}-T_{n2,i}\big) - \dot{m}_{n2}cp_{n2}\dfrac{T_{n2,i}-T_{n2,i-1}}{l\,\Delta x} - h_{p-n2}\big(T_{n2,i}-T_{p2,i}\big) = 0 \qquad (3.47)$

$h_{p-n2}\big(T_{n2,i}-T_{p2,i}\big) - \dfrac{(T_{p2,i}-T_{i,i})}{R_i} = 0 \qquad (3.48)$

$\dfrac{(T_{p2,i}-T_{i,i})}{R_i} - \dfrac{(T_{i,i}-T_{bc,i})}{R_{bc}} = 0 \qquad (3.49)$

$\dfrac{(T_{i,i}-T_{bc,i})}{R_{bc}} - h_{eq(bc-am)}(T_{bc}-T_{am}) = 0 \qquad (3.50)$

For the configurations M-2 and M-4, the subscript "*n1*" has to be replaced by "*w*".

It has to be noted that the heat transfer correlations used for all the configurations are presented in the Appendix A. All other parameters and coefficients involved in solving equations (3.31) to (3.50) are presented in Table 3.9.

Table 3.9: Parameters and coefficients involved in the equations (3.31) to (3.50)

Parameters	Value
A	$1m^2$
l	$1m$
L_c	$0.25m$
D_{h1}	$0.0198m$
D_{h2}	$0.0392m$
e_{n1}	$0.01m$
e_{n2}	$0.02m$
Δx	$0.25m$
α_c	0.05
ε_c	0.9
α_{pv}	0.945
ε_{pv}	0.9
R_p	$5.71 \times 10^{-6} K/W$
T_{am}	$298K$
v_{am}	$1\ m/s$
$\dot{m}$	$0.0104 kg/s$
ϕ_{n2}	$0.1\%, (0.21\text{wt.}\%)$

3.4.2.2 Optical properties of nanofluid optical filter for the M-5 configuration

Silver (Ag) nanoparticles suspended in water was chosen to design a nanofluid-based optical filter. Water was used to absorb the long wavelength whereas the silver nanoparticles were used to absorb shorter wavelength. For the determination of the optical properties (transmittance efficiency), methods described in section **3.3.4.2** have been adopted.

3.4.2.3 Determination of the thermal conductivity of nanofluids

In this analysis, carbon nanotube (CNT) of diameter 15nm suspended in water was chosen to be used in the second channel for the PV/T configurations M-3, M-4 and M-5. Water as a base fluid was selected due to its good performance in cooling applications.

To optimize thermal conductivity of the nanofluid used as a coolant in the second channel, the new correlation, equation (4.1), for the thermal conductivity developed herein was used.

3.4.2.4 Thermal and electrical efficiencies of the investigated PV/T configurations

Due to the interdependence of the different temperatures of the system (PV and thermal units), a coupled iterative method is required to solved simultaneously the equations (3.32) to (3.39) for M-2 and M-3, and equations (3.40) to (3.50) for M-4 and M-5.

Thus, the electrical efficiency of the PV cells for different configurations were calculated as follows:

For the configuration M-1:

$$\eta_{el} = \frac{\left(1 - \beta'(T_{pv} - 298)\right) \int_{0.28}^{2.5\mu m} \eta_{0,\lambda} G_\lambda d\lambda}{G} \tag{3.51}$$

For the configuration M-2 and M-3:

$$\eta_{el} = \frac{\tau_{c1} \left(1 - \beta'(T_{pv} - 298)\right) \int_{0.28}^{2.5\mu m} \eta_{0,\lambda} G_\lambda d\lambda}{G} \tag{3.52}$$

For the configuration M-4 and M-5:

$$\eta_{el} = \frac{\tau_{c1}\tau_{c2}\tau_{c3} \left(1 - \beta'(T_{pv} - 298)\right) \int_{0.28}^{2.5\mu m} \tau_{n1,\lambda}\eta_{0,\lambda} G_\lambda d\lambda}{G} \tag{3.53}$$

For the configuration M-4, the subscript "*n1*" has to be replaced by "*w*".

The numerator in equations (3.51), (3.52) and (3.53) is the electricity produced by the PV cells – a parameter which takes into account the transmittance efficiencies of the cover glass τ_c, and the spectral transmittance efficiency of the nanofluid or water based optical filter; $\tau_{n1,\lambda}$ or $\tau_{w,\lambda}$ determined using equation (3.29). The fraction $\eta_{0,\lambda}$ is the spectral efficiency of the Si PV cells at 298K shown in Figure 3.4, and the quantity

$\left(1 - \beta'\left(T_{pv} - 298\right)\right)$ is a coefficient which takes into account the variation of the PV cells efficiency as function of working temperature T_{pv}, β' is the temperature coefficient equal to 0.005K^{-1}.

It has to be noted that equations (3.51), (3.52) and (3.53) are derived by the author of this thesis.
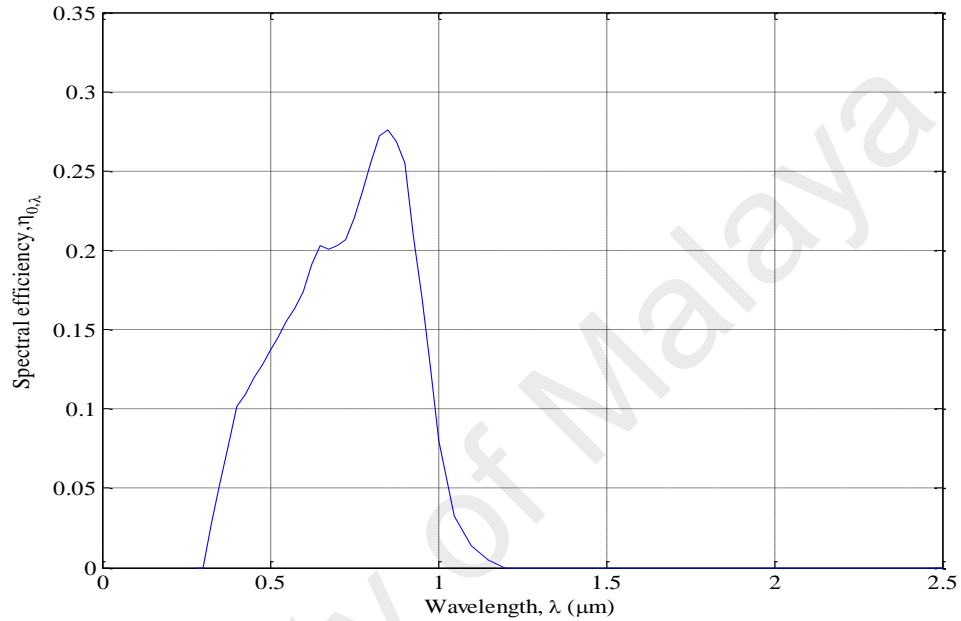
Figure 3.4: Spectral electrical efficiency of the Si PV cells at 25°C (Jing et al., 2015)

When all the unknown temperatures have been computed, the thermal efficiency of the PV/T configurations M-2 and M-3 can be calculated using equation (3.54):

$$\eta_{th} = \dot{m}_n \frac{cp_n\left(T_{n,out} - T_{n,in}\right)}{CGA} \tag{3.54}$$

The subscript "*n*" has to be replaced by "*w*" for the configuration M-2.

The overall thermal efficiencies of M-4 and M-5 are calculated using equation (3.17). The subscript "*n1*" has to be replaced by "*w*" for the configuration M-4.

3.4.2.5 Exergy efficiencies of the investigated PV/T configurations

Electrical and thermal energies are one of the useful output of a PV/T hybrid system. However, they don't have same quality grade. Electrical energy is 100% recoverable as work, and therefore has an exergy equal to its energy (Ayres, Ayres, & Martinás, 1998). Whereas, thermal energy is a low grade energy, and has exergy content less than its

energy content (Wall, 1977). Moreover, thermal exergy is low-grade exergy, while the electricity is high-grade (Lämmle, Kroyer, Fortuin, Wiese, & Hermann, 2016; Müller et al., 2011). Energy analysis method is not a suitable thermodynamic approach to evaluate the usefulness of a renewable energy device, since the energy analysis method does not differentiate the quality of energy (Petela, 2008; Zhao et al., 2011). Therefore, the concept of exergy is adopted in the present study as it includes quality aspect of energy.

The exergy efficiency of the different PV/T configurations can be calculated using the following equations:

For the configuration M-1:
$$\eta_{ex} = \eta_{el} \tag{3.55}$$

For the configurations M-2 and M-3 (T. Otanicar et al., 2010)**:**
$$\eta_{ex} = \eta_{el} + K\left(1 - \frac{T_0}{T_{n,out}}\right)\eta_{th,i} \tag{3.56}$$

For the configurations M-4 and M-5:

The exergy efficiency of the PV/T configurations M-4 and M-5 can be calculated using equation (3.18).

3.4.2.6 Concept of high-grade exergy analysis

The term $\left(1 - \frac{T_0}{T_n}\right)$ in equation (3.18) and (3.56) is the Carnot efficiency which is the maximum work extractable from the thermal energy produced by the PV/T, $\left(1 - \frac{T_0}{T_n}\right)\eta_{th}$ is the exchanged exergy, and K is the fraction of the work converted to electrical output and assumed to be 0.3 for low solar concertation (W. He et al., 2015; Niu, Yu, & Wang, 2009; Zheng, Yan, & Simpson, 2013).

Electrical energy is high grade exergy and is more valuable than the exergy of heat (i.e. $\left(1 - \frac{T_0}{T_n}\right)\eta_{th}$) which is of a low grade (Müller et al., 2011).

Therefore, as a conservative estimate of the useful amount of thermal exergy (i.e. $\left(1 - \frac{T_0}{T_n}\right)\eta_{th}$) in equations (3.18) and (3.56), the conversion factor K is needed to account

for this gradation. In engineering vocabulary, the term "$K\left(1-\frac{T_0}{T_n}\right)\eta_{th}$" is named; thermoelectric conversion rate.

In this analysis, the "high-grade thermal exergy" refers to fraction of thermal energy converted to electricity, and "high-grade exergy" refers to total exergy were produced by the various PV/T configurations.

The concept of high-grade exergy in life cycle exergy analysis is introduced for the first time in the present analysis.

3.4.3 Life cycle exergy analysis

A lot of energy is needed during the manufacturing and operational phases of the PV/T system. Life cycle exergy analysis (LCEA) approach was employed in the present study to determine the cumulative exergy consumption ($CExC$) during the construction and operation phases, and the exergy payback time (ExPBT) period.

Before applying LCEA method to the PV/T collectors, a classical LCA (life cycle assessment) method is necessary to conduct a balance of all embodied energies relative to the different stages of the life cycle. The cumulative energy spent throughout the entire life cycle of the PV/T hybrid system is the sum of embodied energy spent during the manufacturing, balance of system (BOS) and maintenance operation. We assume that the manufacturing zone is quite close to the installation area, therefore the embodied energy due to the transportation was neglected. Moreover, during the operation phase, the energy needed for the maintenance operation is supposed to be supplied by the collectors, hence the embodied energy related to the operation phase is neglected as well.

In order to assess the cumulative energy consumption, the elements constituting the PV/T hybrid systems were assumed of the same material of the PV/T system in reference (T.-T. Chow & Ji, 2012). Table 3.10 presents the resulting cumulative energy for all configurations of the PV/T system.

Table 3.10: Cumulative energy use in different PV/T configurations

Elements		Embodied energy index (MJ/kg)	M-1		M-2		M-3		M-4		M-5	
			Weight (kg)	Energy (kWh)	Weight (kg)	Energy (kWh)	Weight (kg)	Energy (kWh)	Weight (kg)	Energy (kWh)	Weight (kg)	Energy (kWh)
Solar concentrator and tracking system		Estimated from (Cellura, Grippaldi, Brano, Longo, & Mistretta, 2011)	−	504.7	−	504.7	−	504.7	−	504.7	−	504.7
Glass cover		19.7	−	0	7.52	41.15	7.52	41.15	22.56	123.45	22.56	123.45
PV cells		3514[a] (T.-T. Chow & Ji, 2012)	1[a]	976.1	1[a]	976.1	1[a]	976.1	1[a]	976.1	1[a]	976.1
Absorber		219	−	0	10.8	657	10.8	657	10.8	657	10.8	657
Insulation		31.7	−	0	0.9	7.92	0.9	7.92	0.9	7.92	0.9	7.92
Back cover		32.6 (Varun, Sharma, Shree, & Nautiyal, 2012)	−	0	7.85	71	7.85	71	7.85	71	7.85	71
Nanoparticles	Ag	11480 (Kück et al., 2011)	−	0	−	0	−	0	−	0	0.016	51
	CNT	900 (H. C. Kim & Fthenakis, 2013)	−	0	−	0	0.324	81	0.324	81	0.324	81
BOS	Structural support	604[a] (B. Agrawal & Tiwari, 2011)	1[a]	168	1[a]	168	1[a]	168	1[a]	168	1[a]	168
	Inverter + wiring	5% of PV panel (T.-T. Chow & Ji, 2012)	−	48.8	−	48.8	−	48.8	−	48.8	−	48.8
	Storage system (WF[b])	85.6 (T.-T. Chow & Ji, 2012)	−	0	14	333	14	333	28	666	28	666
	Lead-acid Battery	1.19[c] (B. Agrawal & Tiwari, 2011)	−	1773	−	2760	−	2805	−	3630	−	3870
Total				3471		5568		5694		6934		7225

[a] MJ/m^2.

[b] Working fluid.

[c] MJ/Wh$_e$.

70

Embodied energy presented in Table 3.10 is the primary thermal energy. It can be seen that the greater portion of the consumed energy is attributed to the lead acid batteries and PV cells. It has to be noted that the embodied energy due the replacement of battery for every 5 years has also been taken into account.

After obtaining the cumulative energy of the PV/T configuration system using the LCA method, the second step is to switch to LCEA method to assess the cumulative exergetic consumption of the PV/T configurations. In order to do this, the total embodied energy of the system is converted into primary electrical energy assuming a conversion factor of 0.36. This factor presents the output efficiency of a coal power plant (Schivley, Ingwersen, Marriott, Hawkins, & Skone, 2015). It has to be reminded that the exergy content of electricity is essentially 100% of its energy content (Ayres et al., 1998). That is, the cumulative exergy consumption ($CExC$) and primary electrical energy values become identical.

3.4.3.1 Exergy payback time

In order to ascertain the profitability and sustainability of the nanofluid-based PV/T collectors, exergy payback time (ExPBT) has to be estimated. ExPBT can be defined as the time period after which the real economic benefit commences.

In other words, ExPBT is the period of time during which the produced exergy compensates the amount of cumulative exergy spent, and determined using equation (3.57):

$$ExPBT = \frac{CExC}{E} \tag{3.57}$$

where E is the annual exergy produced by the PV/T hybrid system, and calculated using the following proposed equation (3.58);

$$E = \int_0^{365} \eta_{ex} \eta_s Ce_s \, dt \tag{3.58}$$

where $\eta_{ex}, \eta_s, C, e_s$ and t are respectively; the exergetic efficiency of the PV/T calculated using equations (3.18), (3.55) and (3.56), the exergy factor of solar radiation equal to 0.93 (Joshi, Dincer, & Reddy, 2009; Koroneos & Stylos, 2014), the solar concentration, the solar energy received during 4 hours under radiation intensity equal to 992W/m^2, the number of day.

In this study, the LCEA analysis is scaled by the yearly average daily solar irradiance – e.g. for South Malaysia ~4 kWh m^{-2}day^{-1}.

The ExPBT was calculated assuming a lifetime cycle of 25 years for all PV/T configurations.

3.4.3.2 Profitability exergetic index

A new tool for ranking the different PV/T configurations has been introduced in the present study. The profitability exergetic index (PExI) that evaluates the ratio of the exergetic benefit to the exergetic investment. In other words, PExI is the inverse of ExPBT and determined using equation (3.59):

$$PExI(\%) = \frac{1}{ExPBT} \times 100 \tag{3.59}$$

3.4.3.3 Life cycle environmental analysis

Before a new energy technology is completely put into service, its environmental superiority over the competing options should be asserted by assessing its consumption levels of energy throughout its entire life cycle (T.-T. Chow & Ji, 2012). Generally, the energy usage during the manufacturing phase of the PV/T hybrid system is derived from fossil fuels resources (Aman et al., 2015). Consequently, GHG and emissions occur during the first phase of the life cycle of the PV/T hybrid system.

If the primary resource of energy is known, for example coal, the quantity of pollutant emitted from the power plan can be estimated using equation (3.60).

$$PE_i = CExC \cdot F_i \tag{3.60}$$

where $CExC$ is the cumulative exergy of the PV/T systems, F_i is the emission factor and defined as the quantity of a given GHG or air pollutant emitted per unit of electrical energy (g/GJ) presented in Table 3.11, i is the pollutant element.

Similarly, the reduced emission by the exergy generated from the PV/T configurations throughout the post exergy payback time period is estimated using equation (3.61);

$$PS_i = F_i(25 - ExPBT)\, E \tag{3.61}$$

In order to identify best environmental friendly configurations, the amount of pollutants released/avoided to the atmosphere are estimated based on actual emission from a hard coal power plant with an efficiency of 36% (Pulles & Appelman, 2008).

Table 3.11: Fuel-dependent emission factors (g/GJ)

Pollutant	Hard coal	Brown coal	Fuel oil	Other oil	Gas	Ref.
NO_X	292	183	195	129	93.3	European Environment Agency (Pulles & Appelman, 2008)
SO_2	765	1 361	1 350	228	0.68	
CO	89.1	89.1	15.7	15.7	14.5	
PM_{10}	1 203	3 254	16.0	1.91	0.10	

3.4.4 Stability of nanofluids

The stability of nanofluid is indeed a critical issue for nanofluid systems. As mentioned previously in Chapter 2, several researchers (Bandarra Filho et al., 2014; Chen et al., 2015; Hordy et al., 2014; Mesgari, Coulombe, Hordy, & Taylor, 2015) have put significant time/effort into achieving nanofluids which are chemically functionalized to be stable at high temperature and under UV light (both of which are important for solar nanofluids). Since this is a numerical study, it has been assumed that these advanced stabilization techniques can be used in this system and that, if necessary, the nanofluid loop could contain a component to re-sonicate the fluid during operation.

3.5 Summary

This chapter presented a detailed description of the physical model and working principle of the new design nanofluids-based PV/T system. An advanced mathematical modeling has been applied to different PV/T configurations in order to evaluate their electrical and thermal performance.

The electrical model used to evaluate the yield electrical energy of PV/T type D-1 and D-2 has been improved by introducing new empirical constants, and new equations for open-circuit voltage and voltage at the maximum power point.

The thermal conductivity of the thermal nanofluid used for cooling process is a key factor in the energy transfer occurring between the nanofluid and the PV cells, and has to be determined by using a robust numerical model. Therefore, a new correlation has been proposed to predict the thermal conductivity of all the nanofluids designed in this study. The correlation has been established using Vaschy-Buckingham theorem and derived from a large experimental database. An improved algorithm for Mie theorem has been proposed to optimize the transmittance and absorption efficiency of nanofluid based optical filter.

Finally, an explicit methodology on life cycle exergy analysis (i.e. LCEA) including environmental and exergy benefit of the proposed nanofluids-based hybrid PV/T system have been reported. The LCEA method was based on the high grade exergy concept, which is introduced for the first time in the present study.

CHAPTER 4: RESULTS AND DISCUSSION

4.1 Introduction

In this chapter, all the findings obtained from the advanced modeling and simulation conducted throughout this research work will be presented and discussed. The different results obtained all over this study can be divided into three basic categories: 1) validation results of the various theoretical models proposed in this study, 2) analysis of the output performance of the proposed nanofluids-based PV/T with separate channels compared to the conventional double pass channels PV/T systems, 3) analyzing and discussing the output results obtained from life cycle exergy approach that applied on different PV/T configurations including the proposed nanofluid-based PV/T system.

The results presented in this chapter are based on the methodology described in chapter 3.

4.2 Models validation

An accurate model guarantees a faultless prediction data, which brings the simulation close enough to the real problem. Therefore, before exploiting any mathematical models proposed herein, a validation procedure is required.

4.2.1 Correlation for nanofluids thermal conductivity validation

After a nonlinear regression analysis of the data represented in Table 3.4, coefficients and exponents of equation (3.20) have been determined. A statistical analysis has been made, and the results show that the correlation developed, equation (4.1), suits the data with a mean and standard deviations of 2.74 % and 3.63% respectively.

$$\pi_1 = 1.04 + \pi_2^{1.11} \pi_3^{0.33} \pi_4^{-1.7} \left[\frac{1}{\pi_4^{-1.7}} - \frac{262}{\pi_3^{0.33}} + \left(135 \, \pi_5^{0.23} \, \pi_6^{0.82} \, \pi_7^{-0.1} \, \pi_8^{-7} \right) \right] \tag{4.1}$$

As seen in Figure 4.1, the predicted values using the present correlation are very close to the values presented in Table 3.4. Roughly, 86% of the predicted data have been correlated within a mean deviation of $\pm5\%$, while 98% of predicted data belong to an interval of $\pm10\%$. The maximum deviation was found 11.68% for only two points, which represent 1% of the total database presented in the Table 3.4.
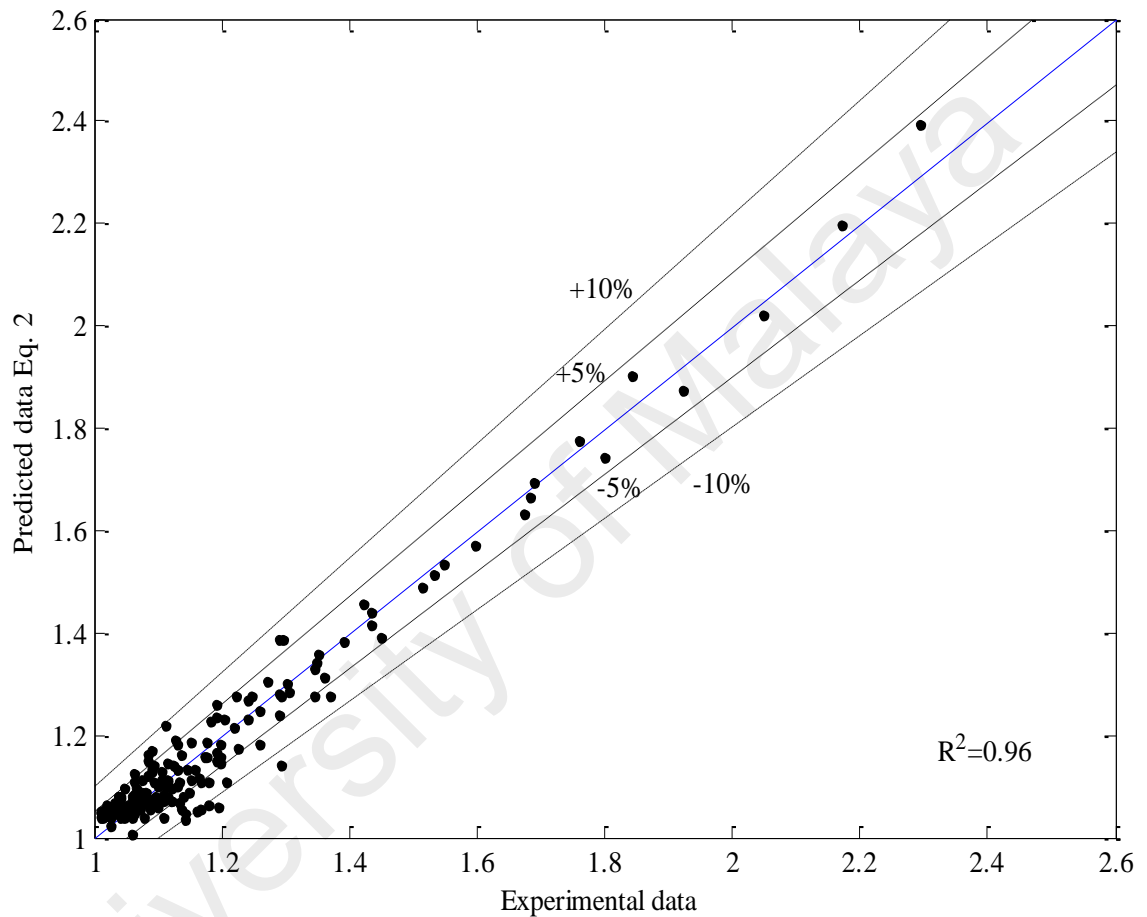
Figure 4.1: Comparison between the predicted data, equation (4.1), and experimental data from Table 3.4

In order to confirm the generalization of the proposed correlation, equation (4.1) was tested with 284 new experimental points which were not included to the database in Table 3.4. The data used for the test are taken from (H. Patel et al., 2010), and presented in Table 4.1.

Table 4.1: Experimental data of thermal conductivity of nanofluids (H. Patel et al., 2010) used for the test

Base fluid	Nanoparticles	Size (nm)	Volume fraction (%)	Temperature (°C)	Number of data
Water	Al_2O_3	$11 - 150$	$0.5 - 3$	$20 - 50$	94
	CuO	31	$0.5 - 3$		
	Cu	80	$0.1 - 1$		
	Al	80	$0.1 - 3$		
Ethylene glycol	Al_2O_3	$11 - 150$	$0.5 - 3$	$20 - 50$	104
	CuO	31	$0.5 - 3$		
	Cu	80	$0.1 - 1$		
	Al	80	$0.1 - 3$		
Water-Ethylene glycol	Al_2O_3	45	$0.5 - 3$	$20 - 50$	16
Transformer oil	Al_2O_3	45	$0.5 - 3$	$20 - 50$	70
	CuO	31	$0.5 - 3$		
	Cu	80	$0.1 - 3$		
	Al	80	$0.1 - 3$		

The present correlation found to be in excellent agreement with the 284 tested data points presented in Table 4.1 since a mean and a standard deviation was 3% and 3.89% respectively. Figure 4. 2 shows the comparison between the predicted data using equation (4.1) and test data presented in the Table 4.1. Approximately, 79% and 98.6% of the experimental data, used for the validity analysis were within $\pm 5\%$ and $\pm 10\%$ of the corresponding value obtained from equation (4.1), respectively. Only 1.4% which represents 4 points of the predicted data above a 10% of deviation, and the maximum deviation has been found to be 12.58%.
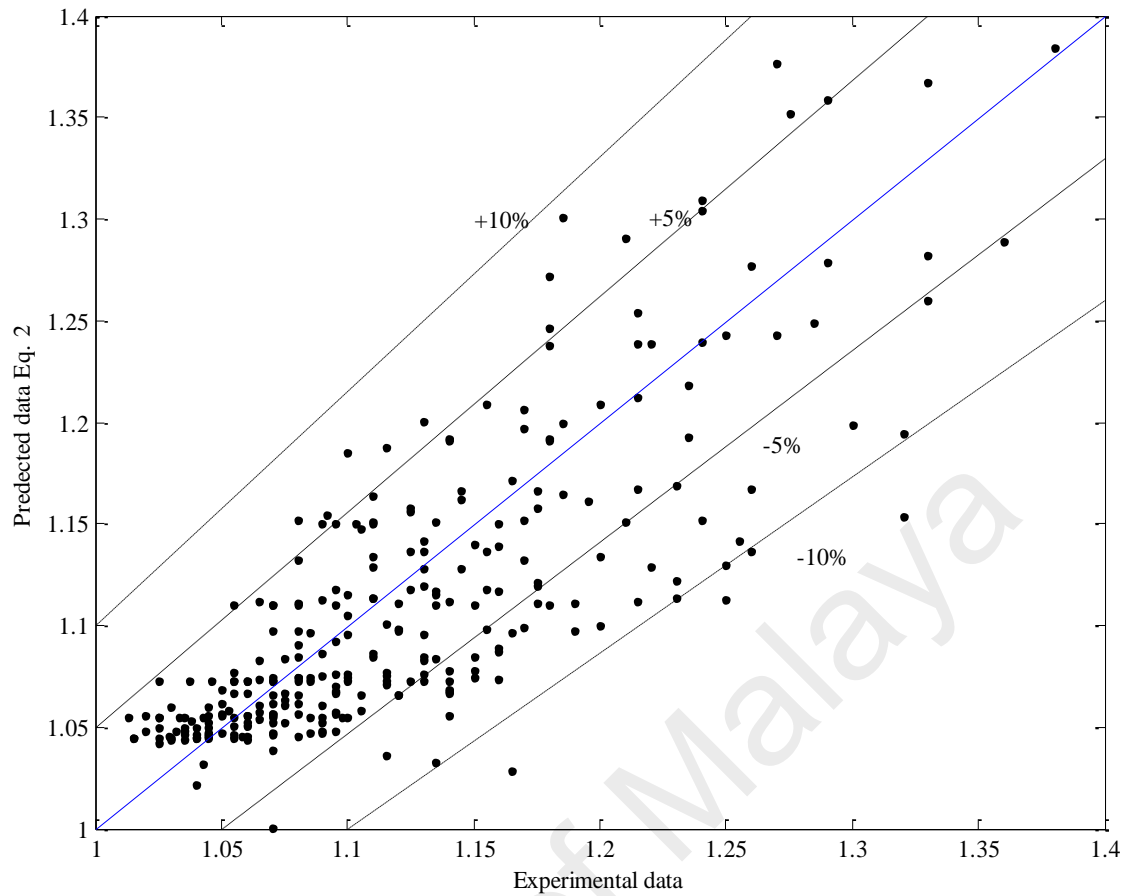
Figure 4. 2: Validity analysis of the proposed correlation

Table 4.2 gives the mean, average and standard deviations for the present correlation compared to the 480 experimental data points mentioned in Table 3.4 and Table 4.1 as a function of base fluids.

Table 4.2: Statistical comparisons of the correlation (i.e. equation (4.1)) with the experimental results

Base fluids	Mean deviation (%)	Average deviation (%)	Standard deviation (%)	Number of data
Water	2.60	−0.19	3.42	180
Ethylene glycol	3.37	−1.44	4.10	153
Methanol	3.20	−1.61	3.80	10
Radiator coolant	1.40	+1.23	1.27	25
R141b	2.13	−2.13	2.53	4
Engine oil	4.27	−1.92	4.95	15
Therminol	3.62	+3.62	0.81	7
Transformer oil	3.23	−1.03	3.92	70
Water-EG	2.29	+1.68	2.40	16
All data	2.94	−0.61	3.79	480

It is obvious from Table 4.2 that the present correlation provides sufficiently accurate predictions with a mean deviation of 2.94% for 480 values of nanofluids thermal conductivity with the experimental data.

In order to verify the accuracy and the strength of the present correlation, the predicted values of the thermal conductivity of the nanofluids obtained from equation (4.1) were compared to other existing correlations, such as Patel et al. (2010; 2008), Corcione (2011), Prasher et al. (2005a), Vajjha and Das (2009), Chon et al. (2005), and Azmi et al. (2012). All these correlations will be applied in their ranges of applicability as well. The results are shown in Table 4.3.

Table 4.3 shows the mean deviation for the nanofluid thermal conductivity predictions obtained from equation (4.1) compared to the previous correlations cited in Table 2.2. The mean deviation has been calculated as a function of types of nanoparticles and base fluids. From Table 4.3, one can see that the present correlation is, generally, suitable for all the analyzed nanofluids, with a maximum mean deviation equal to 7.63% for the case of ethylene glycol with Fe nanoparticles. As for the other correlations, we have found that all of them are in fair agreement with the experimental data within their range of applicability.

Table 4.3: Comparison of the present model correlation with the existing correlations

Particles	Mean deviation (%)								Base fluids
	Present	Patel et al. (2010)	Corcione (2011)	Prasher et al. (2005a)	Vajjha and Das (2009)	Chon et al. (2005)	Azmi et al. (2012)	Patel et al. (2008)	
Al$_2$O$_3$	2.01	1.91	2.89	5.60	4.9	1.66	1.66	–	Water
TiO$_2$	4.96	–	1.07	–	–	–	3.38	–	
Cu	3.31	0.98	–	–	–	–	2.76	–	
CuO	3.11	1.84	1.81	3.15	5.44	–	3.22	–	
Ag	2.13	–	–	–	–	–	–	–	
Al	2.56	2.37	–	–	–	–	–	–	
CNT	4.84	–	–	–	–	–	–	7.29	
Al$_2$O$_3$	3.37	1.97	3.55	3.66	–	–	–	–	Ethylene glycol
TiO$_2$	1.16	–	5.89	–	–	–	–	–	
Cu	4.13	2.51	–	26.59	–	–	–	–	
CuO	3.73	1.72	2.64	3.44	–	–	–	–	
Fe	7.63	4.22	–	–	–	–	–	–	
Al	2.84	2.33	–	–	–	–	–	–	
CNT	3.33	–	–	–	–	–	–	11	
Al$_2$O$_3$	2.11	1.56	–	–	–	–	–	–	Methanol
SiO2	4.29	–	–	–	–	–	–	–	
Al$_2$O$_3$	1.4	4.49	–	–	–	–	–	–	RC
Al$_2$O$_3$	2.13	–	–	–	–	–	–	–	R141b
Al	3.63	2.14	–	–	–	–	–	–	Engine oil
CNT	4.14	–	–	–	–	–	–	2.35	
Cu	3.62	–	–	–	–	–	–	–	TH66
Al$_2$O$_3$	2.59	5.02	–	–	–	–	–	–	Transformer oil
CuO	2.95	1.02	–	–	–	–	–	–	
Cu	4.15	1.47	–	–	–	–	–	–	
Al	3.02	2.10	–	–	–	–	–	–	
Al$_2$O$_3$	2.29	3.48	–	–	10.02	–	–	–	Water-EG

($-$) : the correlation is not in its range of validity.

It has been observed that in the case of TiO$_2$/water, the present correlation has been found less accurate than Corcione's and Azmi's correlations, with mean deviations of 4.91%, against 1.071% for Corcione's correlation and 3.38% for Azmi's correlation. This is due to the characteristics of Azmi`s and Corcione`s correlations where they have used more databases for TiO$_2$ nanoparticles with water. However, for the case of TiO$_2$/EG, the present correlation is more precise than Corcione's correlation, with a mean deviations of 1.16% against 5.89%. Both Prasher et al. (2005a) and Vajjha and Das (2009) correlations have been found less accurate compared to the present correlation except for the case of CuO/ EG where Prasher et al. (2005a) was found slightly accurate with a mean deviation of 3.44% against 3.73% for the present correlation. The origin of the large divergence of Prasher et al. (2005a) for the case Cu/EG is due essentially to the parameter fitting 'm' in their correlation in which it has been found depended on the size and the types of the nanoparticles. One can see that Patel et al. (2010) correlation is slightly more accurate than the present correlation for the case of water, EG and transformer oil. The reason for this is the fact that the Table 4.3 includes 480 experimental data of nanofluids thermal conductivity among them 284 of the data used for the validity test of the present correlation which are taken from Patel et al. (2010) and have been used as the database to derive Patel's correlation. However, for the case of RC and water-EG, the present correlation is more accurate than Patel et al. (2010) correlation, with a mean deviation of 1.4% and 2.29% against 4.49% and 3.48% for Patel's correlation, respectively. It can be seen clearly from Table 4.3 that the range of applicability of the present correlation is wider than the remaining correlations. For example, Azmi et al. (2012) correlation was designed only for water, Corcione (2011) and Prasher et al. (2005a) for water and ethylene glycol, Patel et al. (2010) for base fluids having thermal conductivity of $0.1 - 0.7 \, \text{Wm}^{-1} \, \text{K}^{-1}$. In addition, the type of nanoparticles supported by these correlations is

limited to oxide and metallic particles while the present correlation supports CNTs particles as well. It should be noted that these correlations offer sufficiently good prediction within their range of application.

In general, for all nanofluids combinations investigated in the present work, the proposed correlation, equation (4.1), offers a mean deviation of 2.94%. It is estimated that, the present correlation is valid for nanoparticles of; $10 - 200$nm diameter, thermal conductivity of $1.2 - 419\,\mathrm{Wm^{-1}\,K^{-1}}$, nanoparticles volume fractions of $0.005 - 5\%$, base fluids having thermal conductivity of $0.08 - 0.7\,\mathrm{Wm^{-1}\,K^{-1}}$.
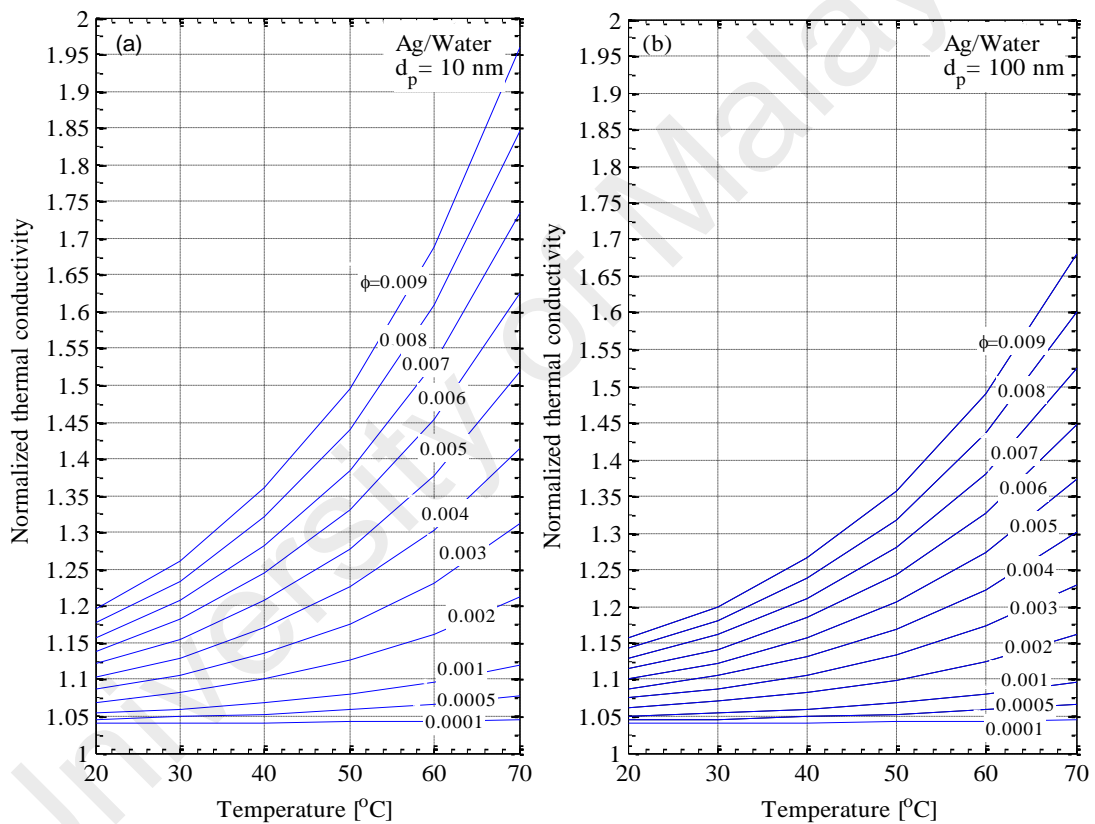
Figure 4.3: Rating chart for normalized thermal conductivity of Ag/Water nanofluid, as a function of temperature and diameter (a) 10 nm (b) 100 nm

Several experimental works show the impact of some physicals parameters on the quality of nanofluids' thermal conductivity enhancement. Diameter of nanoparticles, the volume concentration and temperature variations were found among them. Figure 4.3 and Figure 4.4 show the variation of the thermal conductivity ratio, calculated using equation (4.1),

for water with silver nanoparticles (Figure 4.3), methanol and R141b with alumina nanoparticles (Figure 4.4), as a function of the temperature, the volume fraction and the nanoparticles diameter.
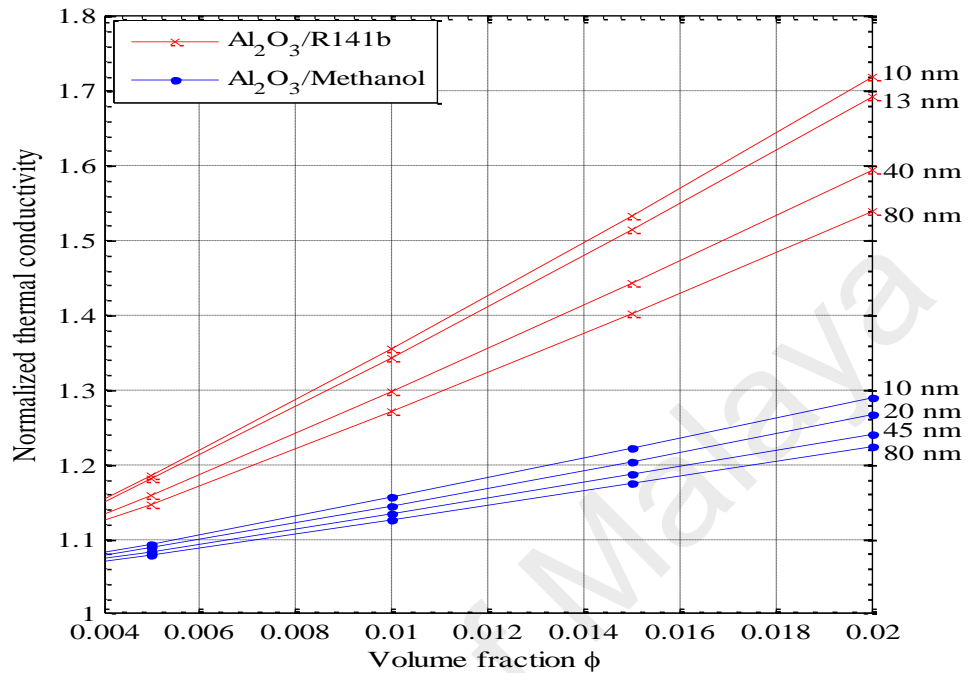
Figure 4.4: Thermal conductivity ratio as a function of volume fraction and diameter of nanoparticles at T=293 K

From Figure 4.4, it can be seen clearly that the reduction in size of nanoparticles contributed more to the enhancement of the thermal conductivity of the nanofluid, and this is due to the large random motion induced by decreasing the particle size, consequently, the convection-like effects become dominant (Jang & Choi, 2004). It can be seen from the Figure 4.3 that the thermal conductivity did not change significantly even though the diameter has been reduced for the small variation in temperature. Unlike at the high temperature, the variation of the thermal conductivity ratio is higher than at the low temperature. The explanation to this phenomenon can be given by Figure 4.5, where the thermal conductivity ratio for ethylene glycol/Cu ($d_p = 20$ nm) and Therminol 66/Cu ($d_p = 20$ nm), has been presented as a function of the dynamic viscosity of the base fluid.
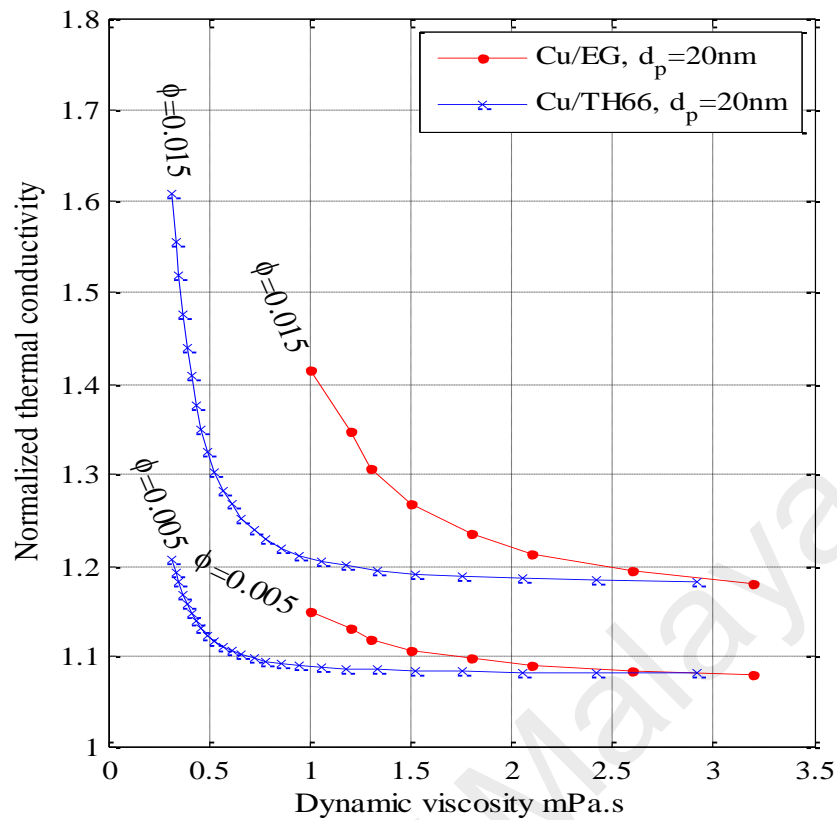
Figure 4.5: Thermal conductivity ratio as a function of dynamic viscosity

From Figure 4.5, it can been seen that the variation of the thermal conductivity ratio of the nanofluids is very sensitive at the low value of the dynamic viscosity. For any kind of fluid, it reaches its lowest value of the dynamic viscosity only when its temperature is near its state saturation. By this fundamental notion, one can understand why the thermal conductivity enhancement at the high temperature is important than at the low temperature. Therefore, decreasing the nanoparticle size as well as reducing the viscosity will play a great role in the enhancement of the thermal conductivity of the nanofluids.

It has to be noted that all the data presented in Figure 4.3, Figure 4.4 and Figure 4.5 have been generated using equation (4.1).

It can be concluded that, equation (4.1) is sufficiently validated and can be used to design and optimize nanofluids involved in the PV/T hybrid systems.

4.2.2 Electrical model validation

Before the set of equations presented in Table 3.3 can be solved, the accuracy of the electrical model, presented in the section **3.3.2**, should be verified. Using the proposed empirical constants indicated in Table 4.4, the simulation results for different outputs of Si and GaAs PV cells at 25℃ and 1 sun (C=1) are compared with experimental data reported in various studies (Green, Emery, Hishikawa, Warta, & Dunlop, 2015) and summarized in

Table *4.5*.

Table 4.4: Parameters and coefficients used in comparison study between PV/T systems type D-1 and D-2

Parameters	Value
A	$1m^2$
l	$1m$
D_{h1}	$0.04m$ for PV/T with Si; $0.095m$ with GaAs
D_{h2}	$0.0392m$
e_{n2}	$0.02m$
Δx	$0.25m$
τ_c	0.95
α_c	0.05
ε_c	0.9
α_{pv}	0.945
ε_{pv}	0.9
K'	0.03
m	1.15
n	0.96
A'	0.99 for Si, 1.1 for GaAs
k	0.8
R_p	$5.71 \times 10^{-6} K/W$
T_{am}	$298K$
v_{am}	$1 \, m/s$

As indicated in Table 4.5, the present model agrees with the experimental data.

Table 4.5: Comparison of different outputs obtained by the present model and experimental data

Cell	$\eta_{el}(\%)$		$J_{sc}(mA/cm^2)$		$V_{oc}(V)$		FF	
	Mod.	Exp.	Mod.	Exp.	Mod.	Exp.	Mod.	Exp.
Si	24.96	25.6	41.652	41.8	0.7455	0.74	0.7976	0.827
GaAs	27.37	28.8	30.17	29.68	1.1254	1.122	0.8	0.865

Moreover, it has been found that at 25℃, 117 and 92 suns, the predicted electrical efficiency for GaAs and Si cells are 30.65% and 28.8%, respectively. These results are comparable to the value of 29.1 ± 1.3% for GaAs and 27.6 ± 1.2% for Si reported by Green et al. (2015).

In addition, Figure 4.6 depicts the evolution of the electrical efficiency normalized to its standard value at 25℃ of Si and GaAs PV cells at a different temperature.
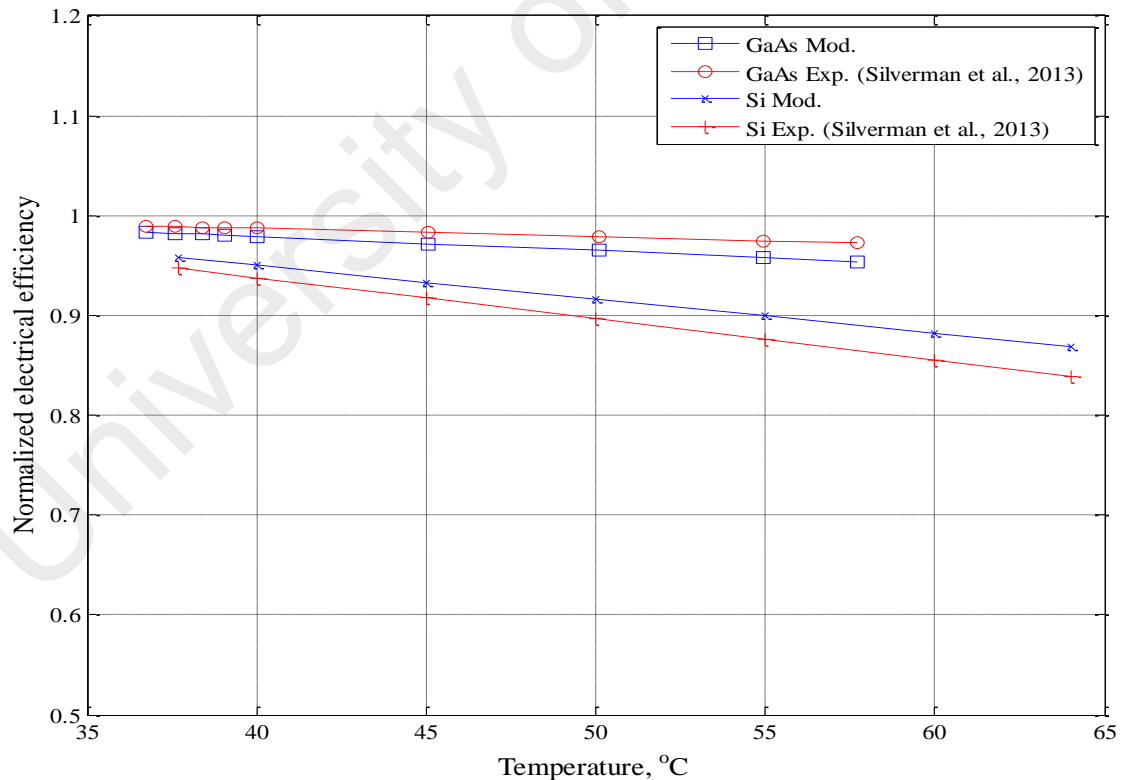
Figure 4.6: Electrical efficiency of Si and GaAs as function of temperature

Figure 4.6 shows that the predicted data obtained by the present model agree well with the experimental results. The electrical efficiency of Si cells decreases more that GaAs with increases of temperature, which is correctly predicted by the present model.

4.2.3 Thermal model validation

The detailed numerical model developed herein includes the optical, thermal and electrical coupling of the system. This systematic study of the salient operational parameters and the physical geometry to determine the performance of the different PV/T configurations represents a big step forward from previous physical PV/T models in the literature.

After researching the current nanofluid PV/T literature, it has been found that an additional experimental study conducted by M. Sardarabadi et al. (2014) that is similar to the PV/T design D-1 (after removing its second thermal unit for optical filtering) and PV/T configurations types M-2 and M-3. Therefore, we have conducted a comparative study between the results obtained by our model and those obtained experimentally by (Sardarabadi et al., 2014). We have reproduced almost all of the experimental conditions. The nanofluid's inlet temperature and wind velocity have been assumed to be 306K and 1m/s, respectively. These two parameters were ignored in their manuscript. The predicted and experimental data are presented in the Table 4.6.

Table 4.6: Numerical and experimental data comparison for thermal model validation

Working fluid	Comparison	Input exergy from the sun (W/m^2)	Thermal exergetic efficiency	Electrical efficiency	Total exergetic efficiency	Thermal exergy (W/m^2)	Electrical exergy (W/m^2)	Total exergy of the system (W/m^2)
Silica/water nanofluid 3 wt%	Experiment	871.1	1.68%	12.59%	14.27%	14.64	109.67	124.31
	Present	873.1	1.72%	12.25%	13.97%	15.02	106.94	121.96
	Deviation	0.23%	2.38%	2.7%	2.1%	2.6%	2.5%	1.9%

The comparative study reveals that the theoretical data are in good agreement with these experimental results. Aside from some slight deviation, the present numerical model can be concluded to be accurate enough for our comparative analysis.

Since there is no experimental data available for the proposed D-1 and M-5 PV/T types, our model for these can be considered as an extrapolation from the validated M-3 configuration.

4.3 Output performance of D-1 and D-2 nanofluids-based PV/T types

In the following subsections, the optical filtering performance of the optimized nanofluids for both Si and GaAs cells are presented firstly. Secondly the main findings on the comparative study between the nanofluids-based PV/T with separate and double pass channels systems (i.e. D-1 and D-2) are presented. The comparative analysis was done in terms of thermal and electrical output performance.

4.3.1 Optimized nanofluid-based optical filters

The nanofluid-based optical filters designed for both PV/T systems D-1 and D-2 corresponding to GaAs and Si PV cells are optimized to match the ideal filter suggested by Robert A. Taylor et al. (2012) for Si and Russo et al. (2014) for GaAs. To find the best volume fraction of nanoparticle and filter thickness (thickness of the first channel), the algorithm presented in Figure 3.2 is used to solve equations (3.25) to (3.30a). Since the PV/T system is expected to run at high solar concentration, a high temperature fluid is needed. Therminol VP-1 was selected to be used as a base fluid for the optical nanofluid. The optical properties of Therminol VP-1 and Ag nanoparticles, along with the real and imaginary parts of the index of refraction, were adapted from (R. Taylor, P. Phelan, T. Otanicar, R. Adrian, & R. Prasher, 2011) and (Babar & Weaver, 2015), respectively. The resulting optical properties of the optimized nanofluid-based optical filters are summarized in Table 4.7.

Table 4.7: Properties of optimized nanofluid optical filter

PV cells	Nap.	Diameter (nm)	Volume fraction (%)	Filter thickness, e_{n1} (mm)	$\tau_{semi} = \int_{\lambda_1}^{\lambda_2} \tau_{n1,\lambda}$	$\int_{0.28}^{2.5} \alpha_{n1,}$	$\int_{0.28}^{2.5} \bar{\alpha}_{n1,\lambda}$
Si	Ag	10	0.003	20	0.813	0.577	0.601
GaAs	Ag	10	0.0002	50	0.821	0.420	0.451

λ_1 and λ_2 are the boundaries of the ideal filter corresponding to each PV cell.

$\bar{\alpha}_{n1,\lambda}$ is the spectral geometric absorption coefficient for optical nanofluid. The parameter $\bar{\alpha}_{n1,\lambda}$ is involved in the calculation of radiative heat transfer coefficients; hr_{c2-n1}, hr_{c3-n1} and hr_{c2-c3} in the equations (3.4), (3.5) and (3.6), respectively. The optical nanofluid in the primary channel runs at high working temperature, therefore, it has been considered as an absorbing and emitting medium, and $\bar{\alpha}_{n1,\lambda}$ quantify the amount of emitted radiation by the nanofluid. However, the emission caused by the nanofluid could be ignored at a low temperature, thus $\bar{\alpha}_{n1,\lambda}$ equal to zero. More details on how $\bar{\alpha}_{n1,\lambda}$ has been determined are available in Appendix A.

To understand the behavior of the solar radiation spectrum within the nanofluid-based optical filter (first channel), equation (3.25) is numerically solved using the finite difference scheme. The simulation results are presented in Figure 4.7.
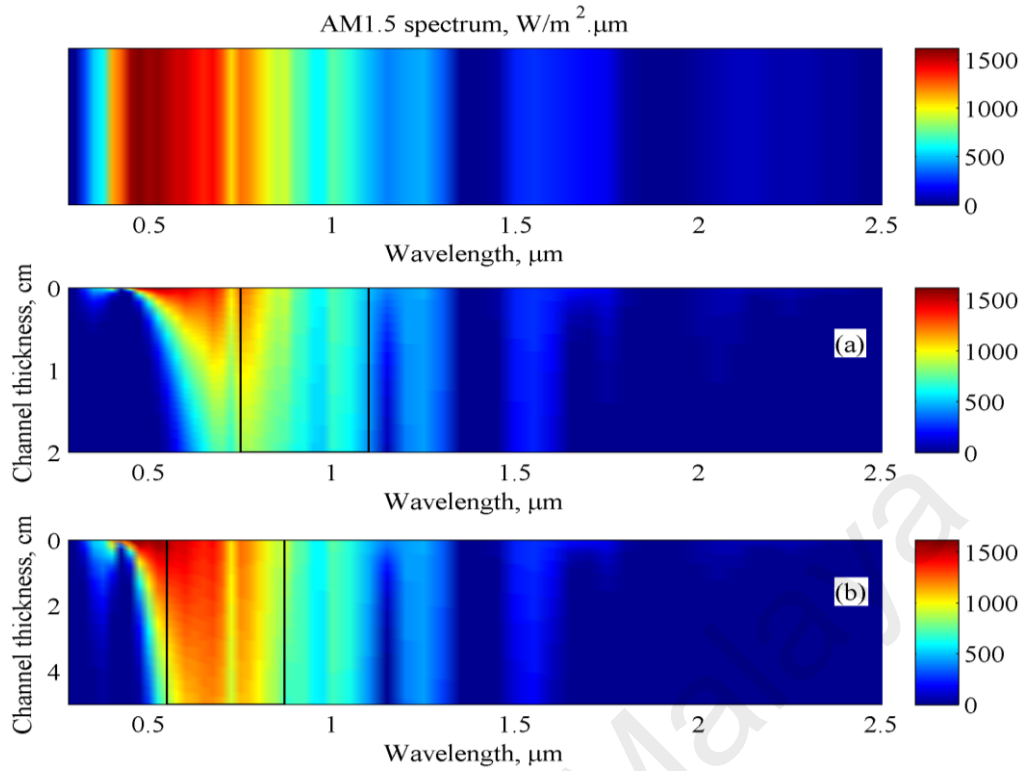
Figure 4.7: AM1.5 spectrum crossing the first channel; (a) Si, (b) GaAs. Solid line presents the ideal filter

Approximately, 81.3% and 82.1% (i.e. τ_{semi}) of the sunlight energy within the interval of the high spectral response of Si $(750\text{–}1100 \text{ nm})$ and GaAs $(550\text{–}875 \text{ nm})$ is transmitted to the PV cells, respectively.

Roughly, both nanofluid-based optical filters are able to absorb the desired UV and near UV spectra completely. Figure 4.7a shows that the UV spectrum at wavelength 500nm backward is absorbed within 1.95cm from the top in the case of the PV/T with Si, as opposed to 3.8cm for GaAs at wavelength 325nm backward, as shown in Figure 4.7b. At the transmission window corresponding to the spectral response of Si and GaAs, the solar radiation intensity is estimated to be almost transmitted to the PV cells. For instance, at wavelength of 1050nm for Si and 850nm for GaAs, the radiation intensity after crossing the path length of the filter is slightly reduced from $654\text{W/m}^2\mu\text{m}$ to $593\text{W/m}^2\mu\text{m}$, and from $894\text{W/m}^2\mu\text{m}$ to $837 \text{ W/m}^2\mu\text{m}$, respectively.

The nanofluids based optical filters absorb partially the IR spectra, and this is due to the optical properties of the base fluid (i.e. Therminol VP-1) which is not a good absorber of long wavelength. The simulation result show that ~34% of the IR spectra at 875 onward was absorbed by the optical nanofluid in the case of GaAs, as opposed to ~45% for Si at wavelength 1100nm onward.

The energy in IR region is not a useful energy for the PV cells, therefore once it is absorbed by the PV will be converted to the heat and then will be removed by the thermal nanofluid under the PV module-i.e. second channel in the PV/T type D-1.

Overall, both nanofluid-based optical filters designed for PV/T with Si and GaAs PV cells are able to absorb 57.7% and 42% of the total incident radiation, respectively.

The volume fraction of the nanoparticles and the thickness of the filter are determined precisely because the performance of the PV modules significantly depends on these two parameters. For example, increasing either of these two parameters reduces the solar radiation intensity that reaches the PV cells and leads to considerable deterioration of the PV module performance. Based on Table 4.7 and Figure 4.7, it can be concluded that both nanofluids optical filters are optimized to absorb the maximum unconvertible energy to electricity, which increases the output of the thermal unit, and to enable the transmission of the maximum convertible energy to electricity.

4.3.2 Electrical and thermal performance of PV/T collector

After the electrical and thermal models are validated, the next step is to check the electrical and thermal performance of the present PV/T design (D-1), and to compare its performance to those of the PV/T with double pass channel (D-2). For this, a MATLAB code was built to simultaneously resolve equations (3.2) to (3.9) for system D-1. Similarly, another Matlab code was built to solve equations relative to the PV/T system D-2.

Figure 4.8 shows the evolution of the electrical efficiency as a function of solar concentration. It can be seen that, when the solar concentration increases the mean electrical efficiency in double-pass channels PV/T type D-2 decreases sharply than in separate channels PV/T type D-1. For instance, at C=45 for the GaAs PV cells, the electrical efficiency is 13.8% for PV/T type D-1, whereas the rate is 4.8% for D-2. Similarly, for Si PV cells at C=30 the electrical efficiency is 9.2% for PV/T type D-1, whereas this is 0.63% for type D-2. In this case, the electrical efficiencies in PV/T type D-1 are boosted by ~8.6% compared with those in D-2.
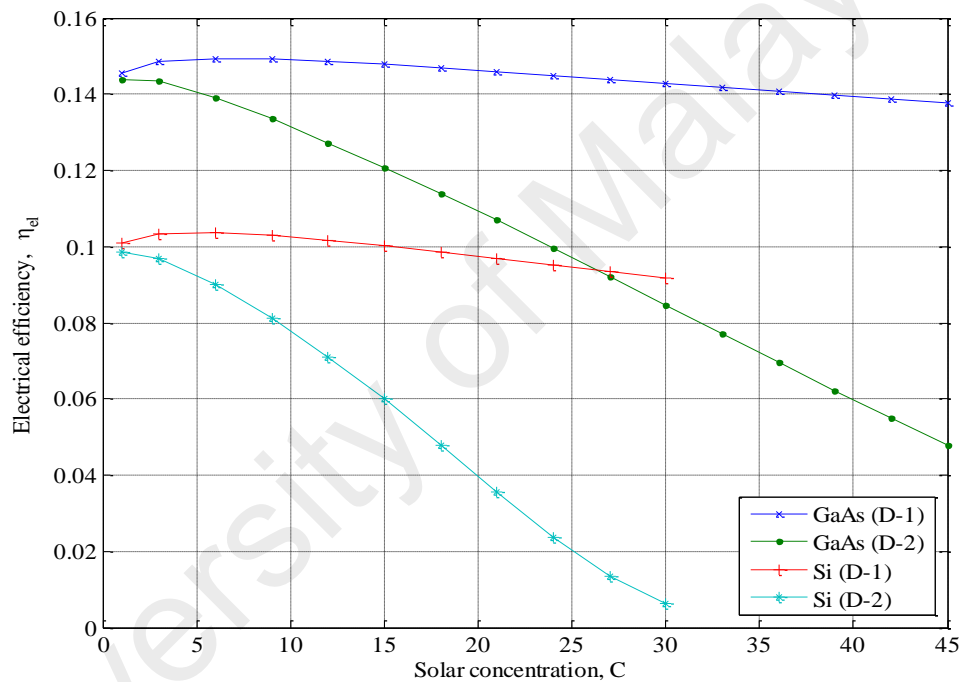
Figure 4.8: Comparison of electrical efficiency as a function of C for Si and GaAs PV cells in the cases of D-1 and D-2. The data are calculated under the following conditions: $m_{n1} = m_{n2} = 0.08kg/s$, $G = 992W/m^2$, $\phi_{n2} = 0.01$

The optimum value of the solar concentration, C, depends on the desired electrical or thermal performance. In present analysis the maximum value of C is determined so that the hottest cells of the GaAs and Si PV modules must operate with a local electrical efficiency greater or equal to 10% and 5%, respectively. The maximum attainable value of C satisfying this condition is obtained from the Figure 4.9.
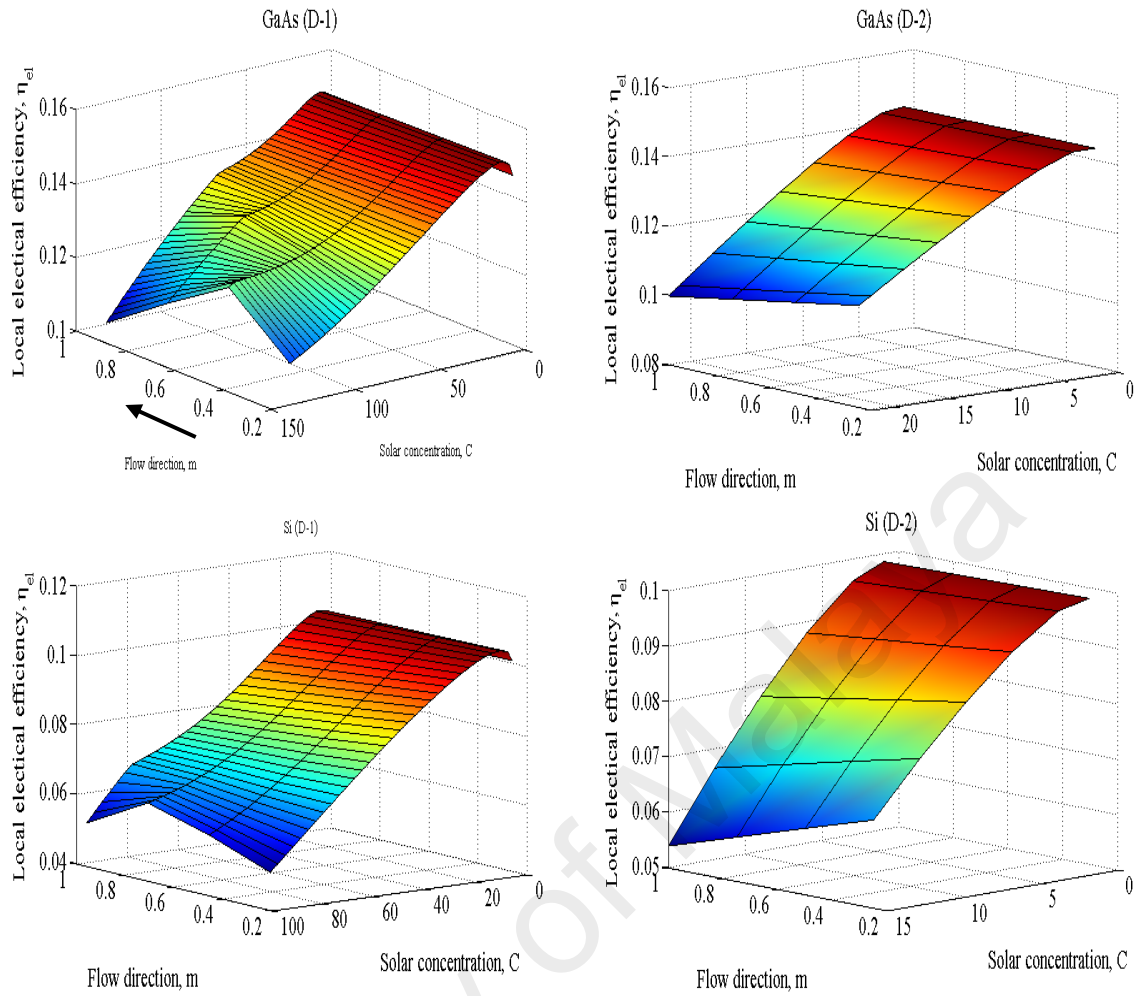
Figure 4.9: Comparison of electrical efficiency, as a function of C, along the direction of flow for Si and GaAs PV cells in the cases of D-1 and D-2. The data are calculated under the following conditions: $\eta_{el,GaAs} \geq 10\%$, $\eta_{el,Si} \geq 5\%$, $m_{n1} = m_{n2} = 0.08 kg/s$, $G = 992 W/m^2$, $\phi_{n2} = 0.01$

Figure 4.9 shows the variation of the electrical efficiency of the PV cells (Si and GaAs) along the flow direction in PV/T collector types D-1 and D-2. The electrical efficiency below C<20, in both cases, decreases when collector length increases. This phenomenon is due to the temperature of the PV panel, which increases along the direction of flow caused by the temperature of the volumetric absorber in the first channel. The present model confirms the suggestion in reference (Baig, Heasman, & Mallick, 2012) that the non-uniformity in temperature within the PV panel can cause a reduction in the PV current, which consequently leads to a reduction in the electrical efficiency.

In addition, the electrical performance of the D-2 design is lower than D-1 as solar concentration increases, and the optimum value of the solar concentration, corresponding to the minimum requirement on electrical efficiency, is much lower in D-2 compared to D-1. The simulation results presented on the Figure 4.9 shows that system D-1 can run at C=132 and that GaAs cells still deliver electricity at 10% efficiency. In contrast, the maximum value of C in system D-2 maintaining the GaAs efficiency at 10% is reached at C=22. Similarly for Si cells, in D-1 the optimum C achieves a Si cell efficiency of 5% at C=96, but this can be achieved at C = 15 for system D-2.

PV cells are highly sensitive at an elevated temperature; thus, the system in D-2 is poorly cooled compared to D-1. Although the double-pass design in D-2 helps the working fluid to increase in temperature, the higher temperature limits the PV module performance. Moreover, the working fluid in the second channel is similar to that in the first channel in the collector type D-2, which is only designed to be applied as an optical filter. Thus, it can be concluded that the low volume fraction of nanoparticles in PV/T type D-2 results in poor thermal conductivity of the nanofluid. This leads to a reduced cooling during the first pass of the nanofluid under the PV module.

In the PV/T collector type D-1, the system uses different nanofluids in two separate channels. The slow decrease in electrical efficiency in D-1 (as shown in Figure 4.8 and 4.9) is due to the high thermal conductivity of the nanofluid in the second channel, which perfectly accomplishes its cooling function.

In Figure 4.9, in the case of the D-1 system, it can be seen that at very high values of solar concentration (C >80) the electrical efficiency of the PV cells has a pick which represents an optimal value along the flow direction of the nanofluids. Indeed, in the second channel the nanofluid cools down the PV cells until it reaches a point of thermal saturation where the solar heat received by the cells is greater than that removed by the thermal nanofluid

in the second channel. In order to increase the heat removal from the solar cells, the volume fraction and/or mass flow rate of the thermal nanofluid in the second channel needed to be increased further. However, this solution has its limitations, because the increase in volume fraction and/or mass flow rate involves a significant increase in pumping power which reduces the overall efficiency of the system.

Figure 4.10 shows the variation of electrical and thermal exergy output performance for both D-1 and D-2 as a function of solar concentration.
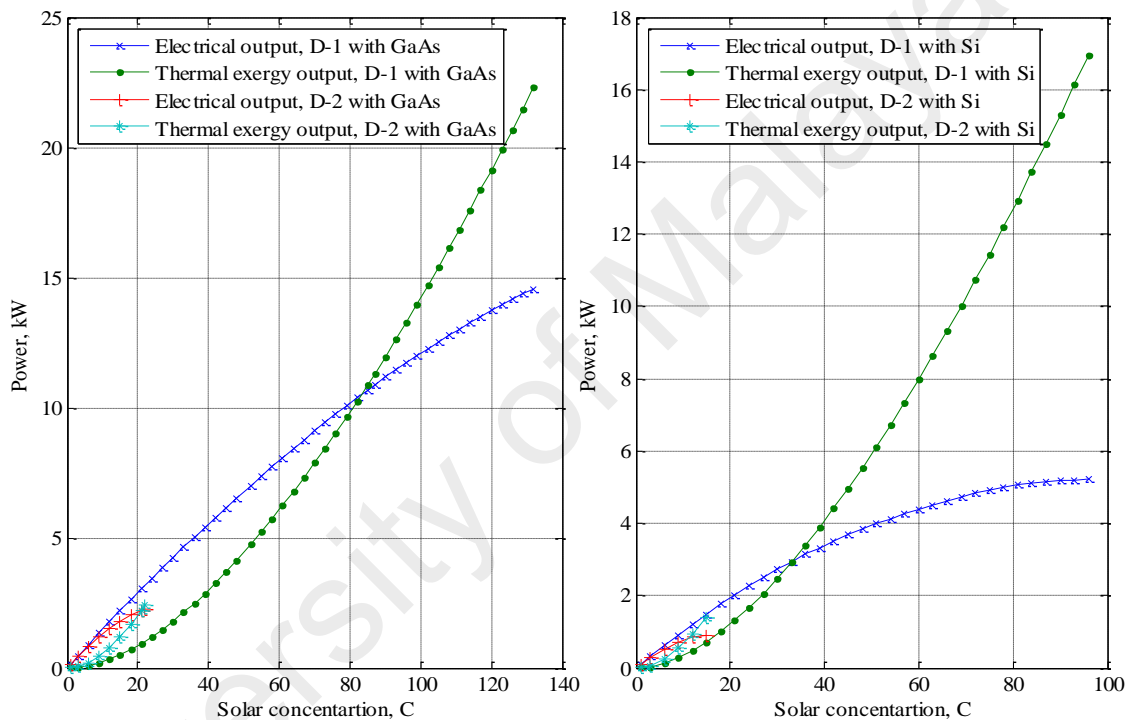
Figure 4.10: Electrical and thermal exergy output of the PV/T as a function of solar concentration of the proposed design D-1 compared with the design D-2. The data are calculated using the following parameters: : $\eta_{el,GaAs} \geq 10\%$, $\eta_{el,Si} \geq 5\%$, $m_{n1} = m_{n2} = 0.08 kg/s$, $G = 992 W/m^2$, $\phi_{n2} = 0.01$

At a lower solar concentration, the PV/T collector type D-2 outperforms D-1 in terms of thermal exergy output. Notably, the Carnot efficiency in D-2 is higher than that in D-1, but due to the minimum requirement performance imposed to the PV cells ($\eta_{el,GaAs} \geq 10\%$, $\eta_{el,Si} \geq 5\%$), the PV/T collector type D-1 can run at higher solar concentration than D-2. Consequently, the electrical and thermal exergy rates in D-2 will be significantly lower in magnitude compared with those in D-1. Overall, it is clear that the PV/T hybrid

system type D-1 is more suitable at high solar concentration based on the results shown in Figure 4.8, Figure 4.9 and Figure 4.10.

4.3.3 Role of the thermal nanofluids volume factions

To emphasize the advantage of the separate channel design and its positive effect on the electrical and thermal performances of a PV/T hybrid system at high solar concentrations, a numerical simulation is conducted by the variation of the volume fraction of the thermal nanofluid in the second channel. The maximum value of the volume fraction should not be exceed the applicably range of the equation (4.1). The volume fraction of the optical nanofluid in the first channel should remain constant because it is optimized only to act as a liquid optical filter. The simulation results are shown in Figure 4.11 and summarized in Table 4.8.
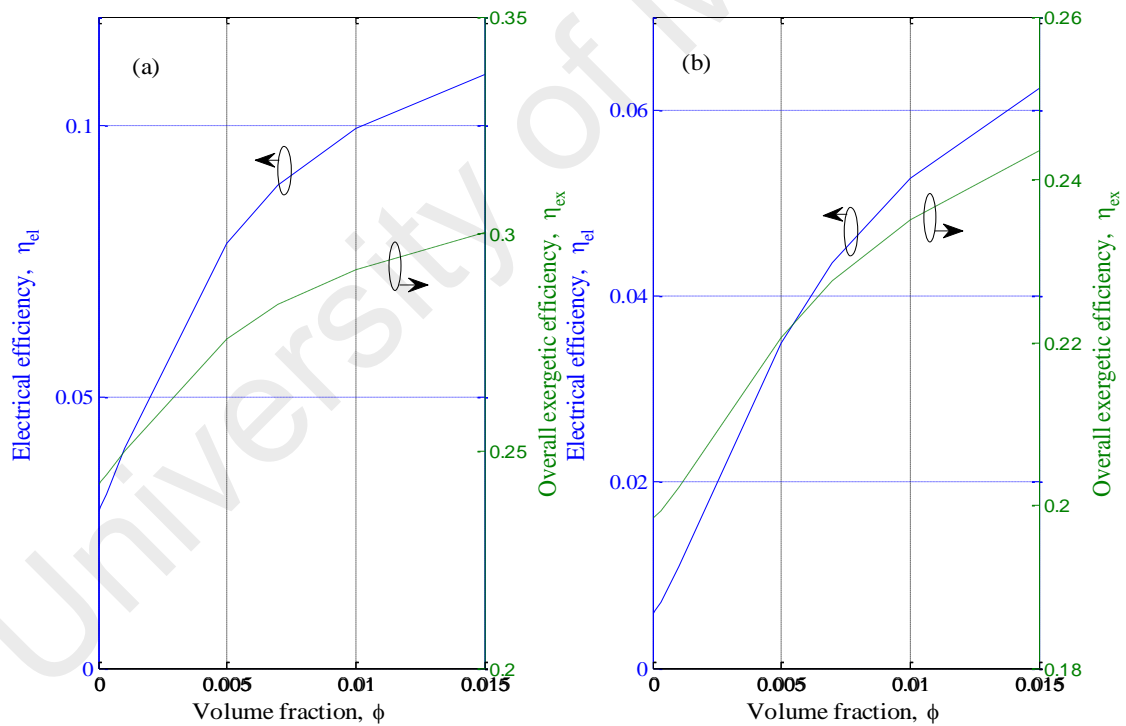
Figure 4.11: Electrical efficiency of (a) GaAs and (b) Si PV cells and overall efficiency of PV/T hybrid collector type D-1 as a function of volume fraction of the thermal nanofluid in the second channel, under the following conditions: $m_{n1} = m_{n2} = 0.08 kg/s$, $C = 160$ for GaAs and $C = 100$ for Si, $G = 992 W/m^2$

It can be seen that the increase in the volume fraction, from 0.001% to 1.5%, for the thermal nanofluid has a significant positive effect on the electrical performance

enhancement of PV/T type D-1 with GaAs PV cells (shown in Figure 4.11a) and of D-1 with Si PV cells (shown in Figure 4.11b). In this instance, the efficiency of GaAs cells has been improved from 3% to 11%, and that of Si cells from 0.6% to 6.2%. Similarly, the overall efficiency of the system D-1 with GaAs and Si cells has been improved from 24.2% to 30%, and from 19.8% to 24.4%, respectively.

Table 4.8: Influence of volume fraction of the thermal nanofluids in the second channel on different parameters of the PV/T hybrid system

Design	C	ϕ_{n2}(%)	T_{n1}(℃)	T_{n2}(℃)	T_{pv}^*(℃)	η_{th-1}	η_{th-2}	η_{el}	η_{ov}
D-1 with GaAs PV cells	160	0.001	402.7	206.7	541.0	0.502	0.386	0.029	0.242
		0.03	400.3	207.8	529.0	0.498	0.387	0.032	0.245
		0.5	378.1	214.6	365.6	0.454	0.383	0.078	0.276
		1	371.7	219.1	290.8	0.442	0.374	0.100	0.292
		1.5	369.3	225.3	254.8	0.437	0.368	0.109	0.300
D-1 with Si PV cells	100	0.001	334.6	120.6	298.2	0.601	0.325	0.006	0.198
		0.03	334.1	121.0	293.1	0.599	0.325	0.007	0.199
		0.5	328.0	122.1	218.8	0.583	0.314	0.035	0.221
		1	325.8	123.1	180.3	0.577	0.302	0.053	0.235
		1.5	324.8	125.4	159.3	0.575	0.295	0.062	0.244

[*] mean temperature.

Table 4.8 shows that the electrical efficiencies of GaAs and Si PV cells are enhanced by 9% and 5.6% by increasing the volume fraction from 0.001% to 1.5%, respectively. Moreover, this increase in volume fraction causes a sharp decrease in PV module temperature. For instance, the mean GaAs cell temperature decreases from 541℃ to 254.8℃, whereas that of Si decreases from 298.2℃ to 159.3℃. The thermal efficiency of the first and second channels decreases marginally because of the effect of the cooling process. This reduction in thermal efficiency is negligible and does not affect the overall efficiency of the system, which is enhanced by 5.8% and 4.6%, respectively. In this case, it can be concluded that the overall efficiency is more sensitive to the electrical performance than to the thermal performance.

Furthermore, at high temperature, the GaAs PV cells are more efficient than the Si PV cells, which confirms the experimental results reported in reference (Silverman et al., 2013). Therefore, GaAs is more suitable at high solar concentrations.

4.3.4 Optimal mass flow rate operating point

In addition to the thermal conductivity of the nanofluid in the second channel, the mass flow rate is a key parameter that significantly contributes to the alteration of overall efficiency. The effect of mass flow rate, and solar concentration on the variation of the performance of the PV/T system type D-1 is presented in Figure 4.12.
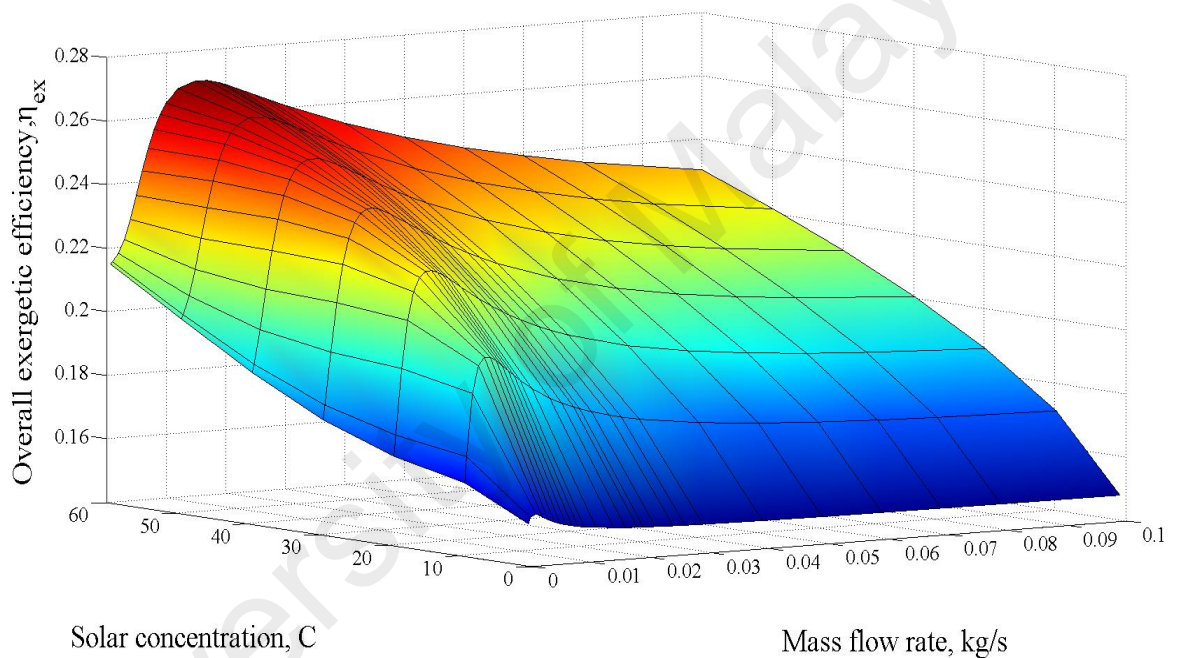
Figure 4.12: Overall efficiency of PV/T hybrid collector type D-1 with GaAs cells as a function of solar concentration and mass flow rate of the thermal nanofluid (second channel) under the following conditions: $m_{n1} = 0.08 kg/s$, $\phi_{n2} = 0.01$, $G = 992 W/m^2$

According to Figure 4.12, the overall efficiency decreases when the mass flow rate increases. This drop in overall efficiency is essentially due to the decrease in the Carnot efficiency. Based on the fundamental definition of Carnot efficiency, the latter is proportional to the temperature of the system. Increasing the mass flow rate reduces the output temperature of the working fluid, which is the principal factor that causes the reduction of overall efficiency. Each value of solar concentration has its own optimum

operating point of mass flow rate corresponding to the maximum value of overall efficiency. For example, at C=30 the optimum mass flow rate is 0.009 kg/s whereas it has been found equal to 0.015 kg/s at C=60. The peaks in Figure 4.12 define the maximum overall efficiency operating point – a point which varies when the solar concentration mass flow rate change. In real life, the operating mass flow rate depends essentially on the desired output performance of the PV/T application.

4.4 Sustainability of the proposed nanofluids-based PV/T system

At the present stage of development (e.g. a detailed design phase), it has been found that an energy analysis is enough to indicate which type of PV/T design is best. According to the simulation results reported in the previous section, the nanofluids-based PV/T system D-1 manifests a superiority in terms of electrical and thermal performance against PV/T system D-2. However, a central question can be asked by an environmentalist which is; *how green is the nanofluids-based PV/T design D-1, really?* To answer this question, the present section presents a comparative study, in terms of exergetic benefit and environmental impact, between the proposed nanofluids-based PV/T system D-1 and three others existing PV/T configurations, namely standard PV (abbreviated as M-1), and standard PV/T system with one channel under the PV cells using water and nanofluid as working fluid (abbreviated as M-2 and M-3, respectively). The nanofluids-based PV/T system D-1 will be analyzed under two configurations named as follow; M-4 with water based optical liquid filter in the upper channel, and M-5 with nanofluid based filter in the upper channel. Both configurations M-4 and M-5 use same nanofluid in the second channel under the PV cells for cooling process.

4.4.1 Nanofluids optical filters' performance for M-4 and M-5 configurations

Pure water was considered as an optical filter for M-4 configuration and Ag/water nanofluid for M-5 configuration. Water is an excellent absorber of sunlight radiation in

the infrared region (Palmer & Williams, 1974), whereas silver nanoparticles (Ag) have a good absorption property at UV spectra. The nanofluid-based optical filters was optimized in such a way so that it allows the transmittance of the maximum visible sunlight laying within the spectral response of the PV cells.

The optical properties of water and Ag nanoparticles, along with real and imaginary parts of the index of refraction were adapted from (Hale & Querry, 1973) and (Babar & Weaver, 2015), respectively. The resulting optical properties of water and optimized nanofluid-based optical filters are summarized in Table 4.9.

Table 4.9: Properties of working fluids as optical filters

Conf.	Working fluids as optical filters	Diameter of nanoparticles (nm)	Volume fraction (%)	Filter thickness, e_{n1} (mm)	$\int_{0.28}^{2.5} \tau_{n1,\lambda}$	$\int_{0.28}^{2.5} \alpha_{n1,\lambda}$
M-4	Water	-	-	10	0.788	0.212
M-5	Ag/water	10	0.001 (0.0104wt.%)	10	0.620	0.380

The intensity variation of solar radiation spectrum within the working fluid as an optical filter (first channel of M-4 and M-5) has been numerically simulated and the results are presented in Figure 4.13.
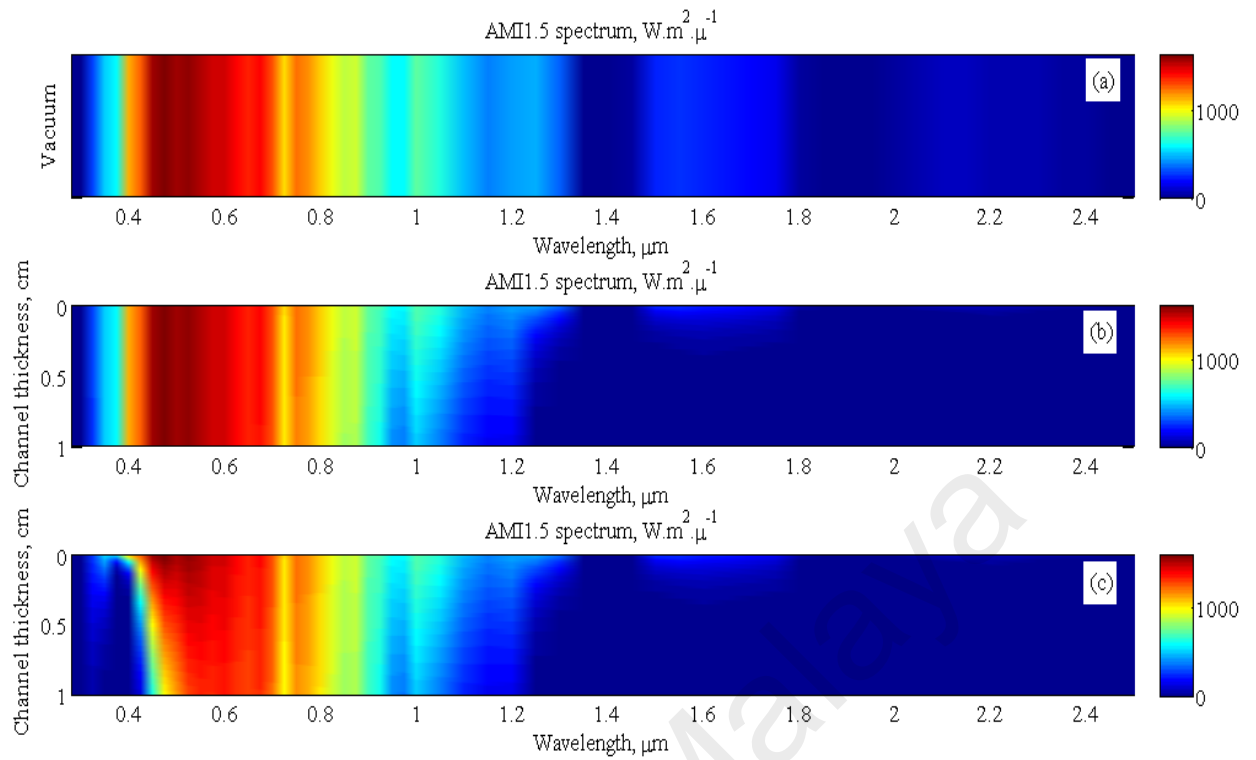
Figure 4.13: AM1.5 spectrum crossing the first channel for three distinct cases; (a) vacuum, (b) water i.e. M-4, (c) Ag nanofluid i.e. M-5

The theoretical results show that the PV cells in M-4 received more sunlight energy than the configuration M-5. Approximately, 78.8% of the sunlight energy is transmitted to the PV cells in M-4 as opposed to 62% in M-5. This implies that the electrical efficiency of the PV cells in M-4 will surpass that in M-5.

Roughly, both working fluids based optical filters are able to absorb the desired IR spectra completely as shown on Figure 4.13b and Figure 4.13c. However, water based optical filter in M-4 has been found to be a poor absorber at UV spectra, and this is due to the optical properties of the water which is not a good absorber at short wavelength. Since PV cells in M-4 received all the UV spectra, this raised PV cells temperature which leads to limit their performance at high solar concentration.

The nanofluid based optical filter in M-5 absorbs the UV spectra better than water in M-4 configuration as shown in Figure 4.13c. This is due to the ability of Ag nanoparticles to absorb the UV spectra.

Overall, both working fluid based optical filters designed for M-4 and M-5 PV/T configurations absorbed 21.2% and 38% of the total incident radiation, respectively.

4.4.2 Exergetic performance of the different PV/T configurations

Once the optical properties of working fluids as optical filters have been determined, the next step is to evaluate the electrical and exergetic performances of the configurations M-1 to M-5. For this, a MATLAB code was built to simultaneously solve the equations shown in Table 3.8. In the code, the temperature distribution along the flow direction is considered in the present analysis.

The output performances of a concentrated PV/T configurations depend on different parameters. One of this parameter is the solar concentration, C. The optimum value of the solar concentration depends on the desired output, and on the maximum allowable working fluid temperature. It is to be reminded that in the present analysis, the different PV/T configurations (i.e. M-1 to M-5) are designed for the domestic use only. Hence all the working fluids have to remain liquid, which means their working temperatures have to be less than 100℃. Therefore, the maximum solar concertation value has to obey the condition of $T_{working\ fluid} < 100$℃. This condition is valid only for the PV/T configurations M-2, M-3, M-4 and M-5. For the PV module M-1, the optimum C was determined in such a way that the electrical output has to be as maximum as possible. The optimal solar concentration C for each configurations is determined using Table 4.10.

Table 4.10: PV module and working fluid temperatures at various solar concentration

Conf.	M-1	M-2		M-3		M-4			M-5		
C	T_{pv}^*	T_{pv}^*	T_f	T_{pv}^*	T_{nf}	T_{pv}^*	T_f	T_{nf}	T_{pv}^*	T_{nf1}	T_{nf2}
1	51.5	37.6	37.7	37.4	37.7	33.2	29.2	33.4	31.5	32	31.7
2	78.5	50.7	51.0	50.2	51.0	41.5	33.9	41.9	38.0	39.3	38.5
3	103.4	63.8	64.5	63.0	64.6	49.7	38.7	50.6	44.7	46.7	45.4
4	126.4	77.0	78.1	75.7	78.3	58.0	43.6	59.4	51.3	54.1	52.4
5	147.7	90.4	91.9	88.3	92.1	66.3	48.5	68.3	58.0	61.5	59.5
6	167.5	NC	NC	NC	NC	74.6	53.4	77.3	64.7	68.9	66.8
7	186	NC	NC	NC	NC	82.9	58.5	86.3	71.4	76.4	74.1
8	203	NC	NC	NC	NC	91.2	63.6	95.5	78.1	83.8	81.4
9	220	NC	NC	NC	NC	NC	NC	NC	84.8	91.2	88.9
10	NC	NC	NC	NC	NC	NC	NC	NC	91.5	98.5	96.5

(*) mean temperature of PV module.

NC: not computed either $T_{pv} > 225°C$ or $T_{working\ fluid} > 100°C$.

Table 4.10 shows the different working temperatures for the PV module M-1 and PV/T configurations M-2 to M-5 as a function of solar concentration. It can be seen that the PV module's temperature in M-1 configuration increased sharply when the C increased compared to the other remaining configurations. On the other hand, the lowest PV modules temperature was found in M-5.

The optimum C in the PV module M-1 was found to be 4 as shown in Figure 4.14. Due to the condition imposed to C in M-2 to M-5, the optimum C was attained once the working fluids reached their near saturation temperature. The simulation results in Table 4.10 showed that the optimum C for M-2 and M-3 was found at $C = 5$, whereas $C = 8$ and 10 in M-4 and M-5, respectively.

With the help of equations (3.17), (3.18) and (3.51) to (3.56), the temperatures shown in Table 4.10 have been used to calculate the exergetic performance of the PV module M-1 and PV/T configurations M-2 to M-5.

4.4.2.1 Electrical performance

Based on the optimal solar concentration for each configurations, the variation of electrical efficiencies along with electricity produced by different PV/T configurations

are presented in Figure 4.14. It can be observed that the electrical efficiency is decreased when C is increased. However, the steepness of lines differ from each other. For example, in the standard PV-only M-1, the efficiency is decreased sharply than the remaining PV/T configurations.
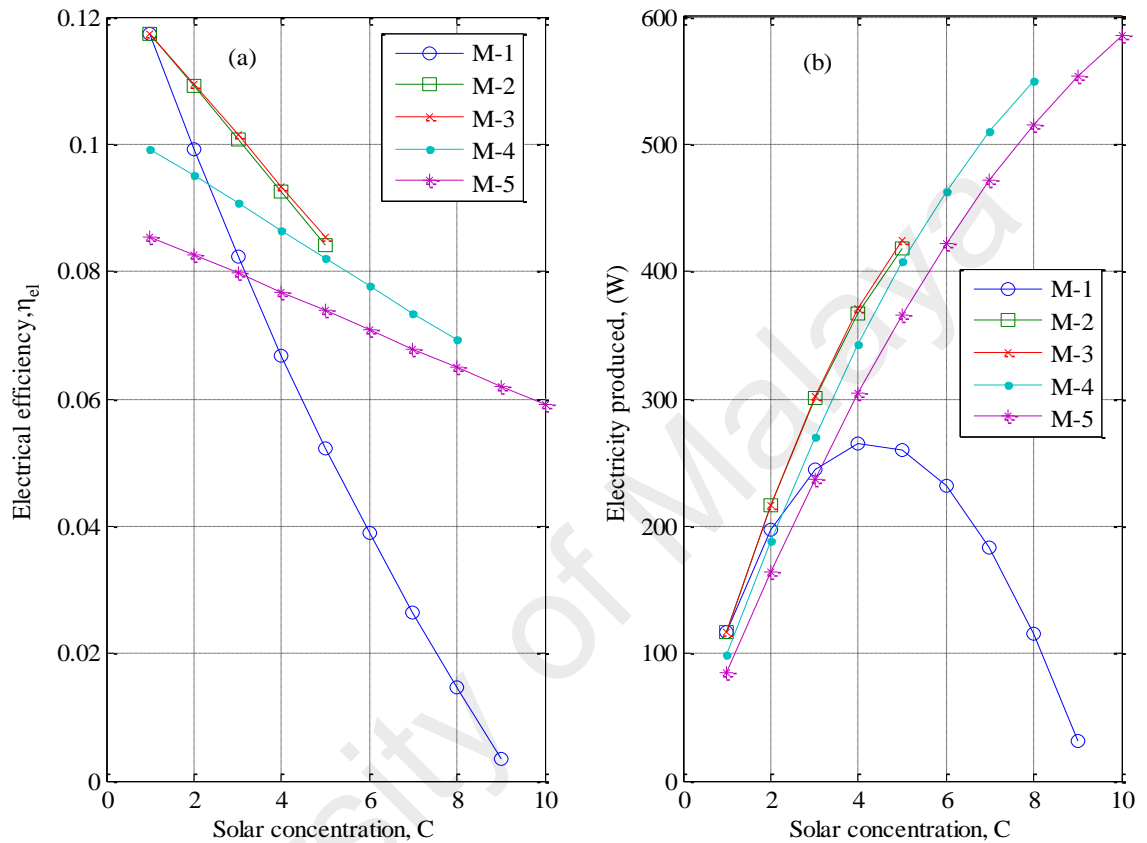
Figure 4.14: Electrical efficiency and electrical power produced by the PV modules as a function of solar concentration

It was also observed that the efficiency line in M-5 has the smallest slope compared to the rest of configurations. This is due to the difference in PV module's temperature between the configurations. Although the configurations M-1, M-2 and M-3 received the same quantity of radiation, M-2 and M-3 are more efficient in terms of electrical efficiency. This is due to the fact that in M-2 and M-3, the PV cells are cooled down by the working fluid placed under the PV module. The electrical efficiency in M-3 is slightly higher than M-2, and this is due to the advantage of the nanofluid which has higher thermal conductivity in M-3, compared to water, in M-2. The electrical efficiency in M-

4 and M-5 found to be the lowest compared to M-2 and M-3, and this is due to the working fluids as optical filters which absorbed a fraction of solar radiation before it reached the PV cells. However, PV/T configurations M-2 and M-3 cannot run with solar concentration above 5, unlike M-4 and M-5 which can run at $C = 8$ and 10 respectively. This produced more electrical power output in the configurations M-4 and M-5 than M-1, M-2 and M-3.

Figure 4.14b, presents electrical power output by the configurations M-1to M-5 as a function of solar concentrations. As predicted before, the amount of electrical power produced by M-5 exceeded all other configurations. For instance, at the optimum value of C in each collector, the electrical power produced found to be $264.7W$ in M-1, $417.9W$ in M-2, $424.3W$ in M-3, $549.6W$ in M-4 and $585.2W$ in M-5.

The proposed novel design in M-4 and M-5 was operated at higher solar concentrations than M-1, M-2 and M-3. Therefore, more electrical and thermal outputs were obtained in M-4 and M-5.

4.4.2.2 High-grade thermal exergetic performance

The high-grade thermal exergetic efficiencies of the thermal units for the various PV/T configurations and the amounts of high-grade thermal exergy produced are shown in Figure 4.15.

From the Figure 4.15a, it has been observed that, at low solar concentration, high-grade thermal exergy efficiencies of M-2 and M-3 are almost similar, and higher than M-4 and M-5. This is due to the fact that Carnot efficiencies in M-2 and M-3 are higher than M-4 and M-5. The high-grade thermal exergy efficiency in PV/T configuration M-5 outperformed than M-4, and this is due to the nanofluid based optical filter in M-5 which has more absorbing capability than the water based optical filter in M-4.
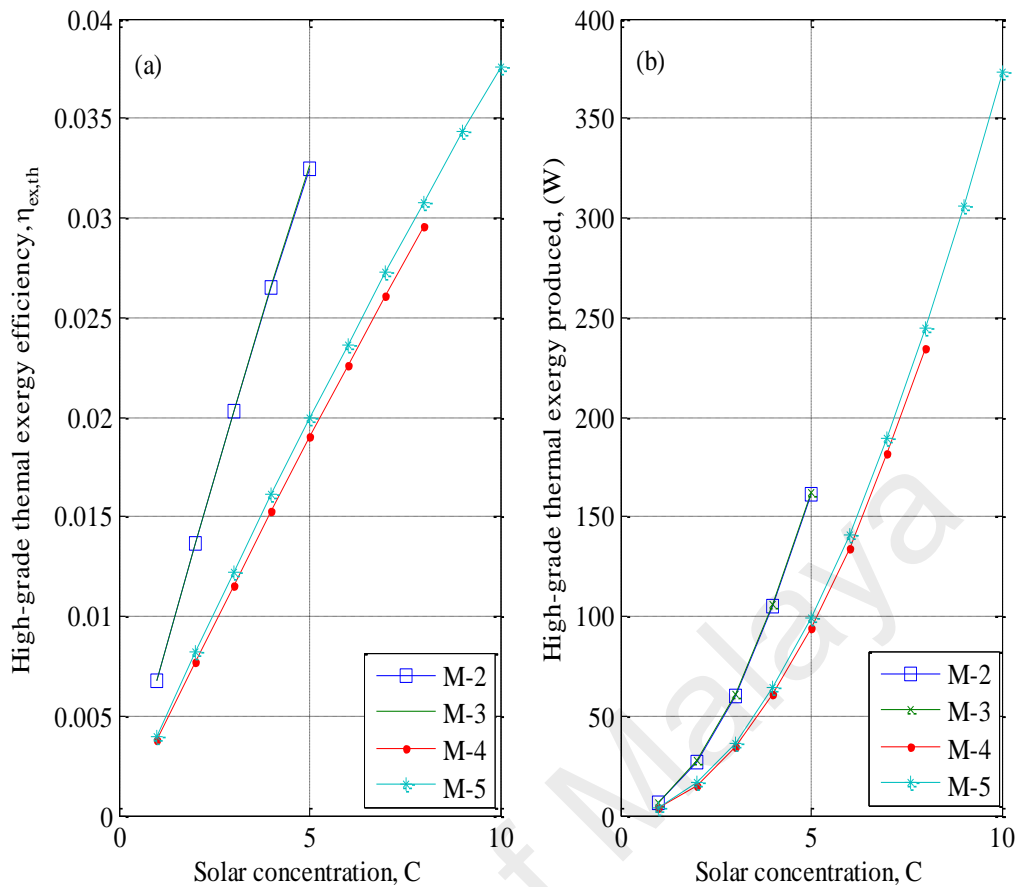
Figure 4.15: (a) High-grade thermal exergetic efficiency, and (b) high-grade thermal exergy generated by the thermal unit as a function of solar concentration

It has to be noted that the nanofluid based optical filter in M-5 absorbed UV and IR spectra, whereas in M-4 water absorbed only IR spectra.

Despite the superiority of M-2 and M-3 in terms of high-grade thermal exergetic efficiency at low solar concentrations, M-4 and M-5 dominated in terms of high-grade thermal exergy output as shown in Figure 4.15b. Again, this is due to the constraint imposed to the optimum value of C which should satisfy the condition of $T_{working\ fluid} <$ 100℃.

The quantitative rate of the high-grade thermal exergy justify the assumption on neglecting the pumping power assumed in Table 3.1. Indeed, using equation (4.2); the model for pumping power described in ref. (Routbort, Singh, Timofeeva, Yu, & France, 2011), the maximum potential pumping power was found to be ~0.4W for M-2 and M-3,

and ~0.73W for M-4 and M-5. These are certainly negligible in comparison to the minimum high-grade thermal exergy (i.e. >100W) produced by various PV/T configurations. This small value of pumping power is due to the low mass flow rate (i.e. $\dot{m}_n = 0.0104 \; kg/s$ for all configurations).

$$P_{shaft} = \frac{\dot{m}_n}{\rho_n} \frac{\left[\rho_n gh + 2\rho_n V_n^2 \left(\frac{L}{d}\right) f + \sum_i K_i \left(\frac{1}{2}\right) \rho_n V_{i,n}^2 \right]}{\eta} \tag{4.2}$$

It should be noted that a marginally increased viscosity of the nanofluids does not significantly alter this fact, since the volume fraction of the thermal nanofluid is $\phi_{n2} <$ 0.001 and that optical nanofluid is $\phi_{n1} < 0.00001$.

This is in agreement with several researchers who have conducted numerical and experimental studies on heat exchangers and solar collectors using nanofluids as their working fluids. That is, if the volume fraction and mass flow rate are both small, the pumping power is insignificant. The Table 4.11 summarizes some of these works.

Table 4.11: Nanofluid system pumping power examples reported from the literature

Authors	Type of study	Volume fraction	Mass flow rate (Kg/s)	Re	Pumping power (W)	Remarks
A. Radwan et al. (2016)	Mod.	2-4%	-	laminar flow	0.11-1.2	The power net is a round 150W
Z. Said et al. (2015)	Exp.	0.02-0.035%	0.0167-0.066	laminar flow	0.01-0.15	Almost negligible effect in the pumping power and pressure drop.
Z. Said et al.(2013)	Mod.	0.02-0.09%	0.017-0.05	laminar flow	0.01-0.1	Almost negligible.
M. Faizal et al. (2015)	Exp.	0.2-0.4%	0.0167-0.05	laminar flow	Negligible	Insignificant impact on the effective efficiency of the system.
Z. Xu et al. (2014)	Mod.	0-4%	-	Turbulent	<1W	The Pumping power to electrical output ratio equal to 0.035.
RA Taylor et al. (2011)	Exp.	< 0.001%	10^{-4}	Laminar	Negligible	Pumping power from frictional losses was found less than 1% of the power plant's electrical output.

4.4.2.3 High-grade exergetic performance

Overall efficiency and the total daily exergy produced (i.e. high-grade exergy) by the different PV/T configurations as a function of C are presented in Figure 4.16.
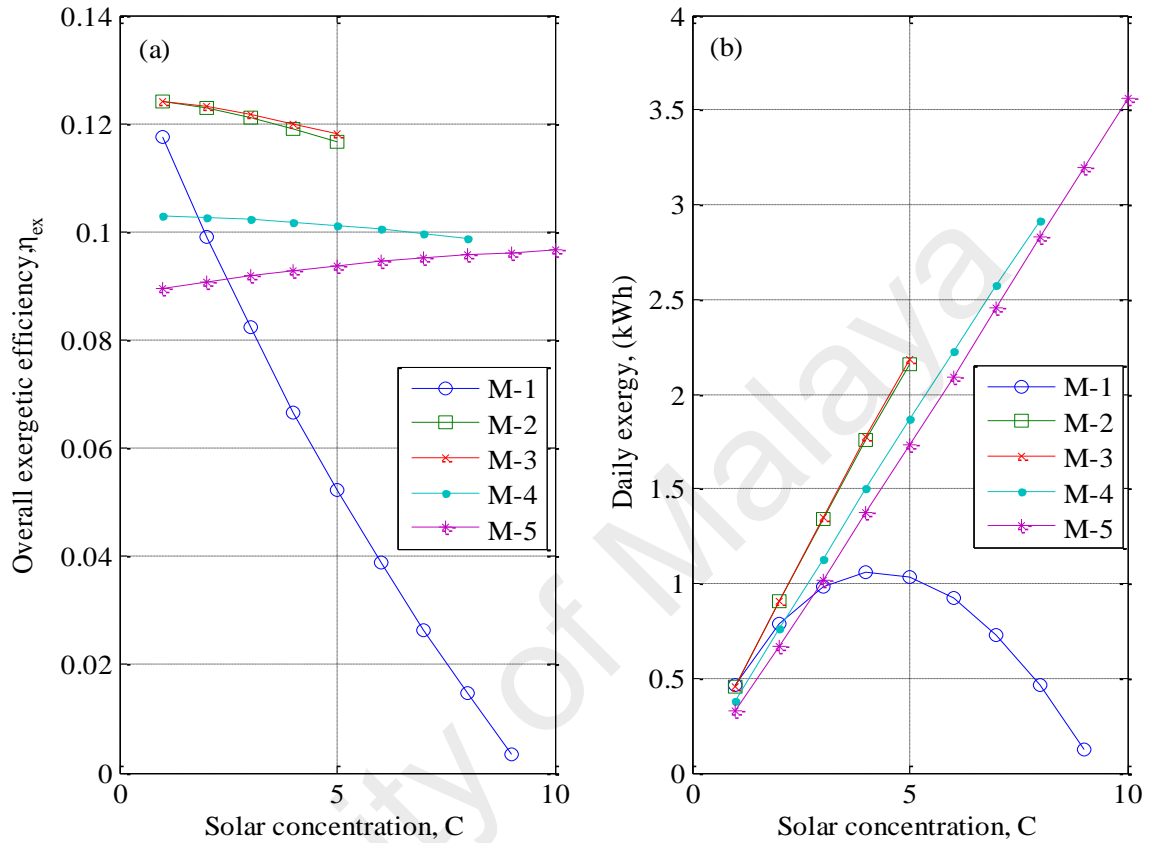
Figure 4.16: (a) Overall efficiency, and (b) daily exergy produced by the corresponding collector as a function of solar concentration

The amount of exergy shown in Figure 4.16b is the combination of electricity and high-grade thermal exergy produced daily during 4 operating hours under a solar radiation flux of 992W/m². It has been clearly observed that M-5 PV/T configuration outperformed than all other configurations in terms of total yield exergy. For instance, at the optimum operating point, M-5 produced $3.56kWh$ per day, while M-4, M-3, M-2 and M-1 produced respectively; $2.92kWh$, $2.18\ kWh$, $2.15kWh$ and $1.06\ kWh$.

The amount of produced exergy is a key factor in the LCEA method in order to determine the sustainability and ecological impact on the ecosystem of each configuration investigated in the present work.

109

4.4.3 Exergy benefit and exergy payback time

Once the output performance of each configuration is evaluated, then the determination of the necessary time to payback the exergetic investment of each configuration is needed. The exergetic investment refers to the cumulative exergy consumption ($CExC$). All the LCEA output parameters have been determined at the optimum operating point and presented in Table 4.12.

Table 4.12: ExPBT and exergy savings comparison for the different PV/T configurations

Model	Exergy consumed (kWh/m^2)	C	η_{ex} (%)	Annual produced Exergy (kWh/ m^2)	ExPBT (years)	Profitability exergetic index (%)	Exergy savings (MWh/ m^2)
M-1	1,250	4	6.70	359	3.48	28.7	7.7
M-2	2,004	5	11.7	786.2	2.55	39.2	17.7
M-3	2,050	5	11.8	795.6	2.58	38.8	17.8
M-4	2,496	8	9.88	1065	2.34	42.7	24.1
M-5	2,601	10	9.66	1301	2	50	29.9

The LCEA revealed that the amount of energy needed to manufacture $1m^2$ of M-5 PV/T configuration was found to be 2,601 kWh, which is approximately double compared to M-1. This is evident since M-5 consist of more elements than M-1 and the rest of configurations. However, the PV/T configuration M-5 has the smallest $ExPT$, and the maximum exergy savings compared to other configurations. According to the simulation results, M-5 PV/T configuration produced 1,301 kWh of high-grade exergy annually with a payback time of 2 years and estimated to save approximately 29.9MWh of exergy throughout the period of post ExPBT. In addition, the best PEI (i.e. Profitability exergetic index) assigned to M-5 PV/T system with 50% of capital exergetic refunded in one year only against 28.7% for M-1, 39.2% for M-2, 38.8% for M-3, and 42.7% for M-4 configuration. Overall, the poorest performance in terms of exergetic benefit is attributed to the standard PV-only configuration M-1.

4.4.4 Environmental impact analysis

The environmental impact of different PV/T configurations throughout the whole life cycle period are resumed in Table 4.13. It can be seen that during the first phase of the life cycle, configuration M-1 seems to be greener than other configurations. On the other hand, configuration M-5 found to be the most pollutant during the manufacturing phase. For instance, during the manufacturing process of $1m^2$ of M-5 emits approximatively; $885kg$ of CO_2, $7.16kg$ of SO_2 and $11.3kg$ of particulate matter (PM_{10}). However, during the second phase of the life cycle, production phase, configuration M-5 outperformed compared to the other configurations in terms of pollution prevention. The simulation results demonstrated that configuration M-5 may prevent the emissions of about $448\ kg\ CO_2 eq.m^{-2}.yr^{-1}$.

Table 4.13: Environmental impact of the different PV/T configurations

Model	Pollutants									
	CO_2		SO_2		NO_x		CO		PM_{10}	
	PE_i^*	PS_i^*	PE_i^*	PS_i^*	PE_i^*	PS_i^*	PE_i^*	PS_i^*	PE_i^*	PS_i^*
M-1	426	2630	3.44	21.3	1.31	8.12	0.401	2.48	5.41	33.4
M-2	682	6007	5.52	48.6	2.11	18.5	0.642	5.66	8.67	76.4
M-3	698	6073	5.65	49.1	2.16	18.7	0.658	5.72	8.88	77.2
M-4	850	8221	6.88	66.5	2.63	25.4	0.801	7.74	10.8	105
M-5	885	10188	7.16	82.4	2.73	31.4	0.834	9.60	11.3	130

* (kg/ m^2).

According to literature review, and to the best of the author's knowledge no studies were conducted on the environmental and exergy life cycle assessment of PV/T system operated with nanofluid such as configurations M-3, M-4 and M-5. Moreover, since the M-5 configuration represents a new type of solar collector, no comparative data on the environmental and exergy life cycle assessment available in the literature. However, some of the data, reported in the literature, on CO_2 reduction rates for PV/T and CPV/T operating with conventional fluids are presented in Table 4.14, and compared to the present funding.

Table 4.14: Comparative data on CO2 reduction rates

Authors	Systems	Type of study	Embodied emissions [$kg\ CO_2eq/m^2$]	CO$_2$ avoidance rates [$kg\ CO_2eq/m^2/yr$]
Present study	CPV/T type M-2 and M-5	Mod.	691-896	271-448
Chow and Ji (2012)	PV/T with water as working fluid	Exp.	513	162
Tripanagnostopoulos, et al. (2005)	Glazed PV/T-liquid	Mod.	400	500
Cellura et al.(2011)	PTC-based CPVT	Exp.	228.1	212.6
T. Kerzmann et al. (2012)	Linear Fresnel lenses-based CPVT system	Mod.	-	10,350 $kg\ CO_2\ /yr.$
S. Agrawal et al. (2013)	Glazed hybrid PV/T module air collector	Exp.	-	1,393 (Energy analysis) 322 (Exergy analysis)

CO$_2$ avoidance rates in some of the works reported in Table 4.14 were given based on unconventional units. Therefore, they have been recalculated to a standard unit "$kg\ CO_2\ eq/m^2/yr$" to facilitate the comparison.

It has been noticed from Table 4.14 that an environmental study of a solar device based on energy analysis overestimates output parameters of the study and does not reflect the reality. For instance, according to the study reported by S. Agrawal et al. (2013), based on energy analysis they have found that their PV/T system can save 1,393 $kg\ CO_2eq/m^2/yr$ but it can save only 322 $kg\ CO_2eq/m^2/yr$ if it is based on exergy analysis.

The present analysis does not include an economic analysis. The reason this was excluded is that it is highly regional. Capital, installation, and electricity costs vary wildly between the world's locations. In addition, early stage technology is exceedingly hard to estimate since prototype costs are much different than mass production cost. Therefore, it has been

concluded that the findings of an economical analysis cannot be generalized, and it is preferable to keep the analysis focused on technical metrics.

Based on the results obtained by the LCEA method presented in both Table 4.13 and Table 4.14, configuration M-5 was ranked the top among the all PV/T configurations in terms of exergy output performance and pollution avoidance. It can be concluded that a cascade nanofluid-based PV/T system with optimized optical and thermal properties represents an enhanced technique towards harvesting more sunlight energy at high solar concentration.

4.5 Summary

The main output results of this research work are presented and discussed in this chapter. Firstly, the different mathematical models proposed to evaluate; the nanofluid thermal conductivity, electrical and thermal performance of the proposed PV/T hybrid systems have been validated against experimental results. The optical efficiency including transmittance and absorption of the optimized optical nanofluid for optical filtering have been analyzed and discussed. Next, thermal and electrical performance of the proposed design of nanofluids-based PV/T hybrid system with separate channels have been compared to those of double-pass nanofluids-based PV/T system. According to obtained results the proposed PV/T with separate channels has been found more suitable at advanced solar concentration and performs better than double-pass PV/T design in terms of yield thermal and electrical energy.

Finally, the results of the life cycle exergy analysis for the proposed nanofluid-based PV/T design compared to conventional standard PV-only and PV/T technology have been reported and discussed. For all analyzed configurations the embodied exergy and emission occurring during the first phase of cycle (i.e. manufacturing period) have been reported, as well as, the amount of annually high-grade exergy produced by each

configuration. Overall, it has been found that the proposed nanofluids-based PV/T design with double nanofluids configuration (i.e. M-5) achieves high level of satisfaction in terms of yield high-grade exergy and pollution prevention comparted to all analyzed configurations.

CHAPTER 5: CONCLUSION AND RECOMMENDATIONS

5.1 Conclusion

In the present thesis, significant research effort has been devoted to establish the importance of using nanofluid as energy carrier in PV/T hybrid system. Application of such heat transfer fluid (i.e. nanofluid) in an optimized geometry design of PV/T system, as reported in the present study, helps to meet the energy needs for society with high performance conversion rate and less harmful to the environment.

In this study, a new configuration of a PV/T hybrid system using two separated nanofluids is proposed. The optical nanofluid is designed to achieve high performance of a liquid optical filter, whereas the thermal nanofluid is designed to act as a coolant fluid under the PV module. In order to optimize the thermal nanofluid a new correlation for nanofluid thermal conductivity has been developed using Vaschy-Buckingham theorem.

The major findings based on the results of the present study can be summarized as follows:

❖ A new correlation for nanofluids thermal conductivity has been developed using a wide range of experimental databases (196 points) taken from the literature. The predictions accuracy was found impeccable with a mean deviation of 2.74%. To confirm the generalization of the proposed correlation, a validation test was done to predict the thermal conductivity of 284 experimental data. The predicted data have been found in good agreement with the validation data test with a mean deviation of 3%.

The applicability and accuracy of the present correlation for wide variety of nanofluid has been verified against other correlations available in the literature. In general, we have found that the range of applicability of the present correlation is wider than the other correlations.

115

The new correlation was applied to predict the influence of particle size, volume fraction and temperature on the thermal conductivity of nanofluids and found that reduction in particle size, and increasing the volume fraction and temperature has positive effect on the thermal conductivity of nanofluids.

Due to the wide range application capability of the developed model, the proposed correlation will be a useful engineering tool for the analysis and thermal design of heat exchangers or solar thermal collectors. Therefore, the present correlation has been used to design the thermal nanofluids used as coolant in the proposed nanofluids-based PV/T systems.

❖ The improved electrical model reported in this research work has been validated against other studies before we had confidence to use the model in simulation. Since the predicted values were indeed in accordance with the data reported by other researchers, the electrical model was then able to use it for this new double fluid design/configuration.

The nanofluid-based optical filter designed for the PV/T systems with both GaAs and Si cells, absorbs practically all the desired UV and partially the IR spectra.

To highlight the advantage of the proposed nanofluids-based PV/T hybrid system with separate channels (D-1), its performance have been compared against the conventional nanofluid-based PV/T with double-pass channels (D-2) system. The results demonstrate that the electrical efficiency of GaAs (at C=45) and Si (at C=30) can be improved by ~8.6% in PV/T type D-1, compared with that in PV/T type D-2.

The simulation results prove that, at these solar concentration ratios, the PV/T with separate channels is more suitable than that with a double-pass channel.

The use of two different nanofluids gives a significant boost to the PV/T hybrid collector. Based on the results of the present study, increasing the volume fraction of the nanofluid-

based coolant, yield enhanced electrical efficiencies for the GaAs and Si PV cells by 9% and 5.6%, and overall efficiency of the system by 5.8% and 4.5%, respectively.

❖ A life cycle exergetic analysis has been carried out to evaluate the high-grade exergy and environmental impact of the proposed design nanofluid-based PV/T hybrid system, and compared its performance to a standard PV and PV/T system.

The cumulative exergies and pollutant emissions during the manufacturing phase were determined by an established method using technical data taken from the literature.

The annual high-grade exergy outputs of the analyzed PV/T configurations were determined using numerical simulation based on validated electrical and thermal models. Ag/water has been used as optical liquid filter for the proposed nanofluid-based PV/T configuration M-5 and water as liquid optical filter for M-4 configuration. It has been found that the designed optical nanofluid absorbed practically all the desired UV and the IR spectra, whereas the water based optical filter in M-4 absorbed only IR spectra.

The simulation results demonstrated that the PV/T configuration M-5 outperformed in terms of high-grade exergy output compared to the standard PV-only and conventional PV/T system.

The life cycle exergy analysis revealed that the PV/T configuration M-5 produced ~1.3 MWh/m^2 of high-grade exergy annually with the smallest exergy payback time of 2 years. This configuration estimated to save approximately ~$30MWh$ of high-grade exergy throughout the post exergy payback time (~23 years).

Although configuration M-5 PV/T system found to be the most pollutant during the manufacturing phase, it outperformed rest of the configurations during the operational phase in terms of pollution prevention. The proposed design M-5 PV/T system may prevent emissions of about $448\ kg\ CO_2eq.m^{-2}.yr^{-1}$.

Overall, the present study proposed a new approach to the efficient use of solar energy in PV/T hybrid configuration systems. A small area of nanofluid-based PV/T system may produce the amount of energy equivalent to a large area of a standard PV-only can produce. The optimized optical and thermal nanofluids-based PV/T hybrid system is a reliable solution to electrify remote off-grid regions at a low cost and to provide a potentially large supply of useful thermal energy.

5.2 Recommendations and suggestions for future work

In this research work, optimal design of new generation of PV/T hybrid system for better harvesting solar energy has been proposed. The advanced mathematical models presented in this thesis demonstrates and determines the potential for using nanofluid as coolant working fluid and liquid optical filter in concentrated photovoltaic solar energy application. It can be recommended that the proposed nanofluids-based PV/T system will be a favorable green solution to satisfy the energy demand at large scale applications such as in residential and office building, hospital, hotel, as well as the remote off-grid regions. In spite of the advanced optimization concept reported in this thesis, so far there are yet several suggestions and further developments that can be expected with this novel generation of nanofluids-based PV/T hybrid system. Therefore, the following are suggestions on which further research works would be beneficial:

i)   At the present stage of development (e.g. a detailed design phase), the author believe that a modeling analysis is enough to indicate the attractiveness in terms of electrical and thermal performance of the proposed PV/T design. However, a prototype is needed to be realized in order to experience various lasting tests, and enlarged tests will need to be carried-out before this new generation of nanofluids-based PV/T system can be introduced in commercial application.

ii) Based on life cycle exergy analysis conducted in this thesis, it is found that the proposed nanofluids-based PV/T system reduces CO_2 emission with high rate annual exergy deliverance. However, these two parameters are not enough for the full assessment of the proposed PV/T system. Therefore, an economic analysis is highly suggested to be considered in the future work based on the actual price of the prototype's components.

iii) The stability issue of the nanofluid is a key parameter in both modeling study and real life application. The present research does not report a definite solution of how to deal with the stability of nanofluid at very high working fluid temperatures. Up to date, the behavior of nanofluids at high temperature application is still not elucidated definitively by the scientific community. Therefore, more scientific research effort should be devoted to achieve long-term nanofluids' stability.

iv) Other nanofluids, their photothermal conversion efficiency, can also be investigated in order to improve the optical filtering performance of the proposed nanofluids-based PV/T system.

v) The proposed nanofluids-based PV/T hybrid system needs further analysis considering the thermal storage, and the thermoelectric conversion rate in order to increase electricity supply dependability.

vi) In this study, the nanofluid-based PV/T system was analyzed under ideal weather condition, therefore more studies, either modeling or experimental, are required considering different weather conditions in different location.

vii) Reducing the required embodied energy is very important in order to minimize emission during manufacturing phase, as well as reducing the exergy payback time which leads to long period of production phase. Therefore, optimizing the materials' compounds constituting the PV/T system will be an interesting axe of research.

REFERENCES

Abdolbaqi, M. K., Azmi, W. H., Mamat, R., Sharma, K. V., & Najafi, G. (2016). Experimental investigation of thermal conductivity and electrical conductivity of BioGlycol–water mixture based Al2O3 nanofluid. *Applied Thermal Engineering, 102*, 932-941.

Agrawal, B., & Tiwari, G. N. (2011). *Building integrated photovoltaic thermal systems: for sustainable developments* (Vol. Energy Series No.4): Royal Society of Chemistry.

Agrawal, S., & Tiwari, G. N. (2013). Enviroeconomic analysis and energy matrices of glazed hybrid photovoltaic thermal module air collector. *Solar Energy, 92*, 139-146.

Al-Shamani, A. N., Yazdi, M. H., Alghoul, M. A., Abed, A. M., Ruslan, M. H., Mat, S., & Sopian, K. (2014). Nanofluids for improved efficiency in cooling solar collectors – A review. *Renewable and Sustainable Energy Reviews, 38*(0), 348-367.

Aman, M. M., Solangi, K. H., Hossain, M. S., Badarudin, A., Jasmon, G. B., Mokhlis, H., . . . Kazi, S. N. (2015). A review of Safety, Health and Environmental (SHE) issues of solar energy system. *Renewable and Sustainable Energy Reviews, 41*, 1190-1204.

Armaroli, N., & Balzani, V. (2007). The Future of Energy Supply: Challenges and Opportunities. *Angewandte Chemie International Edition, 46*(1-2), 52-66.

Aybar, H. Ş., Sharifpur, M., Azizian, M. R., Mehrabi, M., & Meyer, J. P. (2015). A Review of Thermal Conductivity Models for Nanofluids. *Heat Transfer Engineering, 36*(13), 1085-1110.

Ayres, R. U., Ayres, L. W., & Martinás, K. (1998). Exergy, waste accounting, and life-cycle analysis. *Energy, 23*(5), 355-363.

Azari, A. (2015). Thermal conductivity modeling of water containing metal oxide nanoparticles. *Journal of Central South University, 22*(3), 1141-1145.

Azmi, W. H., Sharma, K. V., Mamat, R., Alias, A. B. S., & Misnon, I. I. (2012). Correlations for thermal conductivity and viscosity of water based nanofluids. *IOP Conference Series: Materials Science and Engineering, 36*(1), 012029.

Azmi, W. H., Sharma, K. V., Mamat, R., Najafi, G., & Mohamad, M. S. (2016). The enhancement of effective thermal conductivity and effective dynamic viscosity of nanofluids – A review. *Renewable and Sustainable Energy Reviews, 53*, 1046-1058.

Babar, S., & Weaver, J. H. (2015). Optical constants of Cu, Ag, and Au revisited. *Applied Optics, 54*(3), 477-481.

Babita, Sharma, S. K., & Mital, G. S. (2016). Preparation and evaluation of stable nanofluids for heat transfer application: A review. *Experimental Thermal and Fluid Science,* doi:http://dx.doi.org/10.1016/j.expthermflusci.2016.06.029

Bahaidarah, H. M. S., Baloch, A. A. B., & Gandhidasan, P. (2016). Uniform cooling of photovoltaic panels: A review. *Renewable and Sustainable Energy Reviews, 57,* 1520-1544.

Baig, H., Heasman, K. C., & Mallick, T. K. (2012). Non-uniform illumination in concentrating solar cells. *Renewable and Sustainable Energy Reviews, 16*(8), 5890-5909.

Bandarra Filho, E. P., Mendoza, O. S. H., Beicker, C. L. L., Menezes, A., & Wen, D. (2014). Experimental investigation of a silver nanoparticle-based direct absorption solar thermal system. *Energy Conversion and Management, 84*, 261-267.

Bashirnezhad, K., Bazri, S., Safaei, M. R., Goodarzi, M., Dahari, M., Mahian, O., . . . Wongwises, S. (2016). Viscosity of nanofluids: A review of recent experimental studies. *International Communications in Heat and Mass Transfer, 73*, 114-123.

Battisti, R., & Corrado, A. (2005). Evaluation of technical improvements of photovoltaic systems through life cycle assessment methodology. *Energy, 30*(7), 952-967.

Bohren, C. F., & Huffman, D. R. (2008). *Absorption and scattering of light by small particles*: John Wiley & Sons.

Book, G. (2014). Compendium of Chemical Terminology. *International Union of Pure and Applied Chemistry, Version 2.3.3*.

Botha, S. S., Ndungu, P., & Bladergroen, B. J. (2011). Physicochemical Properties of Oil-Based Nanofluids Containing Hybrid Structures of Silver Nanoparticles Supported on Silica. *Industrial & Engineering Chemistry Research, 50*(6), 3071-3077.

Brekke, N., Otanicar, T., DeJarnette, D., & Hari, P. (2016). A Parametric Investigation of a Concentrating Photovoltaic/Thermal System With Spectral Filtering Utilizing a Two-Dimensional Heat Transfer Model. *Journal of Solar Energy Engineering, 138*(2), 021007-021007.

Bridges, A., Felder, F. A., McKelvey, K., & Niyogi, I. (2015). Uncertainty in energy planning: Estimating the health impacts of air pollution from fossil fuel electricity generation. *Energy Research & Social Science, 6*, 74-77.

Bruggeman, D. A. G. (1935). Berechnung verschiedener physikalischer Konstanten von heterogenen Substanzen. I. Dielektrizitätskonstanten und Leitfähigkeiten der Mischkörper aus isotropen Substanzen. *Annalen der Physik, 416*(7), 636-664.

Buckingham, E. (1914). On Physically Similar Systems; Illustrations of the Use of Dimensional Equations. *Physical Review, 4*(4), 345-376.

Candanedo, L. M., Athienitis, A. K., Candanedo, J. A., O'Brien, W., & YuXiang, C. (2010). Transient and Steady State Models for Open-Loop Air-Based BIPV/T Systems. *ASHRAE Transactions, 116*(1), 600-612.

Cellura, M., Grippaldi, V., Brano, V. L., Longo, S., & Mistretta, M. (2011). Life cycle assessment of a solar PV/T concentrator system. *Fifth International Conference on Life Cycle Management, Berlin*, 28-31.

Cengel, Y. A., & Ghajar, A. J. (2011). *Heat and Mass Transfer: Fundamentals & Applications* (Fourth ed.): McGraw-Hill.

Cess, R., & Tiwari, S. (1972). Infrared radiative energy transfer in gases. *Advances in Heat Transfer, 8*, 229-283.

Che, J., Çagin, T., & III, W. A. G. (2000). Thermal conductivity of carbon nanotubes. *Nanotechnology, 11*(2), 65-69

Chen, M., He, Y., Zhu, J., Shuai, Y., Jiang, B., & Huang, Y. (2015). An experimental investigation on sunlight absorption characteristics of silver nanofluids. *Solar Energy, 115*, 85-94.

Choi, S. U. S., Zhang, Z. G., Yu, W., Lockwood, F. E., & Grulke, E. A. (2001). Anomalous thermal conductivity enhancement in nanotube suspensions. *Applied physics letters, 79*(14), 2252-2254.

Chol, S. (1995). Enhancing thermal conductivity of fluids with nanoparticles. *ASME-Publications-Fed, 231*, 99-106.

Chon, C. H., Kihm, K. D., Lee, S. P., & Choi, S. U. S. (2005). Empirical correlation finding the role of temperature and particle size for nanofluid (Al2O3) thermal conductivity enhancement. *Applied Physics Letters, 87*(15), 153107.

Chow, T.-T., & Ji, J. (2012). Environmental Life-Cycle Analysis of Hybrid Solar Photovoltaic/Thermal Systems for Use in Hong Kong. *International Journal of Photoenergy, 2012*, 1-9.

Chow, T. T. (2010). A review on photovoltaic/thermal hybrid solar technology. *Applied Energy, 87*(2), 365-379.

Corcione, M. (2011). Empirical correlating equations for predicting the effective thermal conductivity and dynamic viscosity of nanofluids. *Energy Conversion and Management, 52*(1), 789-793.

Dagunet, M. (1985). *Les séchoirs solaires: théorie et pratique*. Retrieved from UNESCO

Das, S. K., Choi, S. U., & Patel, H. E. (2006). Heat transfer in nanofluids—a review. *Heat transfer engineering, 27*(10), 3-19.

Das, S. K., Putra, N., Thiesen, P., & Roetzel, W. (2003). Temperature Dependence of Thermal Conductivity Enhancement for Nanofluids. *Journal of Heat Transfer, 125*(4), 567-574.

De Robertis, E., Cosme, E. H. H., Neves, R. S., Kuznetsov, A. Y., Campos, A. P. C., Landi, S. M., & Achete, C. A. (2012). Application of the modulated temperature differential scanning calorimetry technique for the determination of the specific heat of copper nanofluids. *Applied Thermal Engineering, 41*, 10-17.

DeJarnette, D., Otanicar, T., Brekke, N., Hari, P., & Roberts, K. (2015). Selective spectral filtration with nanoparticles for concentrating solar collectors. *Journal of Photonics for Energy, 5*(1), 057008-14.

DeJarnette, D., Otanicar, T., Brekke, N., Hari, P., Roberts, K., Saunders, A. E., & Morad, R. (2014). *Plasmonic nanoparticle based spectral fluid filters for concentrating PV/T collectors*. Proc. SPIE 9175, High and Low Concentrator Systems for Solar Energy Applications IX, 917509 (October 7, 2014).

Duangthongsuk, W., & Wongwises, S. (2010). Comparison of the effects of measured and computed thermophysical properties of nanofluids on heat transfer performance. *Experimental Thermal and Fluid Science, 34*(5), 616-624.

Dubey, S., & Tiwari, G. N. (2008). Thermal modeling of a combined system of photovoltaic thermal (PV/T) solar water heater. *Solar Energy, 82*(7), 602-612.

Duffie, J. A., & Beckman, W. A. (2013). *Solar engineering of thermal processes* (4 ed.): John Wiley, Hoboken, New Jersey.

Eastman, J. A., Choi, S. U. S., Li, S., Yu, W., & Thompson, L. J. (2001). Anomalously increased effective thermal conductivities of ethylene glycol-based nanofluids containing copper nanoparticles. *Applied Physics Letters, 78*(6), 718-720.

Elias, M. M., Mahbubul, I. M., Saidur, R., Sohel, M. R., Shahrul, I. M., Khaleduzzaman, S. S., & Sadeghipour, S. (2014). Experimental investigation on the thermo-physical properties of Al2O3 nanoparticles suspended in car radiator coolant. *International Communications in Heat and Mass Transfer, 54*(0), 48-53.

Ellabban, O., Abu-Rub, H., & Blaabjerg, F. (2014). Renewable energy resources: Current status, future prospects and their enabling technology. *Renewable and Sustainable Energy Reviews, 39*(0), 748-764.

Elmir, M., Mehdaoui, R., & Mojtabi, A. (2012). Numerical Simulation of Cooling a Solar Cell by Forced Convection in the Presence of a Nanofluid. *Energy Procedia, 18*, 594-603.

Faizal, M., Saidur, R., Mekhilef, S., Hepbasli, A., & Mahbubul, I. M. (2015). Energy, economic, and environmental analysis of a flat-plate solar collector operated with

SiO2 nanofluid. *Clean Technologies and Environmental Policy, 17*(6), 1457-1473.

Fan, J. C. C. (1986). Theoretical temperature dependence of solar cell parameters. *Solar Cells, 17*(2–3), 309-315.

Freeman, D. (2010). *Introduction to photovoltaic systems maximum power point tracking*. Retrieved from: www.ti.com/lit/an/slva446/slva446.pdf

Gan, Y., & Qiao, L. (2012). Optical Properties and Radiation-Enhanced Evaporation of Nanofluid Fuels Containing Carbon-Based Nanostructures. *Energy & Fuels, 26*(7), 4224-4230.

Garg, J., Poudel, B., Chiesa, M., Gordon, J. B., Ma, J. J., Wang, J. B., . . . Chen, G. (2008). Enhanced thermal conductivity and viscosity of copper nanoparticles in ethylene glycol nanofluid. *Journal of Applied Physics, 103*(7), 074301.

Ghadimi, A., Saidur, R., & Metselaar, H. S. C. (2011). A review of nanofluid stability properties and characterization in stationary conditions. *International Journal of Heat and Mass Transfer, 54*(17–18), 4051-4068.

Godson, L., Raja, B., Lal, D. M., & Wongwises, S. (2010). Experimental Investigation on the Thermal Conductivity and Viscosity of Silver-Deionized Water Nanofluid. *Experimental Heat Transfer, 23*(4), 317-332.

Good, C. (2016). Environmental impact assessments of hybrid photovoltaic–thermal (PV/T) systems – A review. *Renewable and Sustainable Energy Reviews, 55*, 234-239.

Green, M. A., Emery, K., Hishikawa, Y., Warta, W., & Dunlop, E. D. (2012). Solar cell efficiency tables (version 40). *Progress in Photovoltaics: Research and Applications, 20*(5), 606-614.

Green, M. A., Emery, K., Hishikawa, Y., Warta, W., & Dunlop, E. D. (2014). Solar cell efficiency tables (version 44). *Progress in Photovoltaics: Research and Applications, 22*(7), 701-710.

Green, M. A., Emery, K., Hishikawa, Y., Warta, W., & Dunlop, E. D. (2015). Solar cell efficiency tables (Version 45). *Progress in Photovoltaics: Research and Applications, 23*(1), 1-9.

Hachey, M. A., Nguyen, C. T., Galanis, N., & Popa, C. V. (2014). Experimental investigation of Al2O3 nanofluids thermal properties and rheology – Effects of transient and steady-state heat exposure. *International Journal of Thermal Sciences, 76*(0), 155-167.

Haddad, Z., Abid, C., Oztop, H. F., & Mataoui, A. (2014). A review on how the researchers prepare their nanofluids. *International Journal of Thermal Sciences, 76*(0), 168-189.

Hale, G. M., & Querry, M. R. (1973). Optical Constants of Water in the 200-nm to 200-μm Wavelength Region. *Applied Optics, 12*(3), 555-563.

Hamilton, R. L., & Crosser, O. K. (1962). Thermal Conductivity of Heterogeneous Two-Component Systems. *Industrial & Engineering Chemistry Fundamentals, 1*(3), 187-191.

He, Q., Wang, S., Zeng, S., & Zheng, Z. (2013). Experimental investigation on photothermal properties of nanofluids for direct absorption solar thermal energy systems. *Energy Conversion and Management, 73*(0), 150-157.

He, W., Zhang, G., Zhang, X., Ji, J., Li, G., & Zhao, X. (2015). Recent development and application of thermoelectric generator and cooler. *Applied Energy, 143*, 1-25.

Hj. Othman, M. Y., Yatim, B., Sopian, K., & Abu Bakar, M. N. (2005). Performance analysis of a double-pass photovoltaic/thermal (PV/T) solar collector with CPC and fins. *Renewable Energy, 30*(13), 2005-2017.

Hong, K. S., Hong, T.-K., & Yang, H.-S. (2006). Thermal conductivity of Fe nanofluids depending on the cluster size of nanoparticles. *Applied Physics Letters, 88*(3), 31901.

Hordy, N., Rabilloud, D., Meunier, J.-L., & Coulombe, S. (2014). High temperature and long-term stability of carbon nanotube nanofluids for direct absorption solar thermal collectors. *Solar Energy, 105*, 82-90.

Hwang, Y. J., Ahn, Y. C., Shin, H. S., Lee, C. G., Kim, G. T., Park, H. S., & Lee, J. K. (2006). Investigation on characteristics of thermal conductivity enhancement of nanofluids. *Current Applied Physics, 6*(6), 1068-1071.

International Energy Agency, 2014 Key world energy statistics. (Accessed 09.10.2015). Retrieved from : https://www.iea.org/publications

International, s., ISO, 9845-1. (Accessed in July 2015). Standard Solar Spectra ASTM G-173-03. Retrieved from http://pveducation.org/pvcdrom/appendices/standard-solar-spectra

Ishimaru, A. (1978). *Wave propagation and scattering in random media* (Vol. 2): Academic press New York.

Iyahraja, S., & Rajadurai, J. S. (2016). Stability of Aqueous Nanofluids Containing PVP-Coated Silver Nanoparticles. *Arabian Journal for Science and Engineering, 41*(2), 653-660.

Jang, S. P., & Choi, S. U. S. (2004). Role of Brownian motion in the enhanced thermal conductivity of nanofluids. *Applied Physics Letters, 84*(21), 4316-4318.

Jiang, H., Li, H., Zan, C., Wang, F., Yang, Q., & Shi, L. (2014). Temperature dependence of the stability and thermal conductivity of an oil-based nanofluid. *Thermochimica Acta, 579*(0), 27-30.

Jing, D., Hu, Y., Liu, M., Wei, J., & Guo, L. (2015). Preparation of highly dispersed nanofluid and CFD study of its utilization in a concentrating PV/T system. *Solar Energy, 112*, 30-40.

Joshi, A. S., Dincer, I., & Reddy, B. V. (2009). Performance analysis of photovoltaic systems: A review. *Renewable and Sustainable Energy Reviews, 13*(8), 1884-1897.

Kasaeian, A., Eshghi, A. T., & Sameti, M. (2015). A review on the applications of nanofluids in solar energy systems. *Renewable and Sustainable Energy Reviews, 43*(0), 584-598.

Keblinski, P., Phillpot, S. R., Choi, S. U. S., & Eastman, J. A. (2002). Mechanisms of heat flow in suspensions of nano-sized particles (nanofluids). *International Journal of Heat and Mass Transfer, 45*(4), 855-863.

Kern, E. C. J., & Russell, M. C. (1978). *Combined photovoltaic and thermal hybrid collector systems*. In: Proceedings of the 13th IEEE photovoltaic specialists. Washington, DC, USA. p. 1153–1157.

Kerzmann, T., & Schaefer, L. (2012). System simulation of a linear concentrating photovoltaic system with an active cooling system. *Renewable Energy, 41*, 254-261.

Kim, H. C., & Fthenakis, V. (2013). Life Cycle Energy and Climate Change Implications of Nanotechnologies. *Journal of Industrial Ecology, 17*(4), 528-541.

Kim, S. H., Choi, S. R., & Kim, D. (2006). Thermal Conductivity of Metal-Oxide Nanofluids: Particle Size Dependence and Effect of Laser Irradiation. *Journal of Heat Transfer, 129*(3), 298-307.

Kleinstreuer, C., & Feng, Y. (2011). Experimental and theoretical studies of nanofluid thermal conductivity enhancement: a review. *Nanoscale Research Letters, 6*(1), 1-13.

Koo, J., & Kleinstreuer, C. (2004). A new thermal conductivity model for nanofluids. *Journal of Nanoparticle Research, 6*(6), 577-588.

Koo, J., & Kleinstreuer, C. (2005). Laminar nanofluid flow in microheat-sinks. *International Journal of Heat and Mass Transfer, 48*(13), 2652-2661.

Koroneos, C., & Stylos, N. (2014). Exergetic life cycle assessment of a grid-connected, polycrystalline silicon photovoltaic system. *The International Journal of Life Cycle Assessment, 19*(10), 1716-1732.

Krause, F., Bossel, H., & Müller-Reißmann, K.-F. (1980). *Energie-Wende: Wachstum und Wohlstand ohne Erdöl und Uran, (Energy Transition – Growth and Prosperity without Petroleum and Uranium)*: S. Fischer.

Kück, A., Steinfeldt, M., Prenzel, K., Swiderek, P., Gleich, A. v., & Thöming, J. (2011). Green nanoparticle production using micro reactor technology. *Journal of Physics: Conference Series, 304*(1), 012074.

Kumar, K., Salih, A., Lu, L., Müller, E., & Rodríguez-Reinoso, F. (2011). Molecular Simulation of Hydrogen Physisorption and Chemisorption in Nanoporous Carbon Structures. *Adsorption Science & Technology, 29*(8), 799-818.

Kumaresan, V., & Velraj, R. (2012). Experimental investigation of the thermo-physical properties of water–ethylene glycol mixture based CNT nanofluids. *Thermochimica Acta, 545*(0), 180-186.

Lämmle, M., Kroyer, T., Fortuin, S., Wiese, M., & Hermann, M. (2016). Development and modelling of highly-efficient PVT collectors with low-emissivity coatings. *Solar Energy, 130*, 161-173.

Lee, S.-H., & Jang, S. P. (2013). Extinction coefficient of aqueous nanofluids containing multi-walled carbon nanotubes. *International Journal of Heat and Mass Transfer, 67*(0), 930-935.

Lee, S., Choi, S. U. S., Li, S., & Eastman, J. A. (1999). Measuring Thermal Conductivity of Fluids Containing Oxide Nanoparticles. *Journal of Heat Transfer, 121*(2), 280-289.

Lee, S. W., Park, S. D., & Bang, I. C. (2012). Critical heat flux for CuO nanofluid fabricated by pulsed laser ablation differentiating deposition characteristics. *International Journal of Heat and Mass Transfer, 55*(23–24), 6908-6915.

Li, L., Zhang, Y., Ma, H., & Yang, M. (2008). An investigation of molecular layering at the liquid-solid interface in nanofluids by molecular dynamics simulation. *Physics Letters A, 372*(25), 4541-4544.

Li, X., Zou, C., Lei, X., & Li, W. (2015). Stability and enhanced thermal conductivity of ethylene glycol-based SiC nanofluids. *International Journal of Heat and Mass Transfer, 89*, 613-619.

Li, Y., Zhou, J. e., Tung, S., Schneider, E., & Xi, S. (2009). A review on development of nanofluid preparation and characterization. *Powder Technology, 196*(2), 89-101.

Lin, Y.-S., Hsiao, P.-Y., & Chieng, C.-C. (2011). Roles of nanolayer and particle size on thermophysical characteristics of ethylene glycol-based copper nanofluids. *Applied Physics Letters, 98*(15), 153105.

Liu, M.-S., Ching-Cheng Lin, M., Huang, I. T., & Wang, C.-C. (2005). Enhancement of thermal conductivity with carbon nanotube for nanofluids. *International Communications in Heat and Mass Transfer, 32*(9), 1202-1210.

Liu, M.-S., Lin, M. C.-C., Tsai, C. Y., & Wang, C.-C. (2006). Enhancement of thermal conductivity with Cu for nanofluids using chemical reduction method. *International Journal of Heat and Mass Transfer, 49*(17–18), 3028-3033.

127

Lo, C.-H., Tsung, T.-T., Chen, L.-C., Su, C.-H., & Lin, H.-M. (2005). Fabrication of copper oxide nanofluid using submerged arc nanoparticle synthesis system (SANSS). *Journal of Nanoparticle Research, 7*(2-3), 313-320.

Luo, Z., Wang, C., Wei, W., Xiao, G., & Ni, M. (2014). Performance improvement of a nanofluid solar collector based on direct absorption collection (DAC) concepts. *International Journal of Heat and Mass Transfer, 75*, 262-271.

Mahbubul, I. M., Fadhilah, S. A., Saidur, R., Leong, K. Y., & Amalina, M. A. (2013). Thermophysical properties and heat transfer performance of Al2O3/R-134a nanorefrigerants. *International Journal of Heat and Mass Transfer, 57*(1), 100-108.

Mahendia, S., Tomar, A., Chahal, R. P., Goyal, P., & Kumar, S. (2011). Optical and structural properties of poly (vinyl alcohol) films embedded with citrate-stabilized gold nanoparticles. *Journal of Physics D: Applied Physics, 44*(20), 205105.

Mahian, O., Kianifar, A., Heris, S. Z., & Wongwises, S. (2016). Natural convection of silica nanofluids in square and triangular enclosures: Theoretical and experimental study. *International Journal of Heat and Mass Transfer, 99*, 792-804.

Mahian, O., Kianifar, A., Kalogirou, S. A., Pop, I., & Wongwises, S. (2013). A review of the applications of nanofluids in solar energy. *International Journal of Heat and Mass Transfer, 57*(2), 582-594.

Maïga, S. E. B., Palm, S. J., Nguyen, C. T., Roy, G., & Galanis, N. (2005). Heat transfer enhancement by using nanofluids in forced convection flows. *International Journal of Heat and Fluid Flow, 26*(4), 530-546.

Masuda, H., Ebata, A., Teramae, K., & Hishinuma, N. (1993). Alteration of thermal conductivity and viscosity of liquid by dispersing ultra-fine particles (dispersions of γ-Al2O3, SiO2, and TiO2 ultra-fine particles). *Netsu Bussei, 7*(4), 227-233.

Mathai, J. C., Mori, S., Smith, B. L., Preston, G. M., Mohandas, N., Collins, M., . . . Agre, P. (1996). Functional Analysis of Aquaporin-1 Deficient Red Cells: THE COLTON-NULL PHENOTYPE. *Journal of Biological Chemistry, 271*(3), 1309-1313.

Maxwell, J. C. (1873). *A Treatise on Electricity and Magnetism* (Vol. 1): Clarendon Press.

Menbari, A., & Alemrajabi, A. A. (2016). Analytical modeling and experimental investigation on optical properties of new class of nanofluids (Al2O3–CuO binary nanofluids) for direct absorption solar thermal energy. *Optical Materials, 52*, 116-125.

Menbari, A., Alemrajabi, A. A., & Ghayeb, Y. (2016). Investigation on the stability, viscosity and extinction coefficient of CuO–Al2O3/Water binary mixture nanofluid. *Experimental Thermal and Fluid Science, 74*, 122-129.

128

Mesgari, S., Coulombe, S., Hordy, N., & Taylor, R. A. (2015). Thermal stability of carbon nanotube-based nanofluids for solar thermal collectors. *Materials Research Innovations, 19*(sup5), S5-650-S655-653.

Meyer, J. P., Adio, S. A., Sharifpur, M., & Nwosu, P. N. (2016). The Viscosity of Nanofluids: A Review of the Theoretical, Empirical, and Numerical Models. *Heat Transfer Engineering, 37*(5), 387-421.

Michael, J. J., S, I., & Goic, R. (2015). Flat plate solar photovoltaic–thermal (PV/T) systems: A reference guide. *Renewable and Sustainable Energy Reviews, 51*(0), 62-88.

Minkowycz, W., Sparrow, E. M., & Abraham, J. P. (2012). *Nanoparticle Heat Transfer and Fluid Flow* (Vol. 4): CRC Press, Taylor & Francis.

Mintsa, H. A., Roy, G., Nguyen, C. T., & Doucet, D. (2009). New temperature dependent thermal conductivity data for water-based nanofluids. *International Journal of Thermal Sciences, 48*(2), 363-371.

Mo, S., Chen, Y., Jia, L., & Luo, X. (2012). Investigation on crystallization of TiO2–water nanofluids and deionized water. *Applied Energy, 93*, 65-70.

Mojiri, A., Stanley, C., Taylor, R. A., Kalantar-zadeh, K., & Rosengarten, G. (2015). A spectrally splitting photovoltaic-thermal hybrid receiver utilising direct absorption and wave interference light filtering. *Solar Energy Materials and Solar Cells, 139*(0), 71-80.

Moreira, L. M., Carvalho, E. A., Bell, M. J. V., Anjos, V., Sant'Ana, A. C., Alves, A. P. P., . . . Achete, C. A. (2013). Thermo-optical properties of silver and gold nanofluids. *Journal of Thermal Analysis and Calorimetry, 114*(2), 557-564.

Mukherjee, S., & Paria, S. (2013). Preparation and stability of nanofluids-A Review. *IOSR Journal of Mechanical and Civil Engineering, 9*(2), 63-69.

Müller, A., Kranzl, L., Tuominen, P., Boelman, E., Molinari, M., & Entrop, A. G. (2011). Estimating exergy prices for energy carriers in heating systems: Country analyses of exergy substitution with capital expenditures. *Energy and Buildings, 43*(12), 3609-3617.

Munkhbayar, B., Tanshen, M. R., Jeoun, J., Chung, H., & Jeong, H. (2013). Surfactant-free dispersion of silver nanoparticles into MWCNT-aqueous nanofluids prepared by one-step technique and their thermal characteristics. *Ceramics International, 39*(6), 6415-6425.

Murray-Méthot, M.-P., Ratel, M., & Masson, J.-F. (2010). Optical Properties of Au, Ag, and Bimetallic Au on Ag Nanohole Arrays. *The Journal of Physical Chemistry C, 114*(18), 8268-8275.

Murshed, S., Leong, K., & Yang, C. (2008). Investigations of thermal conductivity and viscosity of nanofluids. *International Journal of Thermal Sciences, 47*(5), 560-568.

Murshed, S. M. S. (2011a). Determination of effective specific heat of nanofluids. *Journal of Experimental Nanoscience, 6*(5), 539-546.

Murshed, S. M. S. (2011b). Simultaneous Measurement of Thermal Conductivity, Thermal Diffusivity, and Specific Heat of Nanofluids. *Heat Transfer Engineering, 33*(8), 722-731.

Murshed, S. M. S., Leong, K. C., & Yang, C. (2005). Enhanced thermal conductivity of TiO2—water based nanofluids. *International Journal of Thermal Sciences, 44*(4), 367-373.

Nagvenkar, A. P., Deokar, A., Perelshtein, I., & Gedanken, A. (2016). A one-step sonochemical synthesis of stable ZnO-PVA nanocolloid as a potential biocidal agent. *Journal of Materials Chemistry B, 4*(12), 2124-2132.

NIST. (accessed December, 2015). Thermophysical Properties of Fluid Systems. *http://webbook.nist.gov/chemistry/fluid/*.

Niu, X., Yu, J., & Wang, S. (2009). Experimental study on low-temperature waste heat thermoelectric generator. *Journal of Power Sources, 188*(2), 621-626.

O'Hanley, H., Buongiorno, J., McKrell, T., & Hu, L.-w. (2012). Measurement and Model Validation of Nanofluid Specific Heat Capacity with Differential Scanning Calorimetry. *Advances in Mechanical Engineering, 4*.

Oliveira, G. A., Cardenas Contreras, E. M., & Bandarra Filho, E. P. (2016). Experimental study on the heat transfer of MWCNT/water nanofluid flowing in a car radiator. *Applied Thermal Engineering,* doi:http://dx.doi.org/10.1016/j.applthermaleng.2016.05.086

Osborn, D. E., Chendo, M. A. C., Hamdy, M. A., Luttmann, F., Jacobson, M. R., Macleod, H. A., & Swenson, R. (1986). Spectral selectivity applied to hybrid concentration systems. *Solar Energy Materials, 14*(3), 299-325.

Otanicar, T., Chowdhury, I., Phelan, P. E., & Prasher, R. (2010). Parametric analysis of a coupled photovoltaic/thermal concentrating solar collector for electricity generation. *Journal of Applied Physics, 108*(11), 114907.

Otanicar, T., Hoyt, J., Fahar, M., Jiang, X., & Taylor, R. A. (2013). Experimental and numerical study on the optical properties and agglomeration of nanoparticle suspensions. *Journal of Nanoparticle Research, 15*(11), 1-11.

Otanicar, T. P., Chowdhury, I., Prasher, R., & Phelan, P. E. (2011). Band-Gap Tuned Direct Absorption for a Hybrid Concentrating Solar Photovoltaic/Thermal System. *Journal of Solar Energy Engineering, 133*(4), 041014-041014.

Otanicar, T. P., Phelan, P. E., Prasher, R. S., Rosengarten, G., & Taylor, R. A. (2010). Nanofluid-based direct absorption solar collector. *Journal of Renewable and Sustainable Energy, 2*(3), 033102.

Otanicar, T. P., Phelan, P. E., Taylor, R. A., & Tyagi, H. (2011). Spatially Varying Extinction Coefficient for Direct Absorption Solar Thermal Collector Optimization. *Journal of Solar Energy Engineering, 133*(2), 024501-024501.

Otanicar, T. P., Taylor, R. A., & Telang, C. (2013). Photovoltaic/thermal system performance utilizing thin film and nanoparticle dispersion based optical filters. *Journal of Renewable and Sustainable Energy, 5*(3), 033124.

Oztop, H. F., & Abu-Nada, E. (2008). Numerical study of natural convection in partially heated rectangular enclosures filled with nanofluids. *International Journal of Heat and Fluid Flow, 29*(5), 1326-1336.

Pak, B. C., & Cho, Y. I. (1998). HYDRODYNAMIC AND HEAT TRANSFER STUDY OF DISPERSED FLUIDS WITH SUBMICRON METALLIC OXIDE PARTICLES. *Experimental Heat Transfer, 11*(2), 151-170.

Palmer, K. F., & Williams, D. (1974). Optical properties of water in the near infrared. *Journal of the Optical Society of America, 64*(8), 1107-1110.

Pang, C., Jung, J.-Y., Lee, J. W., & Kang, Y. T. (2012). Thermal conductivity measurement of methanol-based nanofluids with Al2O3 and SiO2 nanoparticles. *International Journal of Heat and Mass Transfer, 55*(21–22), 5597-5602.

Patel, H., Sundararajan, T., & Das, S. (2010). An experimental investigation into the thermal conductivity enhancement in oxide and metallic nanofluids. *Journal of Nanoparticle Research, 12*(3), 1015-1031.

Patel, H. E., Anoop, K. B., Sundararajan, T., & Das, S. (2008). Model for thermal conductivity of CNT-nanofluids. *Bulletin of Materials Science, 31*(3), 387-390.

Petela, R. (2008). An approach to the exergy analysis of photosynthesis. *Solar Energy, 82*(4), 311-328.

Petroleum, B. (June 2015). *BP Statistical Review of World Energy*. Retrieved from: www.bp.com/en/global/

Pil Jang, S., & Choi, S. U. S. (2006). Effects of Various Parameters on Nanofluid Thermal Conductivity. *Journal of Heat Transfer, 129*(5), 617-623.

Polidori, G., Fohanno, S., & Nguyen, C. T. (2007). A note on heat transfer modelling of Newtonian nanofluids in laminar free convection. *International Journal of Thermal Sciences, 46*(8), 739-744.

Prasher, R., Bhattacharya, P., & Phelan, P. E. (2005a). Brownian-Motion-Based Convective-Conductive Model for the Effective Thermal Conductivity of Nanofluids. *Journal of Heat Transfer, 128*(6), 588-595.

Prasher, R., Bhattacharya, P., & Phelan, P. E. (2005b). Thermal Conductivity of Nanoscale Colloidal Solutions (Nanofluids). *Physical Review Letters, 94*(2), 025901.

Prasher, R., Phelan, P. E., & Bhattacharya, P. (2006). Effect of Aggregation Kinetics on the Thermal Conductivity of Nanoscale Colloidal Solutions (Nanofluid). *Nano Letters, 6*(7), 1529-1534.

Pulles, T., & Appelman, W. (2008). *Air pollution from electricity-generating large combustion plants*. Retrieved from: http://www.eea.europa.eu/publications

Radwan, A., Ahmed, M., & Ookawara, S. (2016). Performance enhancement of concentrated photovoltaic systems using a microchannel heat sink with nanofluids. *Energy Conversion and Management, 119*, 289-303.

Raykar, V. S., & Singh, A. K. (2010). Thermal and rheological behavior of acetylacetone stabilized ZnO nanofluids. *Thermochimica Acta, 502*(1–2), 60-65.

Reinecke, B. N., Shan, J. W., Suabedissen, K. K., & Cherkasova, A. S. (2008). On the anisotropic thermal conductivity of magnetorheological suspensions. *Journal of Applied Physics, 104*(2), 023507.

Renewables 2015: Global status report. (2015). Retrieved from www.ren21.net/wp-content/

Richter, K., Birkner, A., & Mudring, A. V. (2010). Stabilizer-Free Metal Nanoparticles and Metal–Metal Oxide Nanocomposites with Long-Term Stability Prepared by Physical Vapor Deposition into Ionic Liquids. *Angewandte Chemie International Edition, 49*(13), 2431-2435.

Routbort, J. L., Singh, D., Timofeeva, E. V., Yu, W., & France, D. M. (2011). Pumping power of nanofluids in a flowing system. *Journal of Nanoparticle Research, 13*(3), 931-937.

Russo, J. M., Zhang, D., Gordon, M., Vorndran, S., Wu, Y., & Kostuk, R. K. (2014). Spectrum splitting metrics and effect of filter characteristics on photovoltaic system performance. *Optics Express, 22*(S2), A528-A541.

Sadri, R., Ahmadi, G., Togun, H., Dahari, M., Kazi, S. N., Sadeghinezhad, E., & Zubir, N. (2014). An experimental study on thermal conductivity and viscosity of nanofluids containing carbon nanotubes. *Nanoscale Research Letters, 9*(1), 1-16.

Said, Z., Sabiha, M. A., Saidur, R., Hepbasli, A., Rahim, N. A., Mekhilef, S., & Ward, T. A. (2015). Performance enhancement of a Flat Plate Solar collector using Titanium dioxide nanofluid and Polyethylene Glycol dispersant. *Journal of Cleaner Production, 92*, 343-353.

Said, Z., Sajid, M. H., Alim, M. A., Saidur, R., & Rahim, N. A. (2013). Experimental investigation of the thermophysical properties of AL2O3-nanofluid and its effect on a flat plate solar collector. *International Communications in Heat and Mass Transfer, 48*, 99-107.

Said, Z., Sajid, M. H., Saidur, R., Kamalisarvestani, M., & Rahim, N. A. (2013). Radiative properties of nanofluids. *International Communications in Heat and Mass Transfer, 46*, 74-84.

Said, Z., Sajid, M. H., Saidur, R., Mahdiraji, G. A., & Rahim, N. A. (2015). Evaluating the Optical Properties of TiO2 Nanofluid for a Direct Absorption Solar Collector. *Numerical Heat Transfer, Part A: Applications, 67*(9), 1010-1027.

Saidur, R., Leong, K. Y., & Mohammad, H. A. (2011). A review on applications and challenges of nanofluids. *Renewable and Sustainable Energy Reviews, 15*(3), 1646-1668.

Sajid Hossain, M., Saidur, R., Mohd Sabri, M. F., Said, Z., & Hassani, S. (2015). Spotlight on available optical properties and models of nanofluids: A review. *Renewable and Sustainable Energy Reviews, 43*, 750-762.

Sardarabadi, M., Passandideh-Fard, M., & Zeinali Heris, S. (2014). Experimental investigation of the effects of silica/water nanofluid on PV/T (photovoltaic thermal units). *Energy, 66*, 264-272.

Sarkar, J., Ghosh, P., & Adil, A. (2015). A review on hybrid nanofluids: Recent research, development and applications. *Renewable and Sustainable Energy Reviews, 43*, 164-177.

Saroha, S., Mittal, T., Modi, P. J., Bhalla, V., Khullar, V., Tyagi, H., . . . Otanicar, T. P. (2015). Theoretical Analysis and Testing of Nanofluids-Based Solar Photovoltaic/Thermal Hybrid Collector. *Journal of Heat Transfer, 137*(9), 091015-091015.

Schivley, G., Ingwersen, W. W., Marriott, J., Hawkins, T. R., & Skone, T. J. (2015). Identifying/Quantifying Environmental Trade-offs Inherent in GHG Reduction Strategies for Coal-Fired Power. *Environmental Science & Technology, 49*(13), 7562-7570.

Shahrul, I. M., Mahbubul, I. M., Khaleduzzaman, S. S., Saidur, R., & Sabri, M. F. M. (2014). A comparative review on the specific heat of nanofluids for energy perspective. *Renewable and Sustainable Energy Reviews, 38*, 88-98.

Sharma, A. K., Tiwari, A. K., & Dixit, A. R. (2016). Rheological behaviour of nanofluids: A review. *Renewable and Sustainable Energy Reviews, 53*, 779-791.

Sharma, K. V., Sarma, P. K., Azmi, W. H., Mamat, R., & Kadirgama, K. (2012). Correlations to predict friction and forced convection heat transfer coefficients of water based nanofluids for turbulent flow in a tube. *International Journal of*

Microscale and Nanoscale Thermal and Fluid Transport Phenomena, 3(Special Issue in Heat and mass transfer in nanofluids), 1-25.

Shima, P. D., & Philip, J. (2014). Role of Thermal Conductivity of Dispersed Nanoparticles on Heat Transfer Properties of Nanofluid. *Industrial & Engineering Chemistry Research, 53*(2), 980-988.

Sidik, N. A. C., Mohammed, H. A., Alawi, O. A., & Samion, S. (2014). A review on preparation methods and challenges of nanofluids. *International Communications in Heat and Mass Transfer, 54*, 115-125.

Siegel, R., & Howell, J. R. (1992). *Thermal radiation heat transfer* (Third ed.): Hemisphere Publishing Corporation.

Silverman, T. J., Deceglie, M. G., Marion, B., Cowley, S., Kayes, B., & Kurtz, S. (2013, 16-21 June 2013). *Outdoor performance of a thin-film gallium-arsenide photovoltaic module.* Paper presented at the Photovoltaic Specialists Conference (PVSC), 2013 IEEE 39th.

Singh, D., Timofeeva, E. V., Moravek, M. R., Cingarapu, S., Yu, W., Fischer, T., & Mathur, S. (2014). Use of metallic nanoparticles to improve the thermophysical properties of organic heat transfer fluids used in concentrated solar power. *Solar Energy, 105*(0), 468-478.

Solangi, K. H., Kazi, S. N., Luhur, M. R., Badarudin, A., Amiri, A., Sadri, R., . . . Teng, K. H. (2015). A comprehensive review of thermo-physical properties and convective heat transfer to nanofluids. *Energy, 89*, 1065-1086.

Song, D., Wang, Y., Jing, D., & Geng, J. (2016). Investigation and prediction of optical properties of alumina nanofluids with different aggregation properties. *International Journal of Heat and Mass Transfer, 96*, 430-437.

Song, Y. Y., Bhadeshia, H. K. D. H., & Suh, D.-W. (2015). Stability of stainless-steel nanoparticle and water mixtures. *Powder Technology, 272*, 34-44.

Sparrow, E. M., Ramsey, J. W., & Mass, E. A. (1979). Effect of Finite Width on Heat Transfer and Fluid Flow about an Inclined Rectangular Plate. *Journal of Heat Transfer, 101*(2), 199-204.

Syam, S. L., & Singh, M. K. (2013). Convective heat transfer and friction factor correlations of nanofluid in a tube and with inserts: A review. *Renewable and Sustainable Energy Reviews, 20*(0), 23-35.

Taylor, R., Coulombe, S., Otanicar, T., Phelan, P., Gunawan, A., Lv, W., . . . Tyagi, H. (2013). Small particles, big impacts: A review of the diverse applications of nanofluids. *Journal of Applied Physics, 113*(1), 011301.

Taylor, R., Phelan, P., Otanicar, T., Adrian, R., & Prasher, R. (2011). Nanofluid optical property characterization: towards efficient direct absorption solar collectors. *Nanoscale Research Letters, 6*(1), 1-11.

Taylor, R. A., Otanicar, T., & Rosengarten, G. (2012). Nanofluid-based optical filter optimization for PV/T systems. *Light Sci Appl, 1*, e34.

Taylor, R. A., Otanicar, T. P., Herukerrupu, Y., Bremond, F., Rosengarten, G., Hawkes, E. R., . . . Coulombe, S. (2013). Feasibility of nanofluid-based optical filters. *Applied Optics, 52*(7), 1413-1422.

Taylor, R. A., Phelan, P. E., Adrian, R., Prasher, R., & Otanicar, T. P. (2011). Nanofluid Extinction Coefficients for Photothermal Energy Conversion. Paper presented at the ASME/JSME 2011 8th Thermal Engineering Joint Conference.

Taylor, R. A., Phelan, P. E., Otanicar, T. P., Walker, C. A., Nguyen, M., Trimble, S., & Prasher, R. (2011). Applicability of nanofluids in high flux solar collectors. *Journal of Renewable and Sustainable Energy, 3*(2), 023104.

Timofeeva, E. V., Moravek, M. R., & Singh, D. (2011). Improving the heat transfer efficiency of synthetic oil with silica nanoparticles. *Journal of Colloid and Interface Science, 364*(1), 71-79.

Tiwari, A., Raman, V., & Tiwari, G. N. (2007). Embodied energy analysis of hybrid photovoltaic thermal (PV/T) water collector. *International Journal of Ambient Energy, 28*(4), 181-188.

Tripanagnostopoulos, Y., Souliotis, M., Battisti, R., & Corrado, A. (2005). Energy, cost and LCA results of PV and hybrid PV/T solar systems. *Progress in Photovoltaics: Research and Applications, 13*(3), 235-250.

Tyagi, H., Phelan, P., & Prasher, R. (2009). Predicted Efficiency of a Low-Temperature Nanofluid-Based Direct Absorption Solar Collector. *Journal of Solar Energy Engineering, 131*(4), 041004-041004.

Vajjha, R. S., & Das, D. K. (2009). Experimental determination of thermal conductivity of three nanofluids and development of new correlations. *International Journal of Heat and Mass Transfer, 52*(21–22), 4675-4682.

Varun, Sharma, A., Shree, V., & Nautiyal, H. (2012). Life cycle environmental assessment of an educational building in Northern India: A case study. *Sustainable Cities and Society, 4*, 22-28.

Vaschy, A. (1892). *Sur les lois de similitude en physique.* Paper presented at the Annales télégraphiques.

Vorobiev, Y. V., González-Hernández, J., & Kribus, A. (2005). Analysis of Potential Conversion Efficiency of a Solar Hybrid System With High-Temperature Stage. *Journal of Solar Energy Engineering, 128*(2), 258-260.

Wall, G. (1977). Exergy-a useful concept within resource accounting. *Institute of Theoretical Physics, Chalmers University of Technology and University of Göteborg, Sweden, Report no. 77-42*.

Wang, B.-X., Zhou, L.-P., & Peng, X.-F. (2003). A fractal model for predicting the effective thermal conductivity of liquid with suspension of nanoparticles. *International Journal of Heat and Mass Transfer, 46*(14), 2665-2672.

Wen, D., & Ding, Y. (2004). Effective Thermal Conductivity of Aqueous Suspensions of Carbon Nanotubes (Carbon Nanotube Nanofluids). *Journal of Thermophysics and Heat Transfer, 18*(4), 481-485.

Wen, D., & Ding, Y. (2005). Experimental investigation into the pool boiling heat transfer of aqueous based γ-alumina nanofluids. *Journal of Nanoparticle Research, 7*(2), 265-274.

Wen, D., Lin, G., Vafaei, S., & Zhang, K. (2009). Review of nanofluids for heat transfer applications. *Particuology, 7*(2), 141-150.

Witharana, S., Palabiyik, I., Musina, Z., & Ding, Y. (2013). Stability of glycol nanofluids — The theory and experiment. *Powder Technology, 239*, 72-77.

Wu, Y., Zhou, L., Du, X., & Yang, Y. (2015). Optical and thermal radiative properties of plasmonic nanofluids containing core–shell composite nanoparticles for efficient photothermal conversion. *International Journal of Heat and Mass Transfer, 82*, 545-554.

Xu, X., Yang, W., Song, C., Liu, J., & Lin, L. (2003). Hydrogen separation by zeolite membranes. *Preprints of Papers- American Chemical Society, Division of Fuel Chemistry, 48*(1), 284-285.

Xu, Z., & Kleinstreuer, C. (2014). Computational Analysis of Nanofluid Cooling of High Concentration Photovoltaic Cells. *Journal of Thermal Science and Engineering Applications, 6*(3), 031009-031009.

Xuan, Y., & Li, Q. (2000). Heat transfer enhancement of nanofluids. *International Journal of Heat and Fluid Flow, 21*(1), 58-64.

Xuan, Y., Li, Q., & Hu, W. (2003). Aggregation structure and thermal conductivity of nanofluids. *AIChE Journal, 49*(4), 1038-1043.

Xuan, Y., & Roetzel, W. (2000). Conceptions for heat transfer correlation of nanofluids. *International Journal of Heat and Mass Transfer, 43*(19), 3701-3707.

Xue, L., Keblinski, P., Phillpot, S. R., Choi, S. U.-S., & Eastman, J. A. (2003). Two regimes of thermal resistance at a liquid–solid interface. *The Journal of Chemical Physics, 118*(1), 337-339.

Yongjin, F., Boming, Y., Peng, X., & Mingqing, Z. (2007). The effective thermal conductivity of nanofluids based on the nanolayer and the aggregation of nanoparticles. *Journal of Physics D: Applied Physics, 40*(10), 3164.

Younes, H., Christensen, G., Li, D., Hong, H., & Ghaferi, A. A. (2015). Thermal Conductivity of Nanofluids: Review. *Journal of Nanofluids, 4*(2), 107-132.

Yu, W., & Choi, S. U. S. (2004). The role of interfacial layers in the enhanced thermal conductivity of nanofluids: A renovated Hamilton–Crosser model. *Journal of Nanoparticle Research, 6*(4), 355-361.

Yu, W., Hull, J. R., & Choi, S. U. S. (2003). TED-AJ03-384 STABLE AND HIGHLY CONDUCTIVE NANOFLUIDS-EXPERIMENTAL AND THEORETICAL STUDIES. *Proceedings of the ... ASME/JSME Thermal Engineering Joint Conference, 2003*(6), 30.

Yu, W., & Xie, H. (2012). A review on nanofluids: preparation, stability mechanisms, and applications. *Journal of Nanomaterials, 2012*, 1.

Yun, C., & Qunzhi, Z. (2012, 27-29 March 2012). *Study of Photovoltaic/Thermal Systems with MgO-Water Nanofluids Flowing over Silicon Solar Cells.* Paper presented at the Power and Energy Engineering Conference (APPEEC), 2012 Asia-Pacific.

Zhao, J., Song, Y., Lam, W.-H., Liu, W., Liu, Y., Zhang, Y., & Wang, D. (2011). Solar radiation transfer and performance analysis of an optimum photovoltaic/thermal system. *Energy Conversion and Management, 52*(2), 1343-1353.

Zheng, X. F., Yan, Y. Y., & Simpson, K. (2013). A potential candidate for the sustainable and reliable domestic energy generation–Thermoelectric cogeneration system. *Applied Thermal Engineering, 53*(2), 305-311.

Zhou, L.-P., Wang, B.-X., Peng, X.-F., Du, X.-Z., & Yang, Y.-P. (2010). On the Specific Heat Capacity of CuO Nanofluid. *Advances in Mechanical Engineering, 2*.

Zhu, Q., Cui, Y., Mu, L., & Tang, L. (2013). Characterization of Thermal Radiative Properties of Nanofluids for Selective Absorption of Solar Radiation. *International Journal of Thermophysics, 34*(12), 2307-2321.

Zondag, H. A., de Vries, D. W., van Helden, W. G. J., van Zolingen, R. J. C., & van Steenhoven, A. A. (2002). The thermal and electrical yield of a PV-thermal collector. *Solar Energy, 72*(2), 113-128.

LIST OF PUBLICATIONS

Hassani S, Saidur R, Mekhilef S, Hepbasli A. "*A new correlation for predicting the thermal conductivity of nanofluids; using dimensional analysis*". International Journal of Heat and Mass Transfer. 2015; 90(0):121-130. (*ISI-cited publication, IF: 2.85, Q1*)

Hassani S, Taylor R.A, Mekhilef S, Saidur R. "*A cascade nanofluid-based PV/T system with optimized optical and thermal properties*". Energy. 2016; 112 (0) 963-975. (*ISI-cited publication, IF: 4.29, Q1*)

Hassani S, Saidur R, Mekhilef S, Taylor RA. "*Environmental and exergy benefit of nanofluid-based hybrid PV/T systems*". Energy Conversion and Management. 2016; 123(0): 431-444. (*ISI-cited publication, IF: 4.80, Q1*)

Intellectual property rights

Hassani S, Mekhilef S, Saidur R, Taylor RA. "*Nanofluid based solar energy harvester*". Patent number: PI 2016701779, 2016.